AIP | Journal of Applied Physics

Multiferroic magnetoelectric composites: Historical perspective, status, and future directions

Ce-Wen Nan, M. I. Bichurin, Shuxiang Dong, D. Viehland, and G. Srinivasan

Citation: J. Appl. Phys. **103**, 031101 (2008); doi: 10.1063/1.2836410
View online: http://dx.doi.org/10.1063/1.2836410
View Table of Contents: http://jap.aip.org/resource/1/JAPIAU/v103/i3
Published by the American Institute of Physics.

APPLIED PHYSICS REVIEWS—FOCUSED REVIEW

Multiferroic magnetoelectric composites: Historical perspective, status, and future directions

Ce-Wen Nan[a)]
Department of Materials Science and Engineering, State Key Laboratory of New Ceramics and Fine Processing, Tsinghua University, Beijing 100084, People's Republic of China

M. I. Bichurin
Institute of Electronic and Informative Systems, Novgorod State University, B. S.-Peterburgskaya st. 41, 173003 Veliky Novgorod, Russia

Shuxiang Dong[b)] and D. Viehland
Department of Materials Science and Engineering, Virginia Technology, Blacksburg, Virginia 24061, USA

G. Srinivasan
Physics Department, Oakland University, Rochester, Michigan 48309, USA

(Received 18 July 2007; accepted 28 November 2007; published online 5 February 2008)

Multiferroic magnetoelectric materials, which simultaneously exhibit ferroelectricity and ferromagnetism, have recently stimulated a sharply increasing number of research activities for their scientific interest and significant technological promise in the novel multifunctional devices. Natural multiferroic single-phase compounds are rare, and their magnetoelectric responses are either relatively weak or occurs at temperatures too low for practical applications. In contrast, multiferroic composites, which incorporate both ferroelectric and ferri-/ferromagnetic phases, typically yield giant magnetoelectric coupling response above room temperature, which makes them ready for technological applications. This review of mostly recent activities begins with a brief summary of the historical perspective of the multiferroic magnetoelectric composites since its appearance in 1972. In such composites the magnetoelectric effect is generated as a product property of a magnetostrictive and a piezoelectric substance. An electric polarization is induced by a weak ac magnetic field oscillating in the presence of a dc bias field, and/or a magnetization polarization appears upon applying an electric field. So far, three kinds of bulk magnetoelectric composites have been investigated in experimental and theoretical, i.e., composites of (a) ferrite and piezoelectric ceramics (e.g., lead zirconate titanate), (b) magnetic metals/alloys (e.g., Terfenol-D and Metglas) and piezoelectric ceramics, and (c) Terfenol-D and piezoelectric ceramics and polymer. The elastic coupling interaction between the magnetostrictive phase and piezoelectric phase leads to giant magnetoelectric response of these magnetoelectric composites. For example, a Metglas/lead zirconate titanate fiber laminate has been found to exhibit the highest magnetoelectric coefficient, and in the vicinity of resonance, its magnetoelectric voltage coefficient as high as 10^2 V/cm Oe orders has been achieved, which exceeds the magnetoelectric response of single-phase compounds by many orders of magnitude. Of interest, motivated by on-chip integration in microelectronic devices, nanostructured composites of ferroelectric and magnetic oxides have recently been deposited in a film-on substrate geometry. The coupling interaction between nanosized ferroelectric and magnetic oxides is also responsible for the magnetoelectric effect in the nanostructures as was the case in those bulk composites. The availability of high-quality nanostructured composites makes it easier to tailor their properties through epitaxial strain, atomic-level engineering of chemistry, and interfacial coupling. In this review, we discuss these bulk and nanostructured magnetoelectric composites both in experimental and theoretical. From application viewpoint, microwave devices, sensors, transducers, and heterogeneous read/write devices are among the suggested technical implementations of the magnetoelectric composites. The review concludes with an outlook on the exciting future possibilities and scientific challenges in the field of multiferroic magnetoelectric composites. © *2008 American Institute of Physics*. [DOI: 10.1063/1.2836410]

TABLE OF CONTENTS

[a)]Electronic mail: cwnan@mail.tsinghua.edu.cn.
[b)]Electronic mail: sdong@mse.vt.edu.

I. INTRODUCTION

Multiferroic materials[1–3] with coexistence of at least two ferroic orders (ferroelectric, ferromagnetic, or ferroelastic) have drawn increasing interest due to their potential for applications as multifunctional devices. In multiferroic materials, the coupling interaction between the different order parameters could produce new effects, such as magnetoelectric (ME) effect.[4–7] The magnetoelectric response is the appearance of an electric polarization $\boldsymbol{P}$ upon applying a magnetic field $\boldsymbol{H}$ (i.e., the direct ME effect, designated as ME_H effect: $P=\alpha H$) and/or the appearance of a magnetization $\boldsymbol{M}$ upon applying an electric field $\boldsymbol{E}$ (i.e., the converse ME effect, or ME_E: $M=\alpha E$). Magnetoelectricity has been observed as an intrinsic effect in some natural material systems at low temperature, which have been under intensive study recently,[8–15] motivated by potential applications in information storage, spintronics, and multiple-state memories. Although over ten different compound families have been widely investigated as multiferroic ME materials, a high inherent coupling between multiferroic order parameters (especially above room temperature) has not yet been found in a single-phase compound, which hinders their applications. Research progress in single-phase multiferroic ME materials have been summarized and reviewed in a series of conference proceedings on ME interaction phenomena in crystals[4–7] and especially in recent review articles.[2,14,15] Accordingly, this review will not discuss single-phase multiferroic materials.

Alternatively and with greater design flexibility, multiferroic ME composites[16] made by combining piezoelectric and magnetic substances together have drawn significant interest in recent years due to their multifunctionality, in which the coupling interaction between piezoelectric and magnetic substances could produce a large ME response[17] (e.g., several orders of magnitude higher than that in those single-phase ME materials so far available) at room temperature. These ME composites provide opportunities for potential applications as multifunctional devices such as magnetic-electric transducers, actuators, and sensors.

The ME effect in composite materials is known as a product tensor property,[16,18] which results from the cross interaction between different orderings of the two phases in the composite. Neither the piezoelectric nor magnetic phase has the ME effect, but composites of these two phases have remarkable ME effect. Thus the ME effect is a result of the product of the magnetostrictive effect (magnetic/mechanical effect) in the magnetic phase and the piezoelectric effect (mechanical/electrical effect) in the piezoelectric one, namely,[17]

$$\mathrm{ME}_H \text{ effect} = \frac{\text{magnetic}}{\text{mechanical}} \times \frac{\text{mechanical}}{\text{electric}}, \tag{1a}$$

$$\mathrm{ME}_E \text{ effect} = \frac{\text{electric}}{\text{mechanical}} \times \frac{\text{mechanical}}{\text{magnetic}}. \tag{1b}$$

This is a coupled electrical and magnetic phenomenon via elastic interaction. That is, for the ME_H effect, when a magnetic field is applied to a composite, the magnetic phase changes its shape magnetostrictively. The strain is then passed along to the piezoelectric phase, resulting in an electric polarization. Thus, the ME effect in composites is extrinsic, depending on the composite microstructure and coupling interaction across magnetic-piezoelectric interfaces.

Due to technologically viable ME response observed in multiferroic ME composites above room temperature, various ME composites in different systems have been investigated in recent years, including (1) bulk ceramic ME composites of piezoelectric ceramics and ferrites (see, e.g., Refs. 19–46); (2) two-phase ME composites of magnetic alloys and piezoelectric materials (see, e.g., Refs. 47–68); (3) three-phase ME composites (see, e.g., Refs. 69–78); and (4) thin

films (nanostructured composites) of ferroelectric and magnetic oxides (see, e.g., Refs. 79–94). Using the concept of phase connectivity introduced by Newnham *et al.*,[18] we can describe the structures of a two-phase composite using the notations 0-3, 2-2, 1-3, etc., in which each number denotes the connectivity of the respective phase. For example, a 0-3–type particulate composite means one-phase particles (denoted by 0) embedded in the matrix of another phase (denoted by 3). So far, 0-3–, 3-3–, 2-2–, and 1-3–type structured multiferroic ME composites of ferroelectric and magnetic phases have been developed. Some prototype ME devices based on the ME composites have been proposed due their large ME effect at room temperature. In this article, we will give a comprehensive review on the major research topics and developments of multiferroic ME composites from bulk materials to thin films.

This review is divided into eight sections including the Introduction. Section II provides a literature review of prior work since van Suchtelen[16] originally proposed the concept of the product properties in 1972. Sections III–VI are devoted to the current status of fundamental knowledge and experiments of these four kinds of ME composites mentioned above. Applications as novel ME devices are discussed in Sec. VII. Section VIII highlights some of the key issues that need to be addressed in the future.

II. HISTORICAL PERSPECTIVE

van Suchtelen[16] proposed the concept of a product property in two-phase composite materials in 1972, arising from an elastic coupling between two phases of different properties. The ME effect in a composite material having one magnetostrictive and one piezoelectric phase is one such product tensor property, as described by Eqs. (1a) and (1b) above. In this case, the coupling is mechanical. If an input magnetic field is applied to this composite material, then

$$\frac{\partial S}{\partial H} = e^m \tag{2a}$$

for the magnetic phase, and

$$\frac{\partial P}{\partial S} = e \tag{2b}$$

for the piezoelectric phase; where S is the strain and e^m and e are, respectively, piezomagnetic and piezoelectric coefficients. As a result, this two-phase composite material can be characterized by

$$\frac{\partial P}{\partial H} = \alpha = k_c e^m e, \tag{2c}$$

where k_c is a coupling factor ($0 \leqslant |k_c| \leqslant 1$) between the two phases,[95] and α is the ME coefficient of the composite. Thus, a new property (i.e., nonzero ME coefficient α) appears in the composite consisting of magnetic and piezoelectric phases, since neither constituent phase is magnetoelectric. This new ME product response is due to elastic coupling between the two constituent phases. High piezomagnetic and piezoelectric coefficients and strong coupling (large k_c) favor a large ME coefficient.

Soon after the product ME property in the composite combining magnetostrictive and piezoelectric phases was proposed, scientists in Philips Laboratory experimentally found that a large ME effect could be produced in such composites.[19–22] They prepared ceramic composites of $BaTiO_3-CoFe_2O_4$ by unidirectional solidification of eutectic compositions in the quinary Fe–Co–Ti–Ba–O system, and obtained ME voltage coefficients as high as $\partial E/\partial H = 0.13$ V/cm Oe at room temperature. The magnetoelectric effect obtained in this way can reach about hundred times larger than that in single-phase multiferroic one. But unidirectional solidification is complex and requires critical control over composition and processing. At that time, ME composites did not attract attention, and the field of ME composite research went dormant for almost 20 years across the world. Then in the early 1990s, Newnham's group[23] and Russia scientists[24–26] prepared particulate ceramic composites of ferrites and $BaTiO_3$ or $Pb(ZrTi)O_3$ (PZT) by a conventional sintering processing. The sintered ceramic composites were much more easier and cost effective to fabricate in comparison to eutectic composites; and in additional provided the opportunity to combine phases with widely different crystal structures. However, these sintered ceramic composites had lower ME coefficients than the prior eutectic composites in Philips. Although experimental studies of these ME composites in the 1990s did not represent a great step forward, the experiments did inspire significant theoretical work on ME ceramic composites. A few models, such as Green's function approach[17,96] and various micromechanical approaches (see, e.g., Refs. 97–113), were developed to understand coupling between the two ferroic phases and to predict the resultant ME tensor responses in bulk ceramic composites. An upsurge in the multiferroic ME composite research appeared in the early 2000s. In the past few years, various ceramic composites with different connectivity schemes including 0–3–type particulate composites and 2-2–type laminate composites have been reported. The maximum ME coefficient in the 2-2–type laminate ceramic composites is several hundreds mV/cm Oe at room temperature.[31]

A milestone in the development of ME bulk composites was the appearance of ones containing the giant magnetostrictive rare-earth-iron alloy $Tb_{1-x}Dy_xFe_2$ (Terfenol-D) in 2001.[47–49,114] In 2001, by developing Green's function technique,[114,115] it was predicted that both particulate composites with Terfenol-D embedded in a piezoelectric polymer matrix such as poly(vinylidene fluoride-trifluorethylene) copolymer [P(VDF-TrFE)] or a piezoelectric ceramic matrix such as PZT, and laminate composites of Terfenol-D/P(VDF-TrFE) or Terfenol-D/PZT, could exhibit a giant ME (GME) effect. Subsequently, the laminate Terfenol-D/PZT (Refs. 47–49) and Terfenol-D/PVDF composites[116] have been experimentally found to exhibit such a GME effect. In particular, since 2003, Dong and co-workers[49–66] have reported various laminate composites of Terfenol-D and piezoelectric ceramics, and developed various prototype ME devices based on these bulk composites. The GME response (with a ME coefficient of >1 V/cm Oe) of such Terfenol-D based bulk composites made them particularly attractive for technological applications as ME devices.

Recently, in order to overcome brittleness and high eddy current loss of the Terfenol-D disks used in the two-phase Terfenol-D/piezoceramic composites, three-phase ME bulk composites of Terfenol-D/piezoceramics/polymer have been developed.[69,70] Various three-phase composites with different connectivity schemes (including quasi-0-3, 1-3, and 2-2 types) have been reported.[69–78] The maximum ME coefficient in these three-phase composites is 0.1 V/cm Oe orders at room temperature, and over 1 V/cm Oe at resonance.

Most recently, nanostructured composite thin films of magnetic and ferroelectric oxides have been developed. In 2004, Zheng *et al.*[79] reported a pioneering experiment on nanostructured films of the $BaTiO_3/CoFe_2O_4$ system with 1-3 or 2-2 connectivity schemes. In the last two years, a series of experimental[79–93] and theoretical work[117–121] on such multiferroic nanostructured films of ferroelectric and magnetic oxides has been reported. Such multiferroic nanostructures have become the topic of the day in the multiferroic composites field,[94] and they promise potential applications of ME composites in microelectronic devices.

III. BULK CERAMIC COMPOSITES

A. Theories of the ME composites

1. General description

As for piezoelectric composites,[18] the ME composites could have various connectivity schemes, but the common connectivity schemes are 0-3–type particulate composites of piezoelectric and magnetic oxide grains, 2-2–type laminate ceramic composites consisting of piezoelectric and magnetic oxide layers, and 1-3–type fiber composites with fibers of one phase embedded in the matrix of another phase, as shown in Fig. 1. $BaTiO_3$, PZT, $Pb(MgNb)O_3–PbTiO_3$, etc., are usually chosen as the piezoelectric ceramic phase, and ferrites usually as the magnetic phase.

The constitutive equation for describing coupling mechanical-electric-magnetic response in the ME composites to linear approximation can be written by direct notation for tensors as

$$\boldsymbol{\sigma} = \boldsymbol{c}\boldsymbol{S} - \boldsymbol{e}^T\boldsymbol{E} - \boldsymbol{q}^T\boldsymbol{H},$$

$$\boldsymbol{D} = \boldsymbol{e}\boldsymbol{S} + \boldsymbol{\varepsilon}\boldsymbol{E} + \boldsymbol{\alpha}\boldsymbol{H},$$

$$\boldsymbol{B} = \boldsymbol{q}\boldsymbol{S} + \boldsymbol{\alpha}^T\boldsymbol{E} + \boldsymbol{\mu}\boldsymbol{H}, \tag{3}$$

where $\boldsymbol{\sigma}$, $\boldsymbol{S}$, $\boldsymbol{D}$, $\boldsymbol{E}$, $\boldsymbol{B}$, and $\boldsymbol{H}$ are the stress, strain, electric displacement, electric field, magnetic induction, and magnetic field, respectively; $\boldsymbol{c}$, $\boldsymbol{\varepsilon}$, and $\boldsymbol{\mu}$ are, respectively, the stiffness, dielectric constant, and permeability; $\boldsymbol{e}$ and $\boldsymbol{q}$ are the piezoelectric and piezomagnetic coefficients, respectively; $\boldsymbol{\alpha}$ is the ME coefficient. The superscript T means the transpose of the tensor. The tensors $\boldsymbol{c}$, $\boldsymbol{e}$, $\boldsymbol{q}$, $\boldsymbol{\varepsilon}$, $\boldsymbol{\mu}$, and $\boldsymbol{\alpha}$ are (6×6), (3×6), (3×6), (3×3), (3×3), and (3×3) matrices, respectively, by means of the compressive representation. For the piezoelectric phase (e.g., $BaTiO_3$ and PZT) in the composites, $\boldsymbol{q}=0$ and $\boldsymbol{\alpha}=0$; and for the magnetic phase (e.g., Co ferrites and Ni ferrites) in the composites, $\boldsymbol{e}=0$ and $\boldsymbol{\alpha}=0$. But for their composites, the effective ME coefficient $\boldsymbol{\alpha}^* \neq 0$, which depends on details of the composite microstructures, i.e., component phase properties, volume fraction, grain shape, phase connectivity, etc.

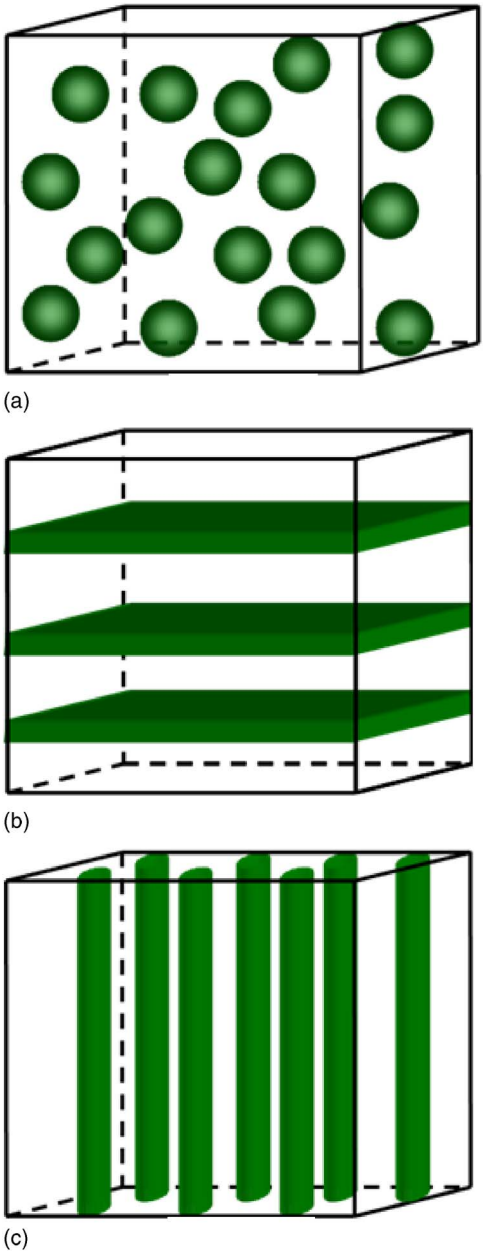

FIG. 1. (Color online) Schematic illustration of three bulk composites with the three common connectivity schemes: (a) 0–3 particulate composite, (b) 2–2 laminate composite, and (c) 1–3 fiber/rod composite.

The first analysis for the ME effect in such bulk ceramic composites was performed by Harshe *et al.*[23] They assumed a relatively simple cube model, in which the 0-3 particulate composites were considered as consisting of small cubes, and then solved the fields in one cube for which the boundary value problem involved is tractable. This simple cube model is an elementary single-grain model. While conceptually straightforward and providing physical insight, this simple model cannot be generalized to other phase topologies. More rigorous treatments of the ME behavior of the composites were performed by using a physically based, Green's function technique (multiple-scattering approach)[17,96] and micromechanics models.[97–113]

2. Modeling of particulate ceramic composites

Green's function technique[17,96] was developed for solving the constitutive Eq. (3) above for the ME composites, and derived the effective properties of the composites, defined as usual in terms of averaged fields. All effective properties of the composites can be got by this approach. Among the effective ME coefficient tensor $\boldsymbol{\alpha}^*$ of the composites was obtained as

$$\alpha^* = \langle (\boldsymbol{e}^* - \boldsymbol{e})\boldsymbol{T}^{13}\rangle \langle \boldsymbol{T}^{33}\rangle^{-1} = \langle (\boldsymbol{q}^* - \boldsymbol{q})\boldsymbol{T}^{12}\rangle \langle \boldsymbol{T}^{22}\rangle^{-1}, \tag{4}$$

where angular brackets denote the microstructural average; $\boldsymbol{e}^*$ and $\boldsymbol{q}^*$ are, respectively, the effective piezoelectric and piezomagnetic coefficients of the composites. $\boldsymbol{T}^{ij}$ are so-called *t*-matrix tensors.[17] The theory developed is formally straightforward and is universal.

As an example, firstly consider a 1-3–type composite (Fig. 1) with piezoelectric (or magnetic) rods aligned in a magnetic (or piezoelectric) matrix. Let the piezoelectric phase be poled along x_3 axis of the composite. Thus the composite has a ∞mm symmetry with ∞ denoting the x_3 axis. The magnetic field is also along the symmetric x_3 axis. In the limit case that the aspect ratio p of the rods approaches infinite, Eq. (4) gives the following simple expression for the ME coefficient along the symmetric x_3 axis:

$$\alpha_{33}^* = -f\frac{e_{31}^* q_{31}}{{}^m k + m^o} = -(1-f)\frac{q_{31}^* e_{31}}{{}^p k + m^o}, \tag{5}$$

where f is the volume fraction of the magnetic phase; $k = (c_{11}+c_{12})/2$ and $m=(c_{11}-c_{12})/2$ are, respectively, transverse in-plane bulk modulus and transverse shear modulus (the superscripts m and p denoting the magnetic and piezoelectric phases; the superscript o denoting a homogeneous reference medium); q_{31} and e_{31} are, respectively, piezomagnetic and piezoelectric coefficients. Different approximations pertain and can be easily obtained from the general solution [Eq. (5)], depending on the choice made for m^0 of the homogeneous reference medium. An intuitive and common choice is to take the host matrix phase as the reference medium. In essence it is a non-self-consistent approximation (NSCA) which is generally valid for matrix-based composites such as a 0-3–type particulate microstructure. Naturally, for the choice $m^0=m^*$, i.e., the constituent phases are embedded into an effective medium with yet unknown m^*, a self-consistent effective medium approximation (SCA) is captured.[96]

For a 1-3–type composite with piezoelectric rods aligned in the magnetic matrix (denoting as 1-3 p/m), the NSCA of Eq. (5) gives

$$\alpha_{33}^* = -\frac{f(1-f)q_{31}e_{31}}{{}^m k + {}^m m + f({}^p k - {}^m k)}. \tag{6a}$$

Inversely, for a 1-3–type composite with magnetic rods aligned in the piezoelectric matrix (denoting as 1-3 m/p), the NSCA of Eq. (5) becomes

$$\alpha_{33}^* = -\frac{f(1-f)q_{31}e_{31}}{{}^m k + {}^p m + f({}^p k - {}^m k)}. \tag{6b}$$

For these two kinds 1-3 microstructures, the SCA of Eq. (5) gives

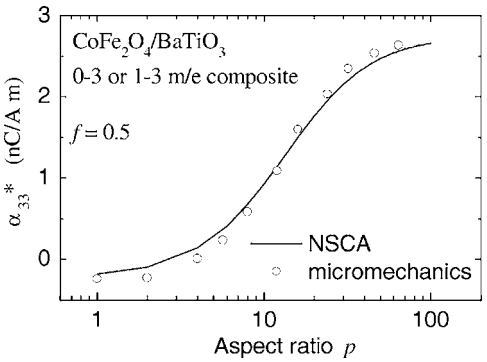

FIG. 2. Comparison of calculated α_{33}^* for 0–3 or 1–3 m/p $CoFe_2O_4/BaTiO_3$ ceramic composites ($BaTiO_3$ being as the matrix phase) by the micromechanical approximation and NSCA [Nan (Ref. 122)].

$$\alpha_{33}^* = -\frac{f(1-f)q_{31}e_{31}}{{}^m k + m^* + f({}^p k - {}^m k)}. \tag{7}$$

Similarly, the constitutive equation [Eq. (3)] for the ME composites can also be solved by using micromechanics methods. Among them, Li[101–105] and Huang[106–108] gave more details about these micromechanics simulations. The micromechanics models are also formally straightforward and universal. It has been already known that micromechanics methods give almost the same approximations as the NSCA from Green's function technique. Figure 2 shows such a comparison between two approaches.[122]

For the extreme case of a 1-3 fiber composites with infinite aspect ratio, Benveniste[97] and Chen[99] proposed a set of relationships between the effective properties including the effective ME coefficients by generalizing Hill's method[123] for the purely elastic case of such a fiber composite. They paid attention to the internal consistency of the solutions for the constitutive coefficient tensors. All these physically based technique and micromechanics models were further expanded by including pyroelectric and pyromagnetic effects.[96,97]

Although it is hard to get such simple expressions for $\boldsymbol{\alpha}^*$ from the general solution [Eq. (4)] for other connectivity schemes, the general expression [Eq. (4)] is easily programmed for numerical calculations of $\boldsymbol{\alpha}^*$ of the composites. Figure 3 further shows a numerical example for the ME response of the 0-3 or 1-3 m/p $CoFe_2O_4/BaTiO_3$ ceramic composites. Here the ME voltage coefficient α_{E33}, describing the ME_H output voltage (on open circuit condition) developed cross the composites along the x_3-axis, is used, i.e.,

$$\alpha_{E33} = \alpha_{33}^*/\varepsilon_{33}^* (= E_3/H_3), \tag{8}$$

which is the figure of merit used to assess the performance of a ME material for a magnetic device. A few points can be drawn from Fig. 3, i.e., (1) the simple cube model[23] overestimates the ME effect of the composites [Fig. 3(a)]; (2) NSCA and SCA predict similar results for this system [Figs. 3(a) and 3(b)]; (3) for 0-3 particulate ceramic composites, the ME voltage coefficient α_{E33} reaches a maximum in the middle concentration region around $f \sim 0.6$, but for 1-3 composites the maximum α_{E33} appear at $f \sim 0.9$. Thus remarkable ME effect could be achieved in the composites with

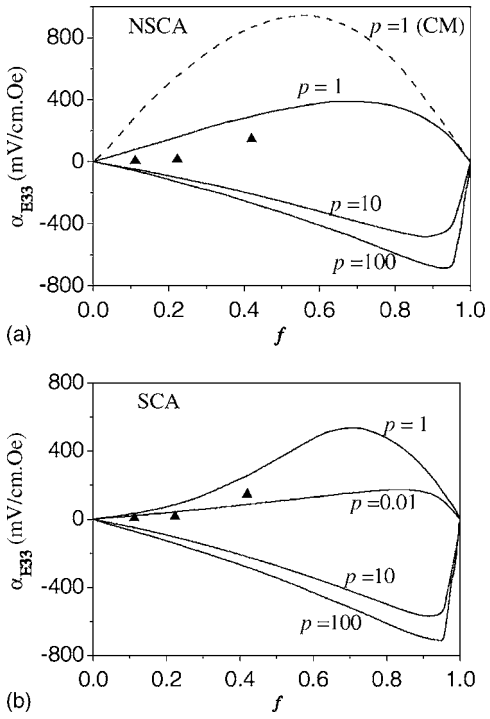

FIG. 3. Calculated α_{E33} for 0–3 or 1–3 m/p $CoFe_2O_4/BaTiO_3$ ceramic composites ($BaTiO_3$ being as the matrix phase). The results from the simple cube model (CM) and three experimental data are also shown for comparison [Nan (Ref. 17)].

high concentration of particulate magnetic phase well dispersed in the piezoelectric phase (see Fig. 4).

It is obvious that the grain shape and phase connectivity have a significant effect on the ME response of the composites. Let us still consider the case as above that the piezoelectric phase is poled along x_3 axis and the magnetic field is also along the symmetric x_3 axis. Figure 5 shows such an example. From 1-3 to 0-3, α_{E33} of this composite system changes its sign around $p=3$. Due to strong anisotropy, the 1-3 structure has maximum α_{E33} along the symmetric x_3 axis, but the present case (i.e., both the magnetic field and electrical poling being along the symmetric x_3 axis) is not optimal one for the 2-2 structure. For example, if the magnetic field and/or electrical poling are perpendicular to the symmetric axis, then we can get more larger ME effect in the 2-2 structure (i.e., α_{E31} or $\alpha_{E11} > \alpha_{E33}$), as shown by Getman[98] who also gave the same results for the extreme 1-3 ($p \to \infty$) and 2-2 ($p \to 0$) composites in 1994. Getman gave explicit expressions for the ME coefficients in the two extreme cases, and especially for the 2-2 ($p \to 0$) composite with the magnetic and electrical polings perpendicular to the symmetric axis, the calculated α_{E11} can reach over 1 V/cm Oe, which is higher than that calculated for the 0-3 particulate ceramic composites.

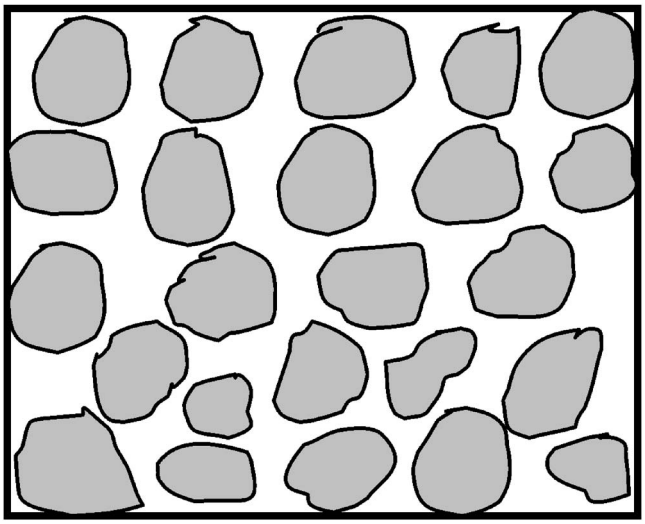

FIG. 4. Schematic illustration of a 0–3 particulate ceramic composite with high concentration of particulate magnetic phase well dispersed in the piezoelectric phase.

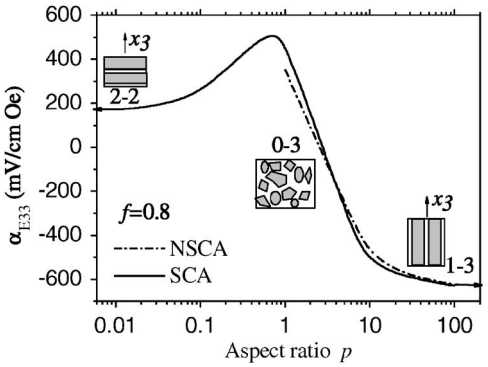

FIG. 5. Effect of the grain shape and phase connectivity on the ME response of m/p $CoFe_2O_4$ (denoted by gray areas; volume fraction $f=0.8$)/$BaTiO_3$ (denoted by white areas) ceramic composites [After Nan (Ref. 17)].

Although the calculations above focus on m/p ferrites/piezoelectric ceramic composites with the piezoelectric phase as the matrix, not high enough resistivity of the ferrite phase would make it hard to obtain high ME response in the 1-3 composites and 0-3 particulate composites with high concentration of ferrite grains (i.e., large f) as expected, due to their large leakage. In comparison, the 2-2 laminate ceramic composites have no such limitation along x_3 because the ferrite layers are separated by the piezoelectric layers. On the other hand, it is easy to prepare the 2-2 laminate ceramic composites in experimental, while such 1-3 ceramic composites are very hard to be prepared. Thus, next we discuss more about modeling of the 2-2 laminate ceramic composites.

3. Modeling of laminate ceramic composites

Static ME effects. Consider a simple bilayered composite of piezoelectric and magnetic ceramic phases with free boundary (Fig. 6). The polarization direction coincides with the axis x_3. For such a simple bilayer structure, the boundary value problem involved is tractable.[98,124] Thus the constitutive equation [Eq. (3)] can be directly solved by an averaging method to estimate effective material parameters.[124–126] For example, when a magnetic field is applied along x_3 (i.e., out-of-plane mode), then the longitudinal ME coefficient is given as[124]

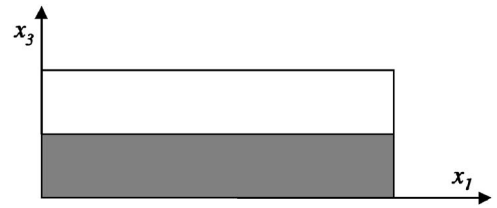

FIG. 6. A simple bilayer composite of piezoelectric and magnetostrictive layers.

$$\alpha_{E33} = \frac{E_3}{H_3} = \frac{2f(1-f)d_{31}q_{31}\mu_0\bar{s}}{(2fd_{31}^2 - {}^p\varepsilon_{33}\bar{s})[\bar{\mu}\bar{s} + 2q_{31}^2(1-f)^2]} \tag{9}$$

with $\bar{s}=f({}^ps_{11}+{}^ps_{12})+(1-f)({}^ms_{11}+{}^ms_{12})$ and $\bar{\mu}=f\mu_0+(1-f){}^m\mu_{33}$, where s_{ij} are compliances; d_{33} is the d-type piezoelectric coefficient; q_{ij} are the piezomagnetic coefficients; μ_0 and ${}^m\mu_{33}$ are, respectively, the permeabilities of the free space and magnetic phase. When the magnetic field is applied along x_1 (i.e., in-plane mode), then the transverse ME coefficient is given as[124]

$$\alpha_{E31} = \frac{E_3}{H_1} = \frac{-f(1-f)(q_{11}+q_{21})d_{31}}{{}^p\varepsilon_{33}\bar{s} - 2fd_{31}^2}. \tag{10}$$

From Eqs. (9) and (10), one can easily calculate the effective ME coefficients of the 2-2 laminate composites.

Figure 7 shows variation of the ME coefficients with the volume fraction f of the magnetic phase in the 2-2 laminate $CoFe_2O_4-BaTiO_3$ ceramic composites. These calculated results are similar to those shown above. For the out-of-plane field mode, a maximum ME coupling appears around $f=0.4$. For the transverse field mode, this maximum shifts to a bit higher f, and the transverse ME coefficient is larger than the longitudinal ME coefficient, which indicates a stronger transverse coupling than the longitudinal case in such 2-2 laminate composites.

In all above simulations, a perfect interface between the magnetic and piezoelectric phases was assumed. This is an ideal case. For such laminate composites, Bichurin *et al.*[125] developed a generalized effective medium method for calculating the composite ME effect by introducing an interface coupling parameter k for characterizing actual bonding conditions at the interface, i.e., $k=({}^pS_i-{}^pS_{i0})/({}^mS_i-{}^pS_{i0})$ $(i=1,2)$, where ${}^pS_{i0}$ is a strain tensor component without frictions between layers.[21] It depends on interface quality and is a measure of differential deformation between piezoelectric and magnetic layers. $k=1$ for an ideal interface and $k=0$ for the case without frictions. In this case, the ME coefficients of the laminate composites can be obtained as[125]

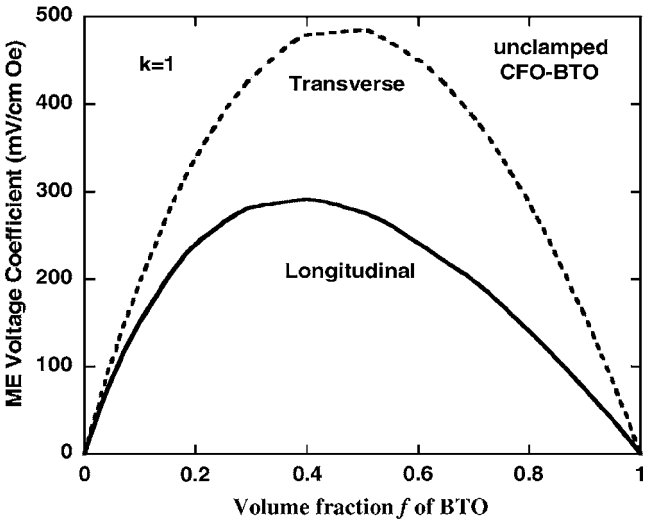

FIG. 7. Transverse and longitudinal ME voltage coefficients for a perfectly bonded 2–2 structure of $CoFe_2O_4/BaTiO_3$ [Bichurin *et al.* (Ref. 125)].

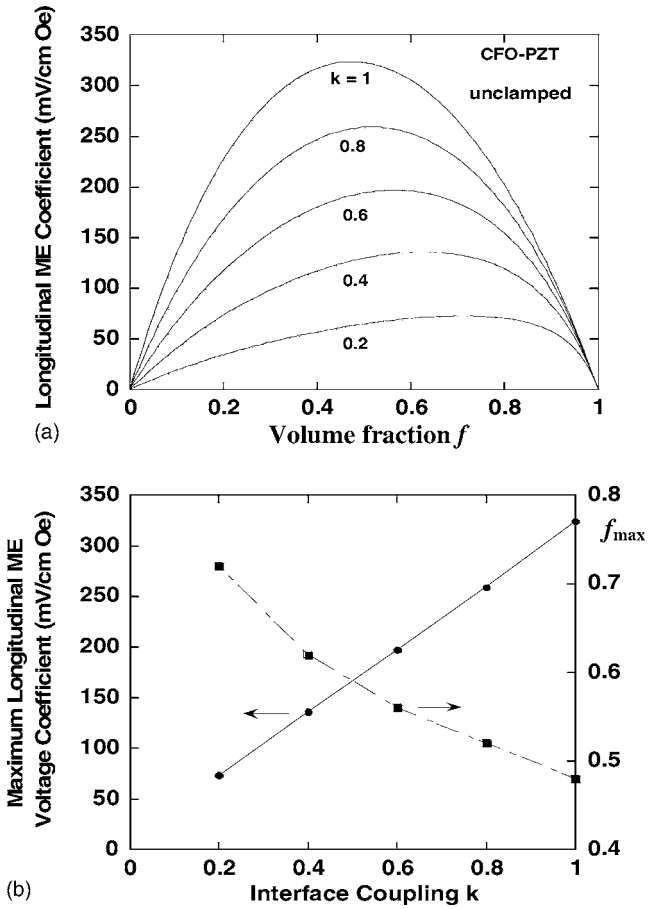

FIG. 8. (a) Estimated dependence of longitudinal ME voltage coefficient on interface coupling k and volume fraction f for $CoFe_2O_4$-PZT bilayer. (b) Variation with k of maximum α_{E33} and the corresponding f_{max} [Bichurin *et al.* (Ref. 125)].

$$\alpha_{E33} = \frac{E_3}{H_3} = \frac{2kf(1-f)d_{31}q_{31}\mu_0\underline{s}}{(2fd_{31}^2 - {}^p\varepsilon_{33}\underline{s})[\bar{\mu}\underline{s} + 2kq_{31}^2(1-f)^2]}, \tag{11}$$

$$\alpha_{E31} = \frac{E_3}{H_1} = \frac{-kf(1-f)(q_{11}+q_{21})d_{31}}{{}^p\varepsilon_{33}\underline{s} - 2kfd_{31}^2}, \tag{12}$$

with $\underline{s}=f({}^ps_{11}+{}^ps_{12})+k(1-f)({}^ms_{11}+{}^ms_{12})$. Obviously, as $k=1$, these two expressions reduce to Eqs. (9) and (10); as $k=0$, the ME effect disappears due to no mechanical coupling between completely unbonded two layers. Any other k values correspond to actual interfaces, and the ME coefficients are between those values for the two extreme cases of $k=0$ and 1. Figure 8 shows an example calculated from the laminate 2-2 composite of PZT and $CoFe_2O_4$ with different k values. Equations (11) and (12) can well fit experiments by choosing k values or facilitate characterization of the interface bonding

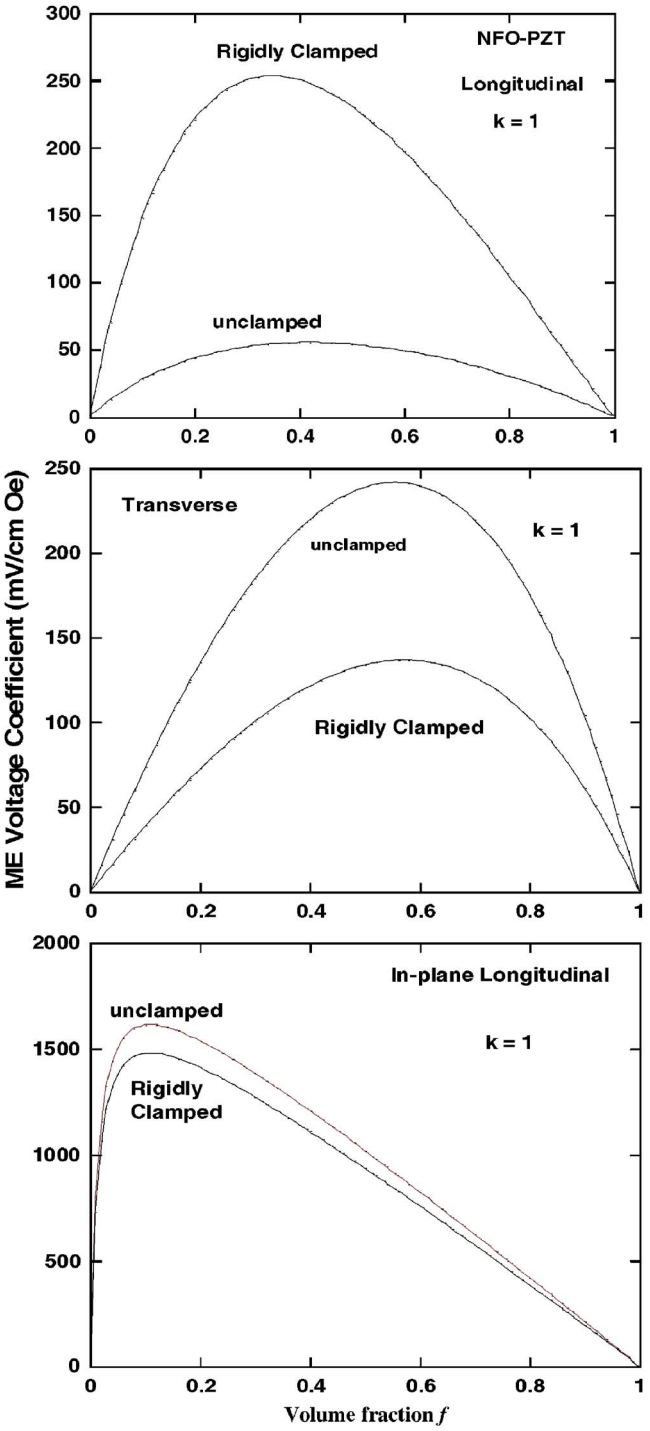

FIG. 9. (Color online) Comparison between f-dependence of the longitudinal, transverse, and in-plane longitudinal ME voltage coefficients for unclamped and rigidly clamped nickel ferrite ($NiFe_2O_4$)-PZT bilayer with $k=1$ [Bichurin *et al.* (Ref. 125)].

status by determining k from the measured ME coefficients.

In these longitudinal and transverse modes, the laminate composite is poled along x_3 and measured in the same x_3 direction. If the composite could be poled with an in-plane electric field (i.e., along x_1) and measured in the same x_1 direction, an in-plane magnetic field would induce a large in-plane longitudinal ME coefficient[125] due to the absence of demagnetization fields and enhanced piezoelectric and piezomagnetic coefficients in this case, as shown in Fig. 9. The maximum ME effect appears at a high f value. This in-plane longitudinal mode in the 2-2 laminate composites is somewhat like the longitudinal mode in the 1-3 fiber composites.

Furthermore, the modeling above for free boundary condition can be generalized to consider the clamped composites.[125] For example, consider the composite be clamped in the x_3 direction. Then the in-plane stresses of the composite $T_1=T_2=0$ (i.e., still free in plane) but the out-of-plane stress $T_3\neq 0$ ($T_3\rightarrow\infty$ for the rigidly clamped case). A significant change in the ME coupling can be expected when the bilayer is subjected to a uniform out-of-plane stress, as shown in Fig. 9. This x_3-clamping, in general, leads to a large increase in α_{E33}. But for the transverse mode, this clamping leads to a substantial reduction in α_{E31} in comparison to the unclamped case. The clamping induced changes in the in-plane longitudinal ME coupling are quite weak compared to the longitudinal or transverse cases.

Enhanced ME effects at resonance. Bichurin *et al.* first developed a theory for the ME effect at electromechanical, ferromagnetic, and magnetoacoustic resonances in the composites.[112,126–131] As the ME effect in the composites is due to mechanical coupling between the piezoelectric and magnetic phases, the ME effect would be greatly enhanced when the piezoelectric or magnetic phase undergoes resonance,[127–131] i.e., electromechanical resonance (EMR) for the piezoelectric phase and ferromagnetic resonance (FMR) for the magnetic phase. Mechanical oscillations of a medium are induced either by alternating magnetic or electric fields, and the wave length is tens of meters and much larger than the composite sizes. Thus it is possible to neglect space changing of the electric and magnetic fields within the sample volume. In order to describe frequency-dependent ME effect, the equations of elastodynamics are needed in addition to the constitutive equations [Eq. (3)]. The equations of elastic dynamics are

$$\rho\frac{\partial^2 u_i}{\partial t^2}=\frac{\partial T_{ij}}{\partial x_j}, \tag{13}$$

where u_i is ith projection of the displacement vector, T_{ij} still denote stress tensors which connect with the strain, electric, and magnetic fields by Eq. (3). The joint solutions of Eqs. (3) and (13) under boundary conditions yield the frequency-dependent ME coefficients.

Solution of Eq. (13) depends on the shape of the sample and orientations of the electric and magnetic fields. Solutions for the composites with different shapes can be ready got. For example, consider a rectangular bilayer shown in Fig. 6 with thickness t, width w, and length L. $L\gg t$ and w. The polarization is still along x_3. Under their boundary conditions, by expressing stress components through strain components and substituting in Eq. (13), we can get the displacement u_x, as[129]

$$u_x(x)=\frac{1}{k}\left\{\left[\frac{\cos(kL)-1}{\sin(kL)}\right]\cos(kx)+\sin(kx)\right\}(d_{31}E_3+q_{31}H_3), \tag{14}$$

where $k=\omega\,(\rho s_{11})^{1/2}$; ω is the angular frequency; ρ, s_{11}, d_{31}, and q_{31} are, respectively, the effective density, compliance,

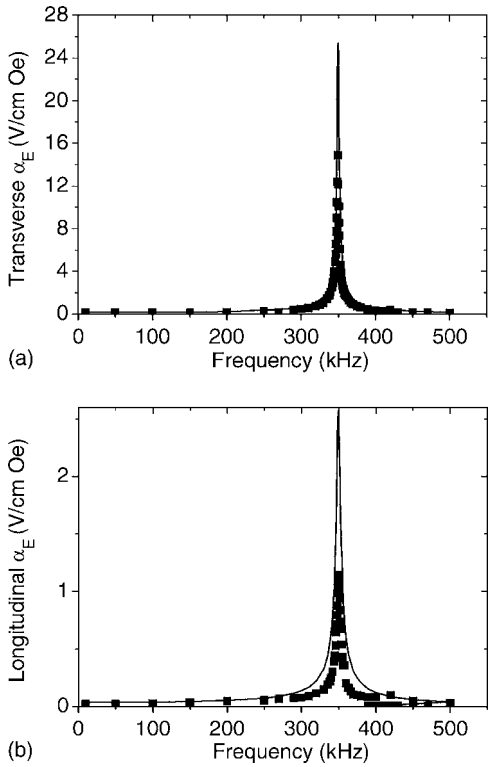

FIG. 10. EMR frequency dependence of the transverse and longitudinal ME voltage coefficients of $CoFe_2O_4$-PZT bilayer [Bichurin *et al.* (Ref. 129)].

and piezoelectric and piezomagnetic coefficients of the composite. Replacement of q_{31} with q_{11} gives the expression for the case of the transverse orientation of fields. Further by using the open circuit condition, i.e., $\int_w dy \int_L D_3 dx = 0$, one can work out the induce voltage E_3 in the composite. Using the definition of ME coefficient as $E_3 = \alpha_{E,L} H_3$ $(=\alpha_{E33} H_3)$ at longitudinal and $E_3 = \alpha_{E,T} H_1$ $(=\alpha_{E31} H_1)$ at transverse orientation, we obtain the dynamic ME coefficients as[129]

$$\alpha_{E,L} = \frac{d_{31} q_{31} N - \alpha_{33} s_{11}}{\varepsilon_{33} s_{11} - d_{31}^2 N}, \tag{15a}$$

$$\alpha_{E,T} = \frac{d_{31} q_{11} N - \alpha_{31} s_{11}}{\varepsilon_{33} s_{11} - d_{31}^2 N}, \tag{15b}$$

with $N = 1 - (2/kL)\tan(kL/2)$. Here all the property parameters denote the effective ones for the composite. As seen from Eqs. (15a) and (15b) at a so-called frequency of an antiresonance where $\varepsilon_{33} s_{11} - N d_{31}^2 = 0$, the ME coefficients sharply grow. This antiresonance frequency is dependent on the effective parameters of the composite and its geometrical sizes. For example, for a bilayer of spinel ferrites and PZT with L of about centimeter, this resonance frequency is around 300 kHz.

For illustration, Fig. 10 shows an example for the laminate PZT-$CoFe_2O_4$ composite rectangular plate with a length of 7.3 mm and width of 2.15 mm. At the frequency of about 300 kHz, the resonance-induced enhancement in the ME effects is observed. The maximal value of the ME coefficient is observed at the transverse orientation of fields, and the resonant value of the ME coefficient is almost ten times higher than its longitudinal orientation value.

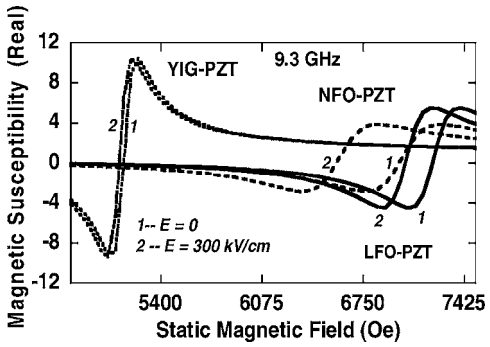

FIG. 11. Theoretical static magnetic field H dependence of the magnetic susceptibility for the bilayers of lithium ferrite (LFO)-PZT, nickel ferrite (NFO)-PZT, and yttrium iron garnet (YIG)-PZT. The susceptibilities at 9.3 GHz are for H and E perpendicular to sample plane and for electric fields of (1) $E=0$ and (2) $E=300$ kV/cm. Notice the downshift in the resonance field when E is increased from 0 to 300 kV/cm [Bichurin *et al.* (Ref. 127)].

The second resonance phenomenon is the FMR. At the FMR, spin-lattice coupling and spin waves that couple energy to phonons through relaxation processes are also expected to enhance the ME interactions. An electric field produces a mechanical deformation in the piezoelectric phase, resulting in a shift in the resonance field for the magnetic phase. Figure 11 shows the estimated resonance profiles with and without electric fields for bilayers of nickel ferrite/PZT, lithium ferrite/PZT, and yttrium iron garnet (YIG)/PZT. The calculations predict a large resonance field shift for the $NiFe_2O_4$ (NFO)/PZT bilayer, and a small shift for the YIG/PZT bilayer.[127]

The third resonance phenomenon of importance is the ME interactions at the coincidence of the FMR and EMR, i.e., at the magnetoacoustic resonance (MAR).[112] Figure 12 provides theoretical estimates on the variation of the ME voltage coefficient α_E with frequency of the ac magnetic field applied to a bilayer of NFO/PZT. The thickness of NFO and PZT layers are 100 and 200 nm, respectively. In Fig. 12(a), the bias field H_0 is smaller than the field H_r for FMR in NFO. The peaks in α_E occur at the fundamental and second harmonic of the EMR for the thickness modes of the bilayer. In Fig. 12(b), H_0 is selected so that FMR in NFO coincides with the fundamental EMR mode, resulting in the enhancement in α_E at the MAR. In Fig. 12(c), the second harmonic of acoustic modes in NFO-PZT coincides with FMR. Thus one observes a dramatic increase in α_E at MAR.

The modeling provides significant implications, e.g., (1) coincidence of the FMR and EMR allows energy transfer between phonons, spin waves, and electric and magnetic fields, and, for example, this energy transfer is found to be very efficient in the ferrite-PZT bilayer; (2) ultrahigh ME coefficients are expected at MAR. This effect is important for miniature/nanosensors and transducers at microwave frequencies.

B. Experiments of bulk ceramic composites

In the past decades, various ceramic composites consisting of piezoelectric and magnetic oxide ceramics have been investigated in experimental, mainly including 0–3 particu-

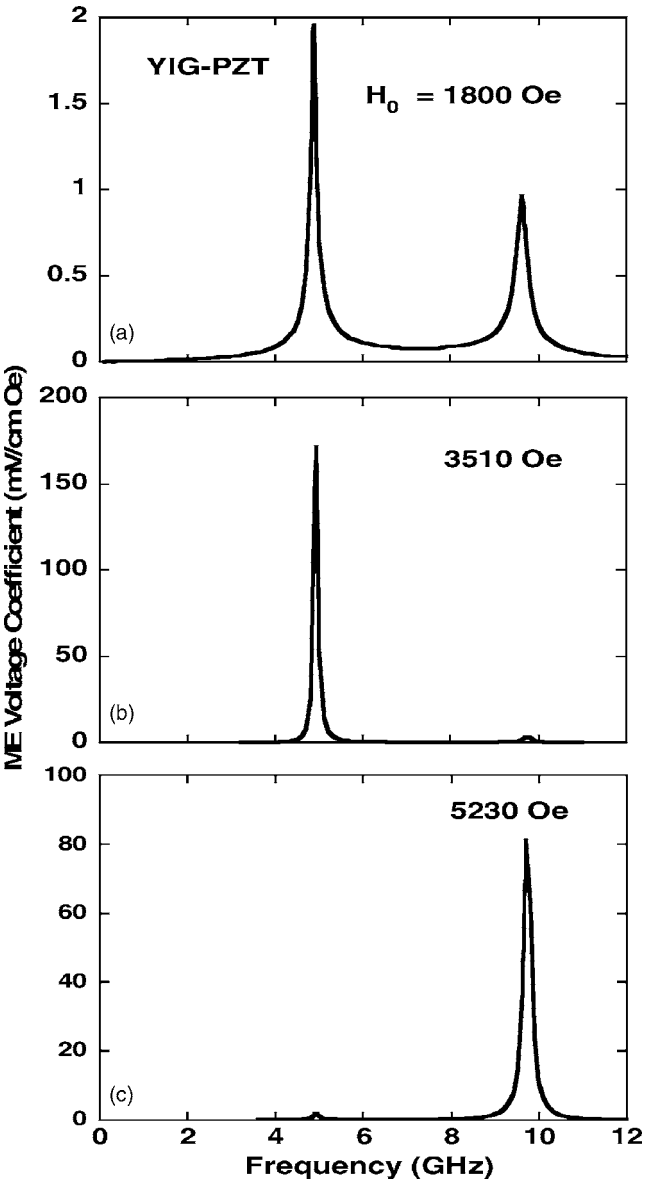

FIG. 12. Theoretical estimates on the variation of ME voltage coefficient α_E with the frequency of ac magnetic field for a bilayer of NFO-PZT. (a) The peaks in α_E occur at the fundamental and second harmonic in EMR for thickness modes for the bilayer; (b) the ME coupling at the coincidence of EMR and FMR, and MAR; (c) similar results as in (b), but for MAR at the second harmonic of acoustic modes [Bichurin *et al.* (Ref. 112)].

late and 2–2 laminate ceramic composites (Fig. 1) in the various systems (see Table I) of $BaTiO_3$ based ferroelectric ceramics and ferrites (or doped ferrites), PZT and ferrites (or doped ferrites), $(SrBa)Nb_2O_5$ (Refs. 43, 132, and 133) and ferrites, and so on. Among them, the particulate ceramic composites are most easily prepared via conventional sintering technique. The powders of piezoelectric ceramics and magnetic oxides (e.g., ferrites) are mixed firstly together, and then the mixed powders are pressed into green bulks followed by sintering at high temperature.

TABLE I. Various constituent phases used for ME ceramic composites.

Piezoelelctric phase	Magnetic phase
$BaTiO_3$ (BTO)	Ni ferrites (e.g., NFO)
PZT	Co ferrites (e.g., CFO)
$Pb(Mg,Nb)O_3$ (PMN)	Li ferrites (LFO)
$PbTiO_3$ (PTO)	Cu ferrite, Mn ferrite
$(Sr,Ba)Nb_2O_5$	Ytttrium iron garnet (YIG)
	$(La,M)MnO_3$ (M=Ca,Sr)

1. Particulate ceramic composites

The original work on *in situ* formation of the ME ceramic composites was done at Philips Laboratories,[19–22] which were prepared by unidirectional solidification of a eutectic composition of the quinary system Fe–Co–Ti–Ba–O. Unidirectional solidification helps in the decomposition of the eutectic liquid into alternate layers of a piezoelectric perovskite phase and a piezomagnetic spinel phase. Their results showed that excess of TiO_2 (1.5 wt %) gives a high ME voltage coefficient α_E=50 mV/cm Oe. However, other compositions showed a lower α_E of about 1–4 mV/cm Oe. In a subsequent work, a high ME coefficient of 130 mV/cm Oe was obtained in a eutectic composition of $BaTiO_3$–$CoFe_2O_4$ by unidirectional solidification. Unidirectional solidification requires critical control over the composition, especially when one of the components is a gas (oxygen). Directional solidifications, such as a Bridgman technique or floating zone method using single ellipsoid furnace, are complex involving tight control over the composition, cooling rate, and temperature.

In comparison, sintering processing is much easier and cheaper for fabrication of ME composite ceramics of piezoelectric ceramic phase and ferrites. The sintered composites exhibit several advantages such as freedoms in the selection of constituent phases, their starting particle sizes, processing parameters. Furthermore, sintering does not require the presence of eutectic or eutectoid transformations and also provides the opportunity to combine phases with widely different crystal structures.

A few groups, for example, from USA,[23] Russia,[25,26] and India,[27] started the preparation of these particulate composite ceramics of BTO or PZT and ferrites via conventional sintering processing in early 1990s. However, the ME coefficients of these particulate composite ceramics were small and around 1 mV/cm Oe orders of magnitude.[23,27,29,30,134–142] Until 2000s, by carefully controlling the sintering processing and composition, higher ME coefficients of about 10–100 mV/cm Oe have been obtained. For example, Ryu *et al.*[28] investigated the effect of the sintering temperature on the sintering behaviors, microstructures, and ME properties of particulate composites of PZT and Ni-ferrite doped. It was found that the sintering temperature has a significant effect on the ME coefficient. Figure 13 shows the maximum ME voltage coefficient of various compositions as a function of sintering temperature. A high ME voltage coefficient of 115 mV/cm Oe at 1 kHz was reported for the 0–3 particulate NFO/PZT composites. This high ME coefficient was attributed to a homogeneous and well-dispersed microstructure, and large grain size of the matrix PZT phase.

The low-frequency ME coefficients of the sintered 0–3 composite ceramics vary from about 10 to 100 mV/cm Oe in the literature,[25,26,28,39,40,132,133,143,144] depending on compo-

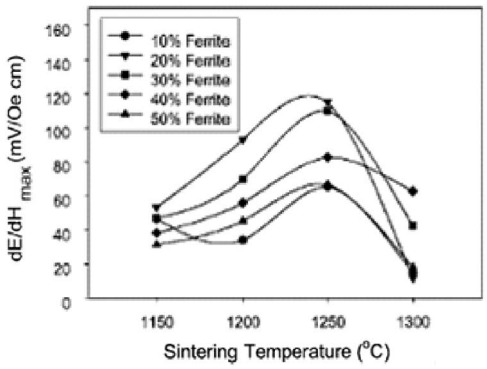

FIG. 13. The maximum ME voltage coefficient of NFO-PZT ceramic composites with various compositions as a function of sintering temperature [Ryu *et al.* (Ref. 28)].

sitions, powders used, and processing. Their ME coefficients can reach up to V/cm Oe orders of magnitude at resonance. So far, these measured values of the ME coefficients are lower than theoretically predicted coefficients. In spite of the promising high ME coefficients in such simple 0–3 particulate composite ceramics, it is difficult to achieve the predicted ones in experimental, which is due mainly to interdiffusion and/or chemical reactions between the piezoelectric and ferrite phases during high-temperature sintering and to thermal expansion mismatch between two phases. The application of high sintering temperature in conventional sintering processes yields the formation of unwanted phases by chemical reaction (for example, undesired phases such as $BaFe_{12}O_{19}$, $BaCo_6Ti_6O_{19}$, or hexagonal $BaTiO_3$ could appear in the case of $BaTiO_3/CoFe_2O_4$ composites) and the interphase diffusion of the constitutional atoms, though difficult to verify, lowers the local eutectic point around the boundary region thus to facilitates the formation of high concentration of defects and liquid phases. These would deteriorate the piezoelectricity and/or magnetostriction of constituent phases and the strain transfer between two phases. Large thermal expansion mismatch between the piezoelectric and ferrite phases harms the densification and leads to the formation of microcracks.

On the other hand, the theories predict that high ME response appears in the 0–3 particulate composite ceramics with high concentration (e.g., $f>0.5$) of ferrites (see Fig. 3). However, the percolation of high concentration of the randomly dispersed ferrite phase with low resistivity makes the electric poling of the composites become difficult and the ME properties are reduced because of leakage problem. Therefore, good dispersion of the low-resistance ferrite particles in the piezoelectric matrix is required in order to suppress percolation. Besides, the porosity would influence the ME effect of bulk composite ceramics. For example, the results[143] show a 60%–70% decrease in the low-frequency ME effect and 96% decrease in the ME effect at EMR, as the porosity increases from 5% to 40%.

Recently, in order to achieve sufficient bulk density while avoid possible reactions between the constituent phases to occur, hot pressing[145] and spark plasma sintering[146] (SPS) techniques have been employed to replace the conventional sintering. Hot-pressed and SPS samples exhibited a

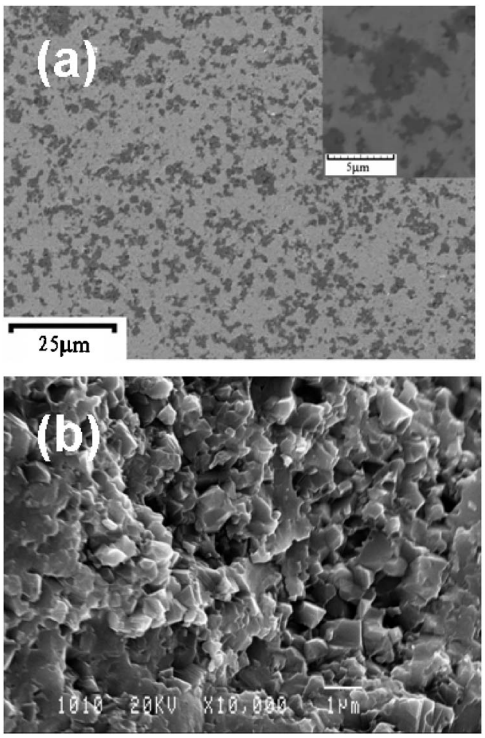

FIG. 14. Scanning electron microscopy (SEM) images of (a) polished surface and (b) fractured surface of the NFO-PZT composite ceramics via SPS [Jiang *et al.* (Ref. 146)].

large improvement in the ME voltage coefficient, as compared to the conventionally sintered samples. Especially, SPS is an efficient sintering method that allows rapid consolidation (e.g., 5 min) at comparatively low temperatures,[147] although the underlying mechanisms for an enhanced mass transport within a limited period of time still remain to be understood. By the dynamic features this SPS method was considered to be feasible for the fabrication of the ME ceramic composites with high density (e.g., as high as 99% of theoretical density[146]) and purity. The short time and low temperature required for densification during SPS process diminish the possibility for unwanted reaction to occur. For example, dense composite NFO-PZT ceramics with relative density of 99% have recently been prepared by SPS consolidation of mechanically mixed powder mixtures.[146] The composite ceramics via SPS exhibit fine microstructure (see, e.g., Fig. 14), and the SPS condition has an essential influence on the ME properties. In comparison to the conventional sintering, SPS leads to an obvious improvement in the ME voltage coefficient, as shown in Fig. 15, though the grain size in the ceramics via SPS is much smaller than that via conventional sintering.

In the composite ceramics synthesized by directly mechanical mixing of the two-phase powders, the randomly mixed ferrite particles have low percolation threshold. In order to achieve good dispersion (see Fig. 4) of a high concentration of ferrite particles in the composite ceramics, wet-chemical processing (e.g., sol-gel method) has recently been employed to *in situ* synthesize the homogeneously mixed composite powders of the piezoelectric and ferrite oxides.[144,148,149] For example, Ren *et al.*[144] added cobalt fer-

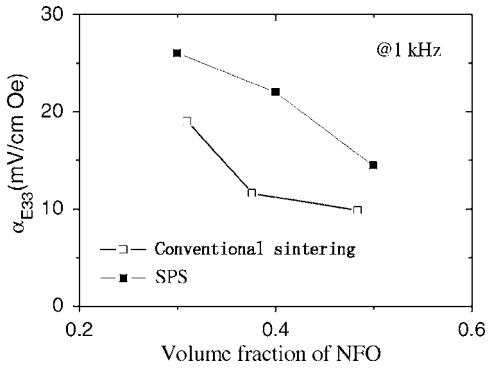

FIG. 15. Comparison of the ME coefficients of the 0–3-type NFO-PZT ceramic composites via SPS and conventional sintering.

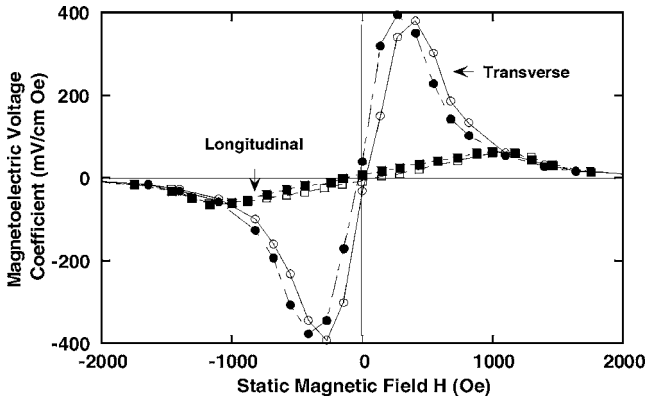

FIG. 16. Transverse and longitudinal ME voltage coefficients vs H at 100 Hz for a multilayer sample with 21 layers of Zn-doped NFO and 20 layers of PZT and a layer thickness of 20 μm [Srinivasan *et al.* (Ref. 31)].

rite nanoparticles obtained by coprecipitation into the precursor gel of BTO, allowing the *in situ* formation of ferrite-core-BTO-shell and thereby restricting the contact of the ferrite particles during sintering. The *in situ* synthesized samples showed a piezoelectric d_{33} constant approximately six times larger and a ME voltage coefficient approximately three times larger than the corresponding mechanically milled samples. The core-shell structured composites with ferrite cores and piezoelectric shell exhibit enhanced ME effect.[144,148–150]

2. Laminate ceramic composites

The leakage problem due to high concentration of the ferrite phase with low resistivity in the particulate composite ceramics can be eliminated in the laminate 2–2 composite ceramics. Laminate composite ceramics are generally fabricated by cofiring ferrite and piezoelectric ceramic layers at high temperature. ME behavior in laminate composite ceramics has been reported for various material couples (see Table I) including PZT or $Pb(Mg,Nb)O_3-PbTiO_3$ (PMN-PT) layers laminated with Ni-ferrite (e.g., NFO), or Co-ferrite (e.g., CFO), or $(La,Ca)MnO_3$ (LCMO) ones. A laminate composite ceramic exhibits higher ME response than its corresponding particulate composite ceramic.

Srinivasan *et al.*[31,32,35,36] prepared such laminate composite ceramics by tape-casting technique. Both bilayers and multilayers of ferrite piezoelectrics were synthesized from thick films prepared by tape casting. The process involves (i) preparation of submicron size powder of NFO and PZT, (ii) thick film tapes by doctor-blade techniques, and (iii) lamination and sintering of bilayers and multilayers. Ferrite powder obtained by standard ceramic techniques and commercial PZT were used. For tape casting, powders of ferrite or PZT was mixed with a solvent (ethyl alcohol) and a dispersant (Blown Menhaden Fish Oil) and ball milled for 24 h, followed by a second ball milling with a plasticizer (butyl benzyl phthalate) and a binder (polyvinyl butyral) for 24 h. The slurries thus obtained were cast into tapes on silicon coated Mylar sheets using a tape caster consisting of a pair of stationary micrometer controlled blades and a movable casting bed. It was possible to obtain 10×20 cm^2 tapes with the thickness in the range of 10–200 μm. The tapes were arranged to obtain the desired structure, laminated under high pressure (3000–5000 psi) and high temperature (400 K), and heated at 1000 K for binder evaporation. The final sintering was carried out at 1400–1500 K.

A high ME voltage coefficients of up to 0.4 V/cm Oe was observed on a laminate NFO/PZT multilayer stack, where NFO was considered to exhibit nearly ideal interface coupling ($k=1$) with PZT. Therefore, an important parameter in the selection of the composite constituent phases is interface coupling [see Eqs. (11) and (12)] between the piezoelectric and ferrite phases, which can vary significantly with the dopant concentration. But the composites with cobalt ferrite or lanthanum manganites and PZT exhibit lower ME effects that are attributable to poor interface coupling ($k\leqslant0.1$). The interface coupling parameter is dependent on surface inhomogeneities and chemical reaction between constituents during sintering as well as misfit strains.

Another remarkable difference between the laminate and particulate composite ceramics is that the laminate ceramics exhibit much larger anisotropy than the particulate ones. Srinivasan *et al.*[31,32,35,36] analyzed the longitudinal and transverse ME responses for PZT in combination with a few magnetic oxides. The ME coefficient α_E was measured for three conditions as discussed earlier: (i) transverse, (ii) longitudinal, and (iii) in-plane longitudinal. Figure 16 shows representative data on H dependence of α_E for nickel zinc ferrite (NZFO) and PZT. They found that the transverse ME effect yields an up to one order of magnitude higher maximum value than the longitudinal ME effect. The dependence of the transverse and the longitudinal ME voltage coefficients on the magnetic bias field is qualitatively different with much higher bias fields for peak longitudinal than for peak transverse ME voltage coefficients. The transverse coefficient is much higher than the longitudinal values due to the absence of demagnetization effects. Further, the strong piezomagnetic coefficient for in-plane magnetic fields is the cause of giant transverse ME coefficients. Saturation of magnetostriction at high field leads to significant decline in the ME voltage coefficient.

The most common 2–2 laminate ME composite is a simple bilayer structure of a ferrite and piezoelectric ceramic layer,[151] or sandwich structure,[44] with a ferrite layer (or piezoelectric ceramic layer) sandwiched between two piezo-

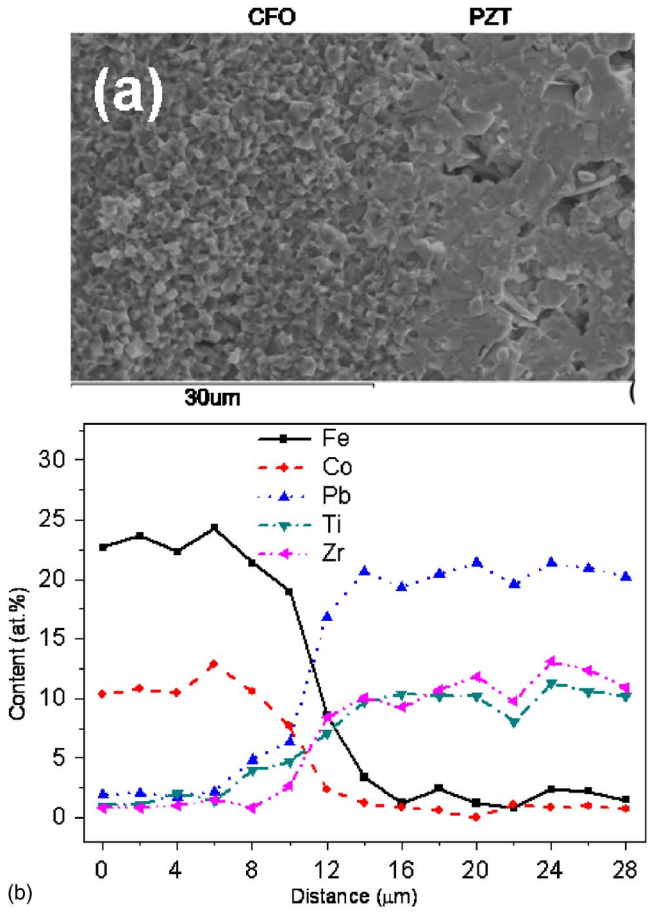

FIG. 17. (Color online) Element distribution across the boundary between CFO and PZT in the sandwich PZT/CFO/PZT ceramics [Zhou *et al.* (Ref. 44)].

electric (or ferrite) ceramic layers, which is easily obtained by a conventional solid state reaction method. The bilayer and sandwich composite ceramics presented similar dependence of the ME voltage coefficients on the magnetic bias field to the multilayer composite ceramics, but a few times smaller ME voltage coefficients than the latter. The ME voltage coefficients of the sandwich ceramics are strong dependent on their relative thicknesses of the two phases.

As in the particulate composite ceramics, there also easily occurs interdiffusion of elements or chemical reactions[44,152] between piezoelectric ceramics layer and ferrite layer during the sintering process at high temperature (Fig. 17), which leads to the change in the properties of the piezoelectric and magnetic phases. Different sintering behaviors of two phases lead to porous in the ceramics (Fig. 17). All these deteriorate the ME response of the composite ceramics.

In order to suppress interdiffusion and chemical reaction of the constituents and improve the quality of the laminate composites moderately, the hot-pressing technique[145] has also been employed. Recently a direct comparison of samples made by conventional sintering and by hot pressing was made.[145] For PZT/NFO bulk composites hot pressing enhanced the ME response by more than one order of magnitude, while for PZT/NZFO multilayers a 100% increase was achieved.

Compared with the particulate composite ceramics, the laminate composite ceramics exhibit high ME coefficients due to elimination of leakage problem. However, high-temperature cofiring processing of the piezoelectric and ferrite ceramic layers is still a big challenge due to different shrinkages, thermal expansion mismatch, and atom interdiffusion and/or chemical reactions, between two ceramic layers during the sintering process at high temperature. Recently, a simple bilayer ceramic composite has been prepared by simply bonding PZT and ferrite ceramic layers together with epoxy,[153] not by cofiring at high temperature. In this case, the ME effect is strongly dependent on the interfacial binder.

IV. TWO-PHASE COMPOSITES OF ALLOYS AND PIEZOELECTRIC MATERIALS

A. Theories

1. Physically based modeling

Rare-earth-iron alloys (e.g., $SmFe_2$, $TbFe_2$, or Terfenol-D) are the best known and most widely used giant magnetostrictive alloys exhibiting much higher magnetostriction (over 10^3 ppm) than the magnetic oxide (e.g., ferrite) ceramics. Thus the composites of these alloys and piezoelectric materials should have much large ME response. By generalizing Green's function technique to treat the composites containing these alloys (e.g., Terfenol-D), Nan *et al.*[114,115,154] calculated the ME response of such composites and predicted their GME effect.

For Terfenol-D based composites, more generally, by considering the coupling interaction between magnetostriction (a *nonlinear* magnetomechanical effect) and piezoelectricity, the coupling response can be described by the following modified constitutive equation as:

$$\boldsymbol{\sigma} = \mathbf{cS} - \mathbf{e}^{\mathrm{T}}\mathbf{E} - \mathbf{cS}^{\mathrm{ms}},$$

$$\mathbf{D} = \mathbf{eS} + \boldsymbol{\varepsilon}\mathbf{E} + \boldsymbol{\alpha}\mathbf{H},$$

$$\mathbf{B} = \boldsymbol{\mu}(\mathbf{S},\mathbf{E},\mathbf{H})\mathbf{H}, \tag{16}$$

where the permeability $\boldsymbol{\mu}$ strongly depends on $\mathbf{S}$ and electric and magnetic fields; and $\mathbf{S}^{\mathrm{ms}}$ is the magnetostrictively induced strain related with the magnetic field dependent magnetostriction constants, λ_{100} and λ_{111}, of the magnetostrictive alloy. The effective ME coefficient of the composites can be solved by using Green's function technique as

$$\boldsymbol{\alpha}^{*}\langle\mathbf{H}\rangle = f\mathbf{e}^{*}\langle[\mathbf{I} - \mathbf{G}^{u}(\mathbf{c} - \mathbf{c}^{0})]^{-1}\mathbf{G}^{u}\mathbf{cS}^{\mathrm{ms}}\rangle_{\mathrm{orient}}, \tag{17}$$

where f is still the volume fraction of the magnetic phase; $\mathbf{c}$ and $\mathbf{c}^0$ are, respectively, the stiffness tensors of the magnetic phase and the homogeneous reference medium; $\mathbf{I}$ is the unit tensor and $\mathbf{G}^u$ is the modified displacement Green's function; $\langle\ \rangle_{\mathrm{orient}}$ denotes averaging over all possible orientations of the magnetic phase in the composites. Under the open circuit measurement condition ($\langle\mathbf{D}\rangle=0$) and a completely mechanically clamped boundary condition ($\langle\mathbf{S}\rangle=0$), the primary ME output voltage can be obtained from equations above as

$$\bar{\mathbf{E}} = -(\boldsymbol{\kappa}^*)^{-1}\boldsymbol{\alpha}^*\langle\mathbf{H}\rangle$$
$$= \boldsymbol{\alpha}_E\langle\mathbf{H}\rangle$$
$$= -f\mathbf{h}^*\langle[\mathbf{I}-\mathbf{G}^u(\mathbf{c}-\mathbf{c}^0)]^{-1}\mathbf{G}^u\mathbf{c}\mathbf{S}^{\mathrm{ms}}\rangle_{\mathrm{orient}}, \quad (18a)$$

where $\mathbf{h}^*$ $(=\boldsymbol{\kappa}^{*-1}\mathbf{e}^*)$ is the effective piezoelectric stress coefficient tensor. To the other extreme, there is a mechanical free boundary condition, i.e., $\langle\boldsymbol{\sigma}\rangle=0$, and in this case, the ME output voltage is

$$\bar{\mathbf{E}}^{\mathrm{free}} = \bar{\mathbf{E}} - \boldsymbol{\kappa}^{*-1}\mathbf{e}^*\bar{\mathbf{S}}^{\mathrm{ms}}. \quad (18b)$$

The first term in the right side of Eq. (18b) corresponds to the primary ME response, and the second term is the secondary ME response measuring the additional ME response produced by the magnetostrictive strain of the composite through the piezoelectric effect of the composite. These equations are the desired formula for the extrinsic linear ME_H coefficient resulting from the coupling interaction between the *nonlinear magnetostrictive* and *linear piezoelectric* effects. The equations also show that a strong ME_H response of the composite could be achieved with the large magnetostrictively induced strain, the high piezoelectricity, and the perfect coupling between the phases (i.e., transferring elastic strains without appreciable losses).

For simple 0-3 particulate composites, the low resistitive Terfenol-D grains should be well dispersed in the piezoelectric matrix to keep the composite insulating, since the conductive Terfenol-D grain percolation path can make it difficult to polarize the composites and cause the charges developed in the piezoelectric phase to leak through this conductive path. Thus the Terfenol-D grains must be not in contact with each other, while the piezoelectric matrix is self-connected thus forming a 0-3 connectivity of phases, and the volume fraction of the alloy grains in the piezoelectric matrix is limited by the percolation. For illustrative purpose, Fig. 18 shows the numerical results in the high magnetic field saturation in the whole volume fraction range for the 0-3 particulate Terfenol-D/P(VDF-TrFE) composite with Terfenol-D grains randomly oriented in the polymer matrix. The NSCA and SCA predict different maximum α_{E33} at different volume fractions (e.g., at $f\sim0.85$ and 0.55 for NSCA and SCA, respectively) and different results at high concentration, but they give very close results in the volume fraction range of $f<0.4$, which means that the theoretical predictions in this volume fraction range of interest are reasonable. The ME coefficients of the particulate composites increase with increasing f in the volume fraction range of $f<0.4$ of interest. The comparison between the flexible Terfenol-D/P(VDF-TrFE) composite and brittle Terfenol-D/PZT composite [Fig. 18(b)] shows that both systems exhibit similar α_{E33} due to their comparable magnetostriction and piezoelectric stress coefficient h_{33}.

Similarly to the ferrites/piezoelectric ceramic composites discussed in Sec. III, although the 0-3–type piezoelectric-matrix composites with Terfenol-D grains embedded are simple, the 2-2 laminate composites are more realizable, since high concentration of conductive Terfenol-D can be easily separated by the piezoelectric layers in the 2-2 composites. Figure 19 shows numerical results for the two 2-2

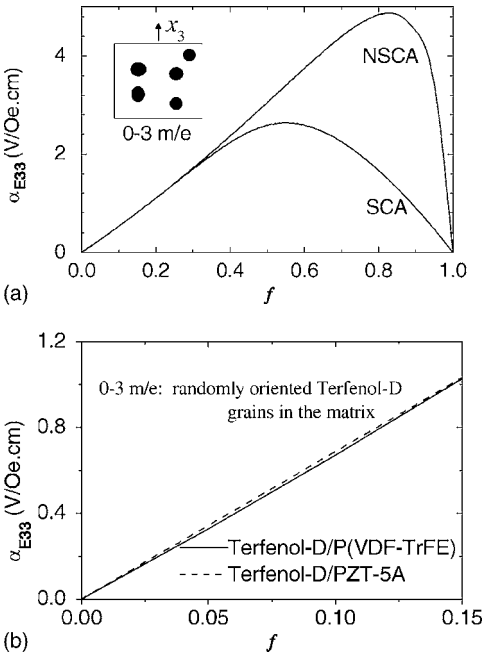

FIG. 18. (a) Calculated α_{E33} for 0–3 m/e Terfenol-D/P(VDF-TrFE) particulate composites by NSCA and SCA. (b) Comparison of calculated α_{E33} for the flexible polymer-matrix composite and brittle PZT ceramic matrix composite filled with randomly oriented Terfenol-D particles [Nan *et al.* (Ref. 114)].

sandwich composites with perfectly interfacial bonding between PZT and Terfenol-D disks. For the sandwich PZT/Terfenol-D/PZT composite, the ME effect nonmonotonically depends on f with a maximum at $f\sim0.85$, while the ME effect of the sandwich Terfenol-D/PZT/Tefenol-D composite nearly linearly increases with f. Of particularly interesting to note is that a GME effect is produced in these two laminate composites with thick Terfenol-D layers but thin PZT layers.

In the calculations above, a perfectly bonded interface between magnetic alloys and piezoelectric phases is assumed, which ensures the perfect coupling between these two phases (i.e., transferring elastic strains without appreciable losses) to obtain exceptional control of the predictability of the ME effect in such ME composites. Any imperfect interfaces will more or less decrease the displacement transfer capability, thereby leading to a decrease in the ME response of the composites. In order to treat the interfacial

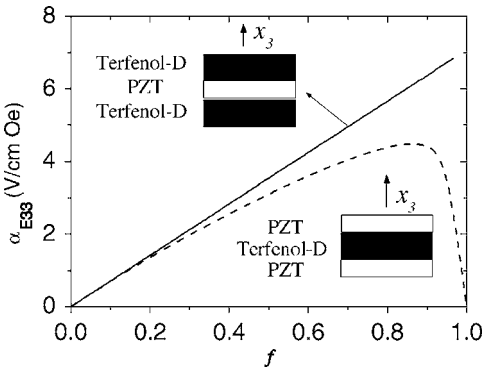

FIG. 19. α_{E33} at high-field saturation of these two sandwiched composites as a function of the volume fraction (or relative thickness ratio) of the Terfenol-D layers [Nan *et al.* (Ref. 114 and 155)].

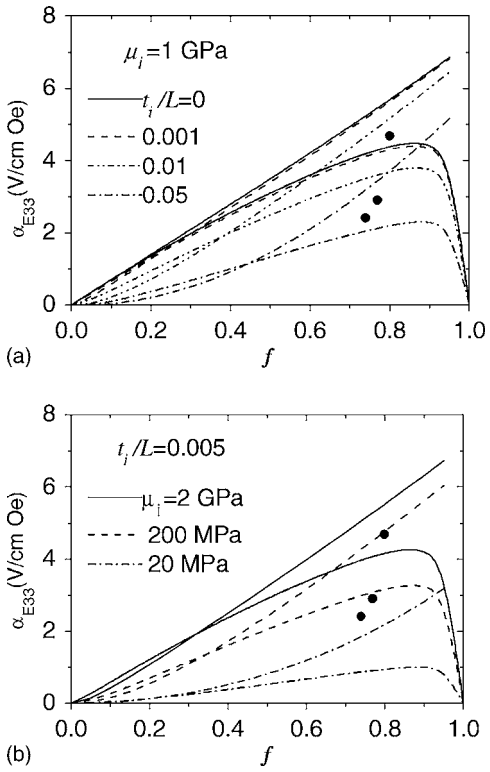

FIG. 20. Effect of (a) relative thickness t_i/L (L being the thickness of the composite) and (b) shear modulus μ_i of the interfacial binder layers on α_{E33} at high-field saturation of these sandwich composites. Recent experimental data available for a Terfenol-D/PZT/Terfenol-D composite are also shown for comparison [Nan *et al.* (Ref. 155)].

bonding effect, we change the shear modulus μ_i and the relative thickness t_i of the interfacial binder.[155] Figure 20 shows the influence of interface properties on α_{E33} of these sandwich composites. The comparison in Fig. 20 shows that the predictions are in reasonable agreement with experimental data available, though the interfacial bonding status in the experiment is not clear. The increase in the thickness t_i of the interfacial binder films between the PZT and Terfenol-D leads to a decrease in the α_{E33} values [Fig. 20(a)]. Figure 20(a) shows that a very thin binder film (e.g., $t_i/L \sim 0.001$) with bonding capability is good enough for producing the GME response. The elastic modulus of the interfacial binder films has a significant effect on the α_{E33} values [Fig. 20(b)]. With decreasing the shear modulus μ_i of the thin binder films (i.e., using a very flexible binder), the interfacial bonding between the PZT and Terfenol-D becomes weak due to the formation of a sliding interface. The weak interfacial contact would lead to appreciable losses of transferring elastic strain/stress from Terfenol-D to PZT, and thus the decrease in the shear modulus μ_i of the thin interfacial binder films results in a large decrease in the ME response of the composites.

If using a piezomagnetic coefficient ($c\partial S^{ms}/\partial H$) to replace the magnetostrictive strain and still using Eq. (3) rather than Eq. (16), the micromechanics modeling and averaging method discussed in Sec. III A 3 could be still applicable for such Terfenol-D based composites.

2. Equivalent-circuit modeling

For the 2-2 laminate composites, Dong *et al.*[156–158] proposed an equivalent-circuit approach which is more convenient for modeling the ME coupling in the dynamic cases. This approach is also based on magnetostrictive and piezoelectric constitutive equations, where the magnetostrictive and piezoelectric layers are mutually coupled through elastic interaction, via an equation of motion that is excited by a magnetic field **H**. We suppose that the magnetostrictive/piezoelectric laminates are long-type configurations (Fig. 21), in which the piezoelectric layer is polarized along either its thickness or length directions and stressed by two magnetostrictive layers along their length (i.e., principal strain) direction. Accordingly, the piezoelectric constitutive equations for one-dimensional motion are

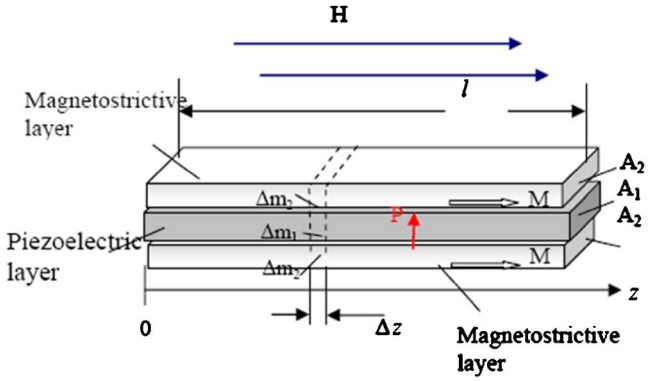

FIG. 21. (Color online) Long-type magnetostrictive/piezoelectric/magnetostrictive laminate [Dong *et al.* (Ref. 156)].

$$S_{1p} = s_{11}^E T_{1p} + d_{31,p} E_3, \quad D_3 = d_{31,p} T_{1p} + \varepsilon_{33}^T E_3. \tag{19a}$$

for the thickness poling case, and

$$S_{3p} = s_{33}^D T_{3p} + g_{33p} D_3, \quad E_3 = -g_{33p} T_{3p} + \beta_{33}^T D_3 \tag{19b}$$

For the length poling case, where D_3 is the electric displacement, ε_{33}^T and β_{33}^T are the dielectric permittivity and impermeability under constant stress T, s_{11}^E and s_{33}^D are the elastic compliances of the piezoelectric material under constant electric field E or constant electric displacement D, $d_{31,p}$ and $g_{33,p}$ are the transverse piezoelectric constant and longitudinal piezoelectric voltage constants, and T_{1p}, T_{3p} and S_{1p}, S_{3p} are the stress and strain of the piezoelectric layer imposed by the magnetostrictive layers.

When **H** is applied parallel to the longitudinal axis of the laminate, a longitudinal strain is excited. The piezomagnetic constitutive equations for the longitudinal mode are

$$S_{3m} = s_{33}^H T_{3m} + d_{33,m} H_3, \quad B_3 = d_{33,m} T_{3m} + \mu_{33}^T H_3, \tag{20}$$

where B_3 is the magnetization along the length direction, μ_{33}^T is the permeability under constant stress, s_{33}^H is the elastic compliance of the magnetostrictive layer under constant **H**, $d_{33,m}$ is the longitudinal piezomagnetic constant, and T_{3m} and S_{3m} are the stress and strain in the longitudinal direction of the magnetostrictive layers imposed on the piezoelectric layer. These constitutive equations are linear relationships, which do not account for loss components. Significant nonlinearities in both piezoelectric and magnetostrictive materials are known to exist, especially under resonance drive. We will introduce a mechanical quality factor Q_m to include these losses later.

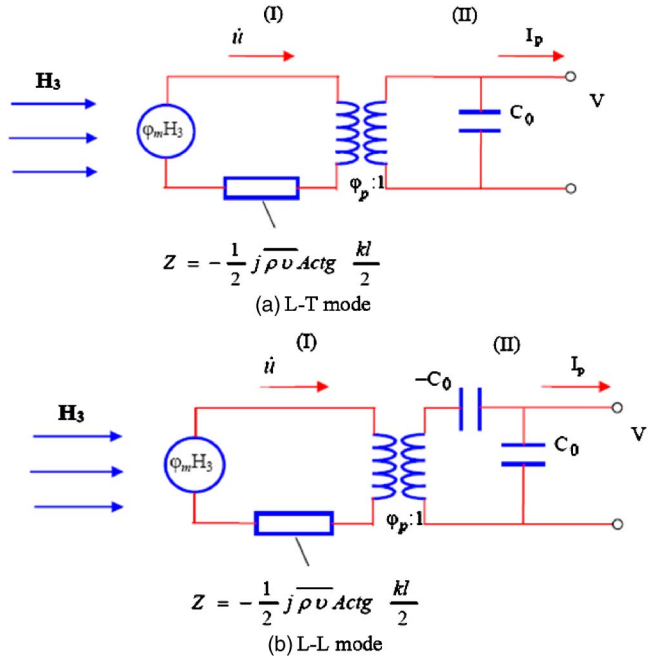

FIG. 22. (Color online) Magneto-elastic-electric bieffect equivalent circuits for (a) *L-T* mode and (b) *L-L* mode [Dong *et al.* (Refs. 156 and 158)].

Assuming harmonic motion, along a given direction z, it will be supposed that three small mass units Δm_i in the laminate have the same displacement $u(z)$. This follows from Fig. 21, by assuming that the layers in the laminate act only in a coupled manner. Following Newton's second law, we then have an equation of motion to couple the piezoelectric and piezomagnetic constitutive equations [Eqs. (19a) and (19b)] as

$$\bar{\rho}\frac{\partial^2 u(z)}{\partial t^2} = n\frac{\partial T_{3,m}}{\partial z} + (1-n)\frac{\partial T_{i,p}}{\partial z} \quad (0 < n < 1, i = 1 \text{ or } 3), \tag{21}$$

where $\bar{\rho}=(\rho_p A_p+\rho_m A_m)/A_{\text{lam}}$ is the average mass density of the laminate, and $n=A_m/A_{\text{lam}}=t_m/t_{\text{lam}}$ is a geometric factor, $t_m=t_{m1}+t_{m2}$ is the total thickness of the magnetic phase layers, A_p and $A_m(=A_{m1}+A_{m2})$ are the cross-sectional areas of the magnetic phase and piezoelectric phase layers, respectively, ρ_p and ρ_m are the mass densities of the piezoelectric and magnetostrictive layers. For a given laminate width w_{lam} and thickness t_{lam}, the total cross-sectional area of the laminate is $A_{\text{lam}}=t_{\text{lam}}w_{\text{lam}}$, and the total thickness is the sum of the layer thicknesses $t_{\text{lam}}=t_p+t_m$, where t_p is the thickness of the piezoelectric layer.

By combining piezoelectric and piezomagnetic constitutive equations [Eqs. (19a) and (19b)], solutions to the equation of motion [Eq. (21)] can be derived for longitudinally magnetized ***M*** and transversely or longitudinally poled ***P*** magnetoelectric modes, respectively, named as *L-T* or *L-L*. Correspondingly, the two magneto-(elasto)-electric (or ME) equivalent circuits for *L-T* and *L-L* modes under free boundary conditions can be derived, as given in Fig. 22,[156,158] where an applied magnetic field ***H*** acts as a magnetic induced "mechanical voltage" ($\varphi_m H_3$), and then induces a "mechanical current" ($\dot{u}_1$ and $\dot{u}_2$) via the magnetoelastic effect with a coupling factor φ_m. In turn, $\varphi_m H_3$ results in an electrical voltage V, and $\dot{u}_1$ and $\dot{u}_2$ result in a current I_p across the piezoelectric layer due to electromechanical coupling. A transformer with a turn ratio of φ_p can then be used to represent the electromechanical coupling. In the circuits of Fig. 22, Z_1 and Z_2 are the characteristic mechanical impedances of the composite, and C_0 is the clamped capacitance of the piezoelectric plate.

Following Fig. 22, open-circuit conditions have been supposed from above, where the current I_p from the piezoelectric layer is zero. Thus, the capacitive load C_0 (and $-C_0$) can be moved to the main circuit loop. Applying Ohm's law to the mechanical loop, the following ME coefficients at low frequency for *L-T* and *L-L* modes can be directly derived as

$$\left|\frac{dE}{dH_3}\right|_{(L\text{-}T)} = \frac{nd_{33,m}g_{31,p}}{ns_{11}^E(1-k_{31,p}^2)+(1-n)s_{33}^H}, \tag{22a}$$

$$\left|\frac{dE}{dH_3}\right|_{L\text{-}L} = \frac{nd_{33,m}g_{33,p}}{ns_{33}^E(1-k_{33}^2)+(1-n)s_{33}^H}. \tag{22b}$$

Thus the ME coefficients are also proportional to the piezomagnetic constant $d_{33,m}$, the piezoelectric voltage constants ($g_{31,p}$ or $g_{33,p}$), and the thickness ratio n of the Terfenol-D layers.

In order to derive the ME coefficients at resonance frequency, we assume the long-type ME laminate composites to be a *L-L* $\lambda/2$-resonator, operating in a length extensional mode, the series angular resonance frequency is $\omega_s=\pi\bar{v}/l$, where l is the length of the laminate and $\bar{v}$ is mean acoustic velocity. Under resonant drive,[158] the mechanical quality factor Q_m of the laminate is finite due to both mechanical and electric dissipations. This limitation of the vibration amplitude must also be included, in order to predict the resonant response. Finite values of Q_{mech} result in an effective motional mechanical resistance of $R_{\text{mech}}=\pi Z_0/8Q_{\text{mech}}$; accordingly, the equivalent circuit of the laminates for the *L-L* mode under resonance drive is given in Fig. 23. At electromechanical resonance ($\omega=\omega_s$), dV/dH of the *L-L* mode reaches a maximum value of

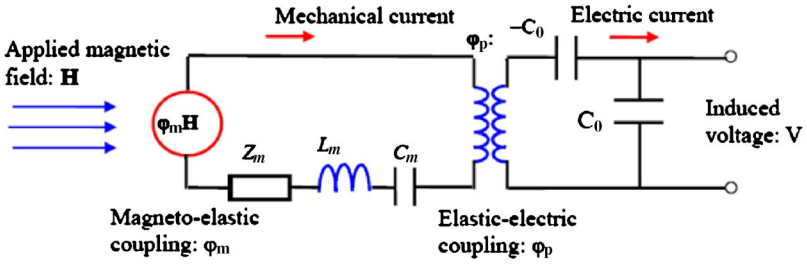

FIG. 23. (Color online) Magneto-elastic-electric equivalent circuits for *L-L* at resonance [Dong *et al.* (Refs. 156 and 157)].

TABLE II. Various constituent phases used for ME laminate composites.

Piezoelectric phase	Magnetic phase
PZT	Terfenol-D
PMN-PT, PZN-PT	Ni, Permendur, Fe–Ga, Ni_2MnGa
PVDF	Metglas

$$\left(\frac{dV}{dH}\right)_{\omega s} = \frac{4Q_m\varphi_m\varphi_p}{\pi Z_0\omega_s C_0}, \tag{23}$$

where Q_m is the effective mechanical quality factor of the laminate composite including contributions from the Terfenol-D and piezoelectric layers, and also from the bonding between layers. Analysis has shown that dV/dH at the resonance frequency is $\sim Q_m$ times higher than that at subresonant frequencies. Using a similar approach, it is ready to obtain the resonance equivalent circuit for the *L-T* mode. The 2-2 laminate structures can also be modeled numerically by using finite-element method.[159,160]

B. Experiments

The GME effect predicted was reported first in the Terfenol-D/PZT laminate by Ryu *et al.*[47,48] and in the Terfenol-D/PVDF laminate by Mori and Wuttig.[116] Since then, in particular, Dong *et al.*[49–66,156–158] have reported the GME effect in a number of laminate composites of Terfenol-D and various piezoelectric materials including PZT ceramics, $Pb(Mg_{1/3}Nb_{2/3}O_3)-PbTiO_3$ (PMN-PT) or $Pb(Zn_{1/3}Nb_{2/3}O)_3-TiO_3$ (PZN-PT) single crystal, or electroactive PVDF copolymers.

The laminate composites are generally fabricated by bonding magnetostrictive and piezoelectric layers (Table II) using an epoxy resin, followed by annealing at a modest temperature of 80–100 °C. Typically, the laminate composites are made of two magnetostrictive layers and a single piezoelectric one, where the piezoelectric layer is sandwiched between the two magnetostrictive ones. However, ME laminates can be made in many different configurations[47–66,156–166] including disk, rectangular, and ring shapes. These various configurations can be operated in numerous working modes including *T-T* (transverse magnetization and transverse polarization), *L-T*, *L-L*, symmetric *L-L* (push-pull) longitudinal vibrations; *L-T* unimorph and bimorph bending; *T-T* radial and thickness vibrations multilayer; and *C-C* (circumferential magnetization and circumferential polarization) vibration modes, as shown in Figures 24–27.

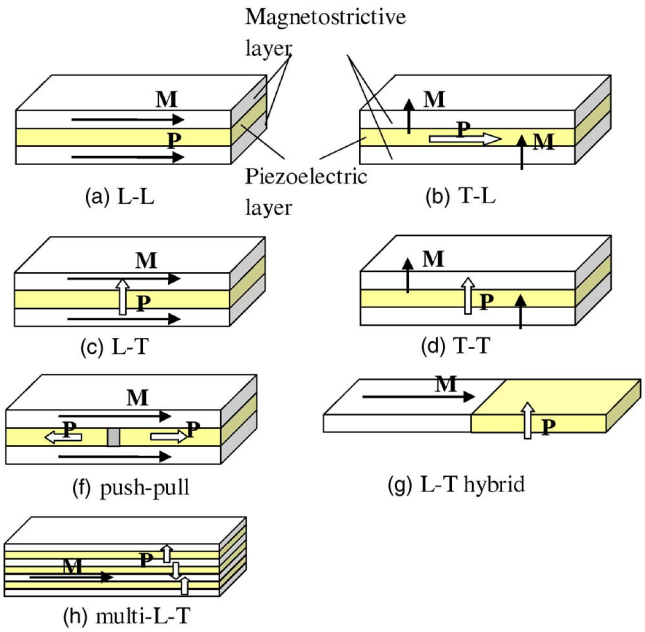

FIG. 24. (Color online) Various rectangular laminates operated in longitudinal vibration mode.

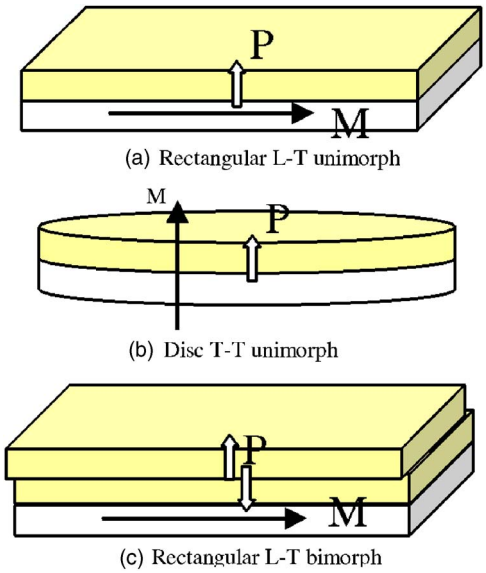

FIG. 25. (Color online) Unimorph and bimorph bending vibration modes.

1. T-T Terfenol-D/PZT laminate

The first studies of Terfenol-D/PZT laminates[48] were performed on disk-shape three layer configurations that were operated in a transverse magnetization and transverse polarization (*T-T*) mode. Relatively large ME voltage coefficients of α_E=4.8 V/cm Oe was reported by Ryu *et al.*[48] under dc magnetic field bias of $H_{dc} \geqslant 4000$ Oe; although later, other investigators repeated the actual value to be α_E =1.3 V/cm Oe.[164,165] Figure 28 shows these later (repeated) experimental results for a *T-T* laminate, where a maximum ME voltage of 66 mV/Oe (or 1.32 V/cm Oe) was observed under $H_{dc} \approx 4000$ Oe. This discrepancy might be due to the interfacial bonding,[155] as calculated in Fig. 20.

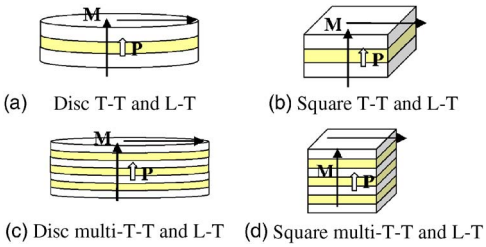

FIG. 26. (Color online) Radial and thickness vibration modes of disk- and square-type ME laminates.

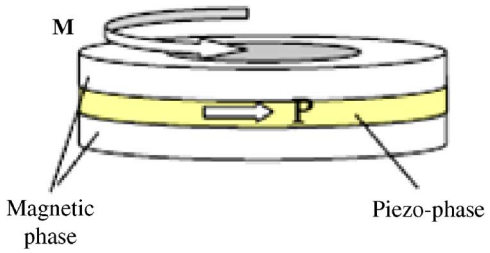

FIG. 27. (Color online) *C-C* mode of ring ME laminate [Dong *et al.* (Ref. 53)].

The main problem with the *T-T* mode laminates is that a quite high dc magnetic bias H_{dc} is required to obtain a maximum value of α_E. This high H_{dc} is caused by a large demagnetization factor in transversely magnetized Terfenol-D layers.

2. L-T Terfenol-D/PZT and PMN-PT laminates

To reduce the demagnetization factor effect, a long-type configuration (Fig. 21) that uses a longitudinal magnetization was designed.[49–51] This dramatic decrease in the demagnetization factor results in a large reduction in the H_{dc}, required to achieve the maximum ME coefficient.[51] Long rectangular-shaped Terfenol-D/PZT/Terfenol-D and Terfenol-D/PMN-PT/Terfenol-D three layer laminates with a longitudinal magnetization and transverse polarization (*L-T*) were then reported[49–51] based on this consideration. Experimental results confirmed that at low magnetic biases of H_{dc} <500 Oe much large values of α_E could be obtained for *L-T* laminates relative to *T-T* ones. For example, Fig. 29 shows these measurements taken under an ac magnetic excitation of $H_{ac}=1$ Oe at $f=1$ kHz. It can be seen that the induced ME voltage for the *L-T* Terfenol-D/PZT laminates under H_{dc} $=500$ Oe was 0.085 V/Oe (or $\alpha_E=1.7$ V/cm Oe) and for *L-T* Terfenol-D/PMN-PT ones $\sim$0.11 V/Oe (α_E $=2.2$ V/cm Oe); whereas that for the *T-T* mode of Terfenol-D/PZT laminate under $H_{dc}=500$ Oe was only $\sim$0.015 V/Oe ($\alpha_E=0.3$ V/cm Oe). Clearly, long type *L-T* laminates have significantly higher ME voltage coefficients than *T-T* ones under modest magnetic biases.

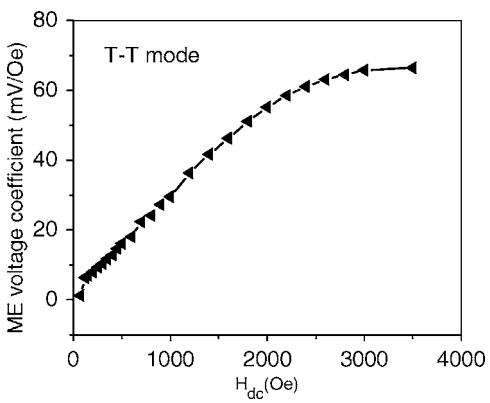

FIG. 28. ME voltage coefficient as a function of the applied dc magnetic field bias H_{dc} [Dong *et al.* (Ref. 165)].

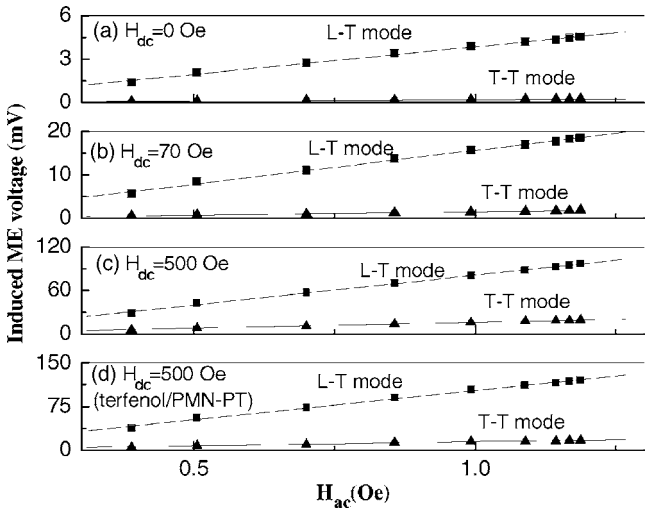

FIG. 29. Induced ME voltage as a function of H_{ac} for a laminate of Terfenol-D and PZT-5 ceramic: (a) $H_{dc}=0$ Oe, (b) $H_{dc}=70$ Oe, and (c) $H_{dc}=500$ Oe; and (d) for a laminate of Terfenol-D and a ⟨001⟩-oriented PMN-PT crystal. The measurement frequency was 10^3 Hz [Dong *et al.* (Ref. 50)].

3. L-L and push-push terfenol-D/PZT and PMN-PT laminates

To achieve a high output voltage, a *L-L* mode of Terfenol-D/PZT/Terfenol-D or Terfenol-D/PMN-PT/Terfenol-D laminate is a good choice due to its large dielectric displacement along the length (longitudinal) direction.[52,156,165] For a long-type ME laminate, the length of the piezoelectric layer is much larger than its thickness, in addition, the longitudinal electromechanical coupling coefficient $k_{33,p}$ and piezoelectric voltage constant $g_{33,p}$ are higher than the corresponding transverse $k_{31,p}$ and $g_{31,p}$. Following Eq. (23), a Terfenol-D/PZT laminate operated in an *L-L* mode should have a much higher induced voltage V_{ME} under magnetic field excitation. For example, Fig. 30 shows measurements for an *L-L* mode terfenol-D/PZT laminate, which exhibits a maximum $V_{ME}=3.5$ V/Oe at 1 kHz (or α_E $=2.4$ V/cm Oe) at $H_{dc}=500$ Oe. Although *L-L* ME laminates have the highest induced voltage (in V/Oe), its ME charge coefficient (in C/Oe) is quite low. This is because *L-L* ME laminates have a low capacitance. For a ME laminate with small capacitance, direct measurements of the induced ME

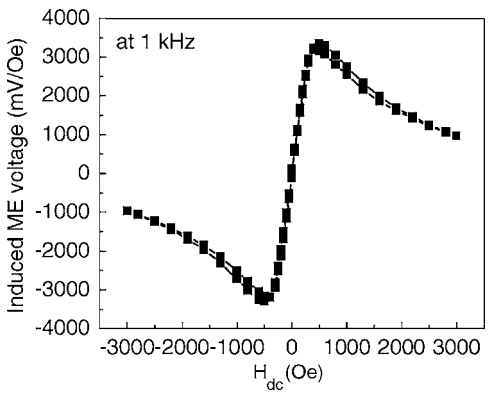

FIG. 30. Induced ME voltage in the *L-L* Terfenol-D/PZT/Terfenol-D laminate [Dong *et al.* (Ref. 156)].

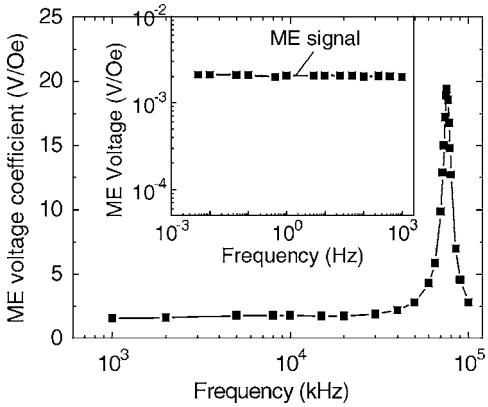

FIG. 31. ME voltage coefficients as a function of ac magnetic field frequency [Dong *et al.* (Ref. 166)].

voltages using a lock-in amplifier may result in big error.[156] In this case, a charge measurement method may be more reliable for obtaining the correct values.

A double (or symmetrically poled) *L-L* configuration has been designated as push-pull mode [Fig. 23(f)].[59,158,166] The push-pull configuration is a compromised design, which takes advantages of the high induced voltage of *L-L* mode and the large ME charge of the *L-T* one. Figure 31 shows measurements of the ME voltage coefficients for a push-pull laminate, which had a maximum ME induced voltage of 1.6 V/Oe (or α_E=2.5 V/cm Oe) at 1 kHz and ~20 V/Oe (~31 V/cm Oe) at 75 kHz. Although this value is similar to an *L-L* mode, its ME charge coefficient was two times higher than that in *L-L* one.[166]

4. L-T bending mode of Terfenol-D/PZT laminates

A single longitudinally magnetized Terfenol-D layer laminated together with one or two transversely poled piezoelectric PZT or PMN-PT layers is an *L-T* bending mode (Fig. 25).[164] Under an external magnetic excitation, the stress applied to the piezoelectric layer by the Terfenol-D one is asymmetric, resulting in a bending motions rather than a longitudinal one for the *L-T* mode. In general, the ME voltage coefficients of the bending mode are smaller (~1.2 V/cm Oe) than those of the *L-T* or *L-L* ones, simply because the bending mode contains only a single Terfenol-D layer. However, the bending mode does have better low-frequency response to magnetic fields than either the *L-T* or *L-L*, making it suitable for low-frequency magnetic sensor applications. Figure 32 shows the induced charge response of the bimorph ME laminate [see Fig. 25(c)] to low-frequency magnetic field variations. The ME charge coefficient of this bimorph was ~800 pC/Oe at 10^{-2} Hz.

5. C-C Terfenol-D/PZT and PZN-PT laminates

In many situations, magnetic fields are excited by electric currents. In this case, the excited magnetic fields are vortexes. A ME ring-type laminate operated in circumferential magnetization and circumferential polarization has been designated as the *C-C* mode (see Fig. 27). Experimental investigations have shown that Terfenol-D/PMN-PT/Terfenol-D three layer laminate ring has a very high ME coefficient with maximum values of up to 5.5 V/cm Oe at 1 kHz in response to a vortex magnetic field.[58] High ME coupling in the *C-C* mode is due to the magnetic loop of the ring ME-type configuration, and which is suitable for capturing a vortex-type field. We will see later that this *C-C* ME laminate ring has potential for electric current sensor applications.

6. ME laminates based on non-Terfenol-D materials

Although Terfenol-D has the highest magnetostriction amongst all known magnetostrictive materials, this rare-earth iron alloy is quite costly, and also very brittle. Thus alternatively, there are other magnetostrictive metallic materials (see Table II)—such as Permendur, Ni, Metglas, and other

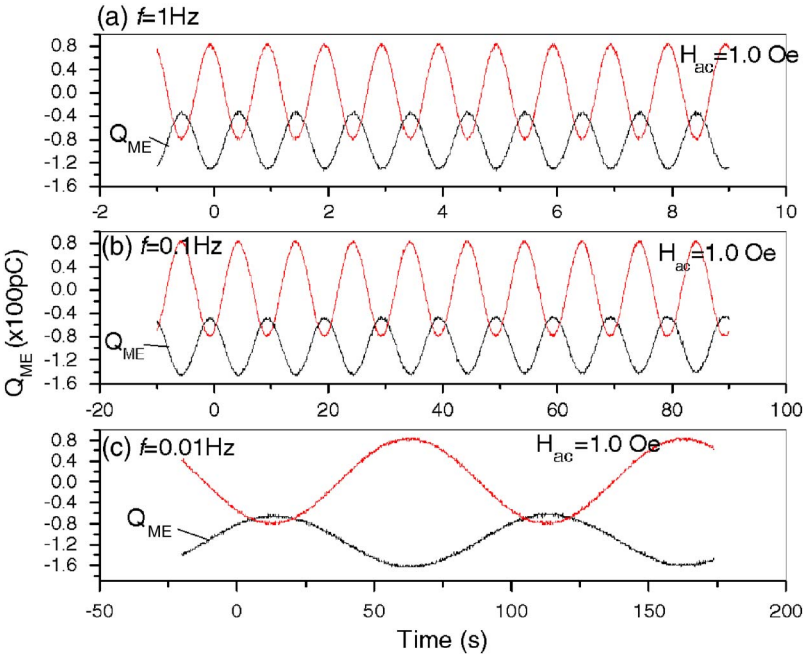

FIG. 32. (Color online) The ME response of a bimorph-type ME laminate [Dong *et al.* (Ref. 164)].

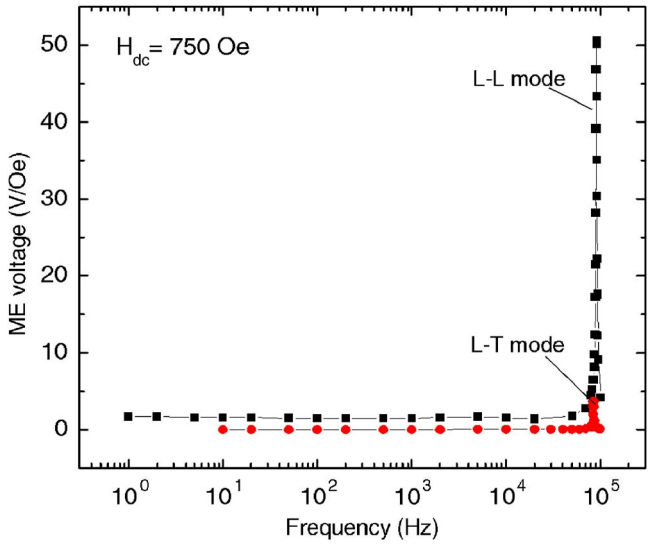

FIG. 33. (Color online) ME voltage coefficients of Fe–Ga/PMN-PT laminates as a function of magnetic field frequency [Dong *et al.* (Ref. 60)].

magnetic alloys, to be used.[59,60,167–171] Dong *et al.* developed new ME laminate composites of magnetostrictive Fe 20 at. % Ga alloys with PZT ceramics and piezoelectric single crystals, which exhibited a large ME coupling.[59,60] The maximum ME voltages observed for *L-T* Fe–Ga/PMN-PT laminates were ~1 V/cm Oe at 1 kHz and 70 V/cm Oe at resonance, as shown in Fig. 33. Although the low-frequency ME performance of the Fe–Ga/PMN-PT laminates is not as good as that of Terfenol-D/PZT laminates, its resonance ME performance is better than that of Terfenol-D/PZT laminates, due to a higher Q-factor.

Recently, a thin (<100 μm) and flexible laminate of Metglas and PVDF piezopolymer films has been reported.[167] The results showed that in both unimorph and three-layer configurations very low dc magnetic biases (as low as 8 Oe) can induce GME effect with ME voltage coefficients of 7.2 V/cm Oe at low frequency, and up to 310 V/cm Oe at resonance. Zhao *et al.*[168] reported a Ni_2MnGa/PZT laminate and observed a distinct peak of the ME coefficient near the martensitic transformation temperature (ca. 30 °C) of the Ni_2MnGa alloy. This enhancement results from the martensitic transition in the magnetic Ni_2MnGa alloy.

V. THREE-PHASE COMPOSITES

A. Quasi-0-3-type particulate composites

In the two-phase Terfenol-D based laminates, the eddy current loss in bulk Terfenol-D is quite large at high frequency, which limits the applications of this laminate structure, and the GME response of the laminated composites is strongly influenced by the interfacial binders,[155] as discussed above. In addition, Terfenol-D thin layers are very brittle. In order to overcome these difficulties in two-phase Terfenol-D/PZT laminate composites, a three-phase composite of Terfenol-D, PZT, and a polymer has been developed.[69] Such three-phase composites can be easily fabricated by a conventional low-temperature processing, and especially the three-phase particulate composites can be fabricated into a variety

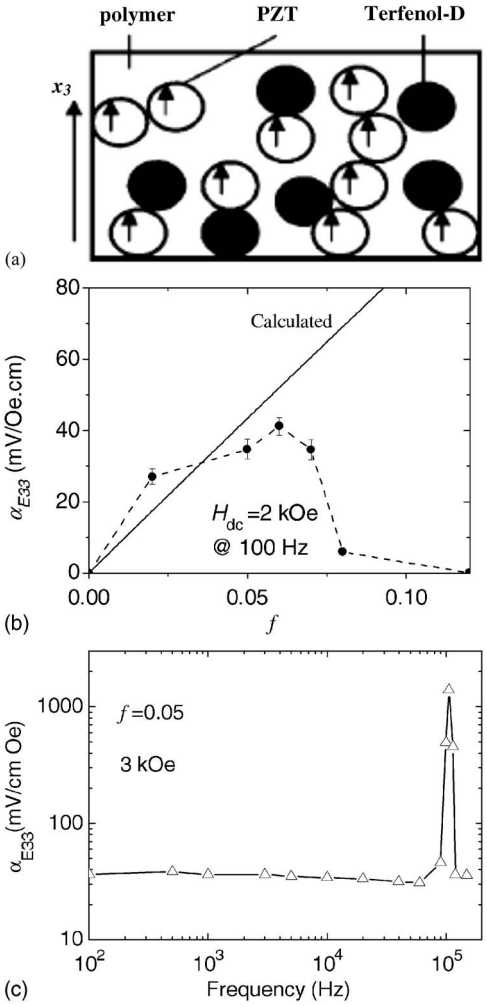

FIG. 34. (a) Schematic representation of the particulate Terfenol-D/PZT/polymer composites. All grains are randomly embedded in the polymer matrix. The polarization in PZT particles (denoted by the arrows within the open circles) is assumed to be parallel to the x_3 direction. (b) Calculated (solid line) and measured (dots) α_{E33} at high field saturation for the f Terfenol-D/(0.7−f)PZT/0.3 polymer composites. (c) Measured frequency-dependent α_{E33} for the 0.05Terfenol-D/0.65PZT/0.3polymer composite [Nan *et al.* (Ref. 71) and Shi *et al.* (Ref. 172)].

of forms such as thin sheets and molded shapes, and they exhibit greatly improved mechanical properties.

The simplest three-phase ME composite is quasi-0-3-type particulate composites where Terfenol-D grains are randomly oriented in the mixture matrix of PZT and polymer.[69,71] The conductive Terfenol-D grains are well dispersed in the PZT/polymer matrix to keep the composite insulating, as schematized in Fig. 34(a), thus forming a 0-3-3 connectivity of phases. Figure 34(b) shows a micrograph of the three-phase particulate composite. In the three-phase ME composites, the inactive polymer is just used as a binder. Such a three-phase particulate composite shown in Fig. 34 can be denoted as fTerfenol-D/(1-f_m-f)PZT/$f_m$polymer, where f and f_m are the volume fractions of Terfenol-D and polymer, respectively. The ME response of the 0-3-3 composites can also be calculated by using Green's function technique as discussed above.[172] The solid line in Fig. 34(b) shows calculated α_{E33} (under the boundary condition of completely mechanically clamped in the x_3 direction but free in

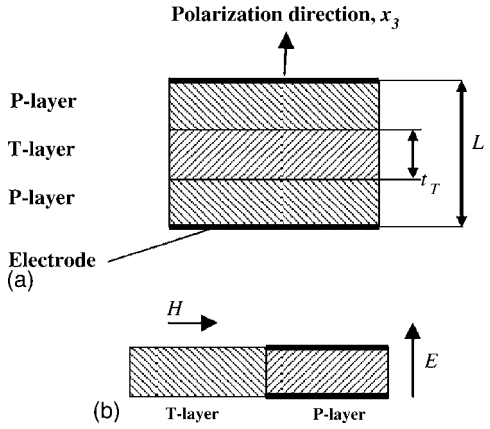

FIG. 35. Schematic illustrations of (a) a three-phase laminate *P-T-P* composite and (b) a three-phase transverse *P-T* composite.

the transverse direction as in experimental measurement) of the fTerfenol-D/(0.7-f)PZT/0.3polymer composite. As shown, in the low volume fraction range of $f<0.1$, the α_{E33} values at high-magnetic-field saturation increase approximately linearly with increasing f. This increase in α_{E33} is attributed to the increase in magnetostrictively induced strain of the composites with f. Comparison in Fig. 34(b) shows that there is a good agreement between the experimental and calculated and measured α_{E33} as $f<0.07$. However, as $f>0.07$, the measured α_{E33} values decline with f, which is due to formation of a Terfenol-D grain percolation path through the composites, though the magnetostrictively induced strain of the composites still increases with f. The maximum α_{E33} value of the composites at 2 kOe is about 42 mV/cm Oe at $f=0.06$, which is comparable with those measured for the ferrite/PZT ceramic particulate composites (see Sec. III B). At high resonance frequency, α_{E33} is as high as over 1500 mV/cm Oe [Fig. 34(c)]. The peak ME response is attributed to enhanced coupling elastic interaction at the resonance.

As observed, the ME effect in the Terfenol-D/PZT/PVDF particulate composites is mainly limited by the concentration threshold of the Terfenol-D grains allowed in the composites due to the low resistance of Terfenol-D, which is dependent on the composite microstructure. If f allowed in the composites is higher, the α_{E33} values will increase. The results imply that the ME response of the three-phase composites could be further improved by carefully controlling processing to achieve homogeneity and higher loading of the Terfenol-D grains well isolated in the PZT/polymer mixture.

B. Quasi-2-2-type laminate composites

In order to eliminate this limitation on the low volume fraction of Terfenol-D in the quasi-0-3-type particulate composites, 2-2–type laminate composites containing Terfenol-D/polymer and PZT/polymer layers have been made by laminating the Terfenol-D/polymer (denoted as *T*-layer) and the PZT/polymer (denoted as *P*-layer) particulate composite layers and then simply hot molding these layers together.[72–75] Such a simple hot-pressing procedure ensures a good interfacial bonding between composite layers, since the polymer used in the *T*-layer and *P*-layer is the same just as a matrix

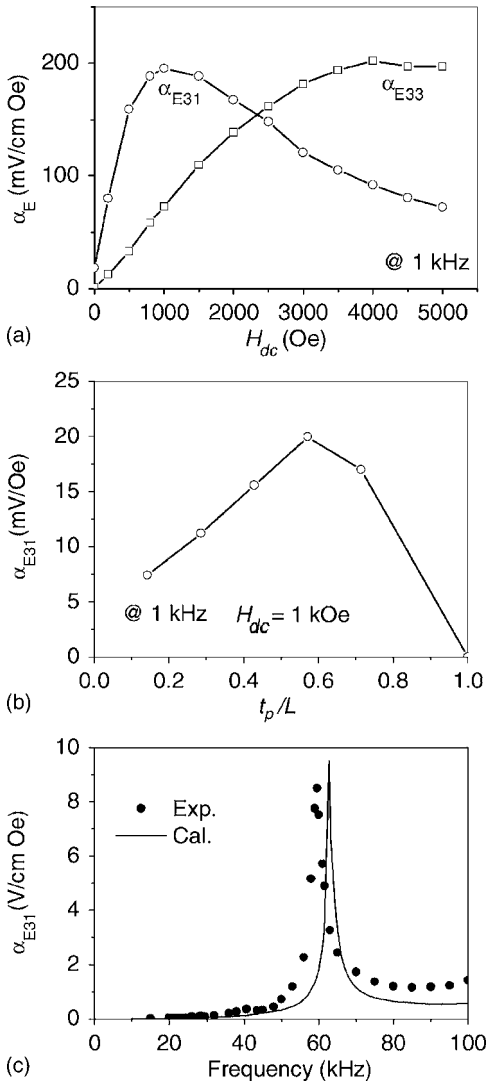

FIG. 36. The ME coefficients measured at 1 kHz for the laminate *T-P-T* composites as a function of (a) the bias magnetic field and (b) t_p/L [Nan *et al.* (Ref. 75)]. (c) Comparison of frequency dependencies of the ME coefficient measured (solid dots) and calculated (solid line) for the transverse structure of *P*-layer and *T*-layer [Filippov *et al.* (Ref. 173)].

binder. Different laminate structures, can be obtained, e.g., sandwich structure of *P*-layer/*T*-layer/*P*-layer (abbreviated as the *P-T-P* composite), or *T*-layer/*P*-layer/*T*-layer (abbreviated as the *T-P-T* composite), or transverse structure of *P*-layer and *T*-layer, as shown in Fig. 35.

In comparison with the quasi-0-3-type particulate composites, the quasi-2-2-type laminate composites exhibit strong anisotropy, and thus different longitudinal ME coefficient α_{E33} and transverse ME coefficient α_{E31} [see, e.g., Fig. 36(a)]. α_{E33} increases first rapidly with the bias field and slowly changes with the magnetic field in the high bias field range where the effective magnetostriction becomes to approach its saturation. α_{E31} nonmonotonically depends on the bias field with a peak at about 1.5 kOe. Such a nonlinear ME response of the composites is closely related to the magnetostrictive behavior of the Terfenol-D. The difference between α_{E33} and α_{E31} is due to different magnetostrictions arising from the out-of-plane bias and in-plane bias in the anisotropic laminate composite samples. At high magnetic

fields the magnetostriction gets saturated more faster under the in-plane bias than the out-of-plane bias producing a nearly constant electric field in the PZT, thereby decreasing α_{E31} with increasing bias field.

The ME effect of these composites is strongly dependent on the thickness ratio t_p/L and volume fraction of the polymer matrix. For example, Fig. 36(b) shows that both α_{E33} and α_{E31} of the *P-T-P* composites nonmonotonically depend on t_p/L with a maximum ME effect in the middle range of t_p/L. Both α_{E33} and α_{E31} of the composites first increase with t_p/L, which is attributed to the increase in the effective piezoelectric constant the composites with t_p/L. However, with further increasing t_p/L, the ME coefficient declines after a maximum value, which is due to the reduction in magnetostrictively induced strain of the laminated composites with increasing t_p/L, since much thinner *T*-layer than the *P*-layers leads to much lower magnetostrictively induced strain and thereby lower ME coefficient of the composites.

These 2-2 laminate composites exhibit similar frequency dependence [Fig. 36(c)] of the ME coefficient to those 0-3 particulate composites, i.e., their ME coefficients keep at stable values in the low-frequency range but get greatly enhanced at resonance frequency. For example, the maximum ME coefficient values of these 2-2 laminate composites are about 100 mV/cm Oe order of magnitude in the low-frequency range, which are comparable to those for the PZT/ferrite ceramic composites; but reach up to several V/cm Oe at resonance.

A similar dependence of the ME effect of the composites on the volume fraction f_P of the polymer is also observed. $f_P<0.3$, the low quality of the samples due to low concentration of the polymer binder leads to the large loss of stress/strain transfer from the *T*-layer to the *P*-layer and thus low ME response. As $f_P>0.5$, the ME coefficient also declines with the increase in f_P. This decrease is attributed to the decrease in the concentration of the piezoelectric phase and magnetostrictive phase, which lead to low magnetostrictively induced strain and low piezoelectricity of the composites.

In comparison with the quasi-0-3-type particulate composites, these quasi-2-2-type laminate composites exhibit higher the ME effect. The ME response of the three-phase polymer-based laminate composites could be further improved by optimization of their structures, and processing; and would be an important smart multiferroic material for magnetic-electric devices.

Recently, it has been reported that a simple bilayered composite containing thin PZT ceramic chip and Terfenol-D/epoxy layer has large capacitance and large ME charge output of about 300 pC/Oe at the resonance frequency.[78] Three resonance modes including the first-order flexural mode, second-order flexural mode, and radial mode, have been observed in this simple three-phase composite bilayer. The measured phase spectra showed a significant phase change around each resonance frequency. The thinner PZT chip is benefit for higher flexural resonance ME effect. The ME effects measured under open and short electric boundary conditions show different behaviors.

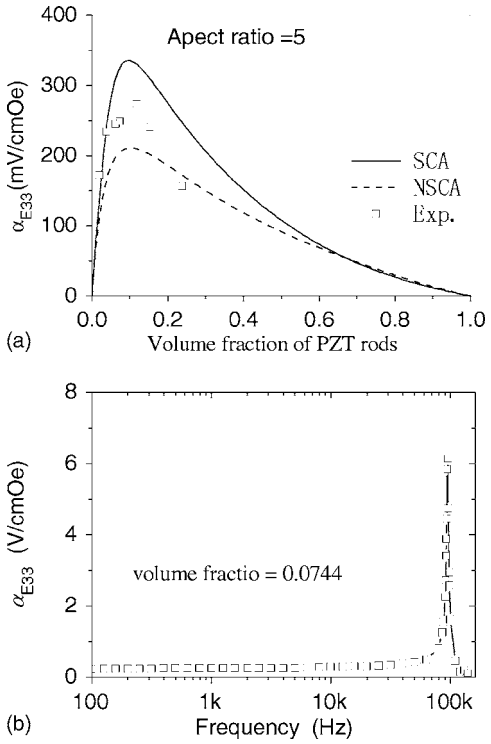

FIG. 37. Variation in the ME coefficient of the pseudo-1–3-type multiferroic composites with (a) the volume fraction of PZT rods at low frequency and (b) frequency, at 2 kOe bias field. Solid and dashed lines in (a) are calculated results by SCA and NSCA [after Shi *et al.* (Ref. 76)].

C. Quasi-1-3-type rod-array composites

Besides 0-3 and 2-2 structures, the 1-3 structure, i.e., a fiber (or rod) reinforced composite, is another important structure. As for the 1-3 piezoelectric composites,[18] such 1-3 multiferroic ME composite[76,77] can be prepared via a dice-and-fill process. According to the designed volume fraction of PZT rods, a PZT bulk is diced to get a PZT rod array, and then the gap of the PZT rod array is filled with a mixture of Terfenol-D particles and epoxy. When the epoxy hardens, the pseudo-1-3-type multiferroic composite is obtained [see the inset of Fig. 37(a)].

The dependence of the ME coefficients on the volume fraction f_{PZT} of PZT rods is presented in Fig. 37(a). The calculations and experiments all show that the ME coefficient increases with increasing f_{PZT} due to the increasing piezoelectric effect. After reaching a maximum, the ME coefficient decreases when $f_{PZT}>0.1$. This decrease is attributed to the decrease in the volume fraction of the magnetostrictive Terfenol-D/epoxy matrix. The maximum α_{E33} reaches about 300 mV/cm Oe at 2 kOe, which is comparable with that for the pseudo-2-2-laminate ME composites and larger than that for the 0-3 particulate ME composites.

Figure 37(b) is a typical frequency dependence of the ME coefficient of the pseudo-1-3-type multiferroic composite with $f_{PZT}=0.0744$. A GME coefficient of about 6.2 V/cm Oe at 90 kHz is observed. This GME effect at high frequency is also attributed to the piezoelectric resonance which significantly enhances the magnetic-mechanical-electric coupling between matrix and rods. The transverse ME coefficient of such 1-3–type ME composites

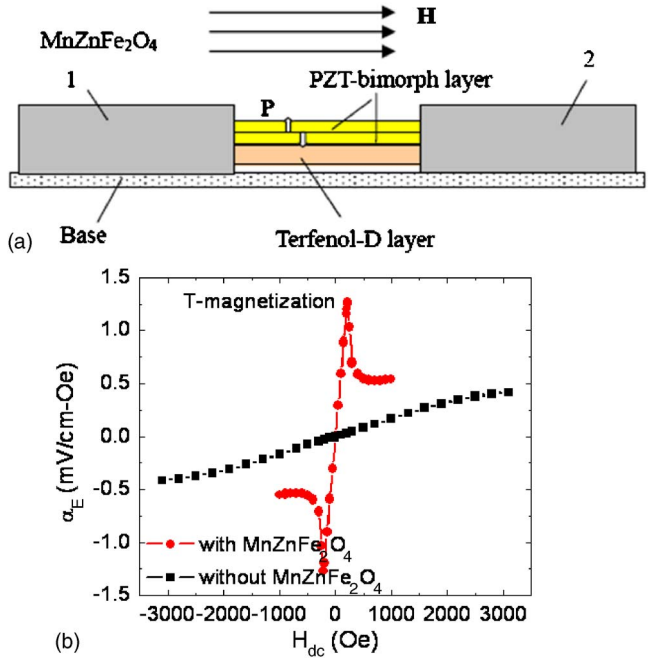

FIG. 38. (Color online) (a) Configuration of three-phase $MnZnFe_2O_4$/Terfenol-D/PZT laminate; (b) the effect of high-μ phase on its ME voltage coefficient [Dong *et al.* (Ref. 174)].

is lower than the longitudinal one in the test frequency range, resulting from the large anisotropy of the rod reinforced composites.[76,77]

D. Other three-phase composites

Other three-phase ME composites have also been available. In the Terfenol-D based composites above, a high magnetic field is needed to achieve a maximum ME coefficients, which is due to the low magnetic permeability μ_r of the Terfenol-D alloys. Typically, μ_r in magnetostrictive Terfenol-D or Fe–Ga is as low as 3–10. However, by incorporating a third phase ferromagnetic layers with a high-permeability into Terfenol-D/PZT laminates, the effective permeability of the resultant three-phase ME composites can be dramatically increased, which in turn results in a larger effective piezomagnetic coefficient and thus a stronger ME coupling at lower magnetic field. For example, Fig. 38(a) illustrates a configuration of three-phase $MnZnFe_2O_4$/Terfenol-D/PZT laminate.[174] The comparison in Fig. 38(b) clearly shows the largely enhanced ME effect in the three-phase composite due to the incorporation of high-permeability $MnZnFe_2O_4$ layers.

VI. NANOSTRUCTURED COMPOSITE THIN FILMS

Recently, motivated by a pioneer work of Zheng *et al.*,[79] multiferroic nanocomposite thin films of ferroelectric [e.g., BTO, PTO, PZT, and $BiFeO_3$ (BFO)] and magnetic oxides (e.g., CFO, NFO, and LCMO) prepared via physical deposition techniques [e.g., pulsed laser deposition (PLD)] and chemical solution processing (e.g., sol-gel spin-coating method) have become new routes to multiferroic ME composites.[94] In comparison to bulk multiferroic ME composites, the nanostructured thin films provide more degrees of freedom, such as lattice strain or interlayer interaction, to modify the ME behavior. It also offers a way to investigate the physical mechanism of ME effect in nanoscale. The coupling interaction between two oxides in the multiferroic nanostructures is still due to elastic interaction as was the case in bulk composites. However, the mechanical constraint arising from the film on substrate and the good bonding between the two phases in the nanostructurd composite films could significantly affect the ME coupling interactions.

Similarly to bulk ceramic composites shown in Fig. 1, according to the microstructure of the nanostructured composite films, there are also three kinds of nanostructured composite films, i.e., (1) 0-3–type structures with magnetic spinel nanoparticles (e.g., CFO and NFO) embedded in the ferroelectric films (e.g., PZT), (2) 1-3–type heterostructures (vertical heterostructures) consisting of magnetic spinel pillars (e.g., CFO) vertically embedded into a ferroelectric films (e.g., BTO, PTO, or BFO), and (3) 2-2–type heterostructures (horizontal nanostructures) consisting of alternating layers of a ferroelectric perovskite and magnetic oxide.

Few works were reported on the 0-3–type nanostructure.[82,90] Wan *et al.*[82] prepared a PZT-CFO composite thin film using a sol-gel process and spin-coating technique. The phase separation of the CFO and PZT phases in the films was verified by x-ray diffraction. The films exhibited both good magnetic and ferroelectric properties, and the ME effect of these films was found to be strongly dependent on the magnetic bias and magnetic field frequency. In comparison, more publications were reported on 1-3 and 2-2 heterostructures.

A. 1-3–type vertical heterostructures

The prototypical 1-3 vertical heterostructure consists of a magnetic spinel phase epitaxially embedded into the ferroelectric matrix. The first example was reported by Zheng *et al.*,[79] where arrays of magnetic CFO nanopillars with diameters of 20–30 nm were embedded in a ferroelectric BTO matrix films (Fig. 39). Other different combinations of $PbTiO_3$–$CoFe_2O_4$ and $BiFeO_3$–$CoFe_2O_4$ have also been grown on $SrTiO_3$ single crystal substrates. The morphologies of the component phases in such vertical composite films containing either magnetic or ferroelectric nanopillars vary markedly with the substrate orientation and phase fractions,[87,88,175] as was inferred from their microscopy observations. However, the design and control of such heterostructures remain a challenge.

Recent work has demonstrated substantial ME coupling in such nanostructures, through switching of the magnetization on reversal of the ferroelectric polarization,[81,176] which was attributed to (1) a reduced clamping effect by the substrate in the vertical architecture, and (2) efficient strain coupling resulting from a larger interfacial surface area and intrinsically heteroepitaxial in three dimensions. Detailed studies suggest that the switching is mediated by strong mechanical coupling between the two lattices, which leads to a time dependent modulation of the magnetic anisotropy in the nanopillars. But controllable switching of the magnetization

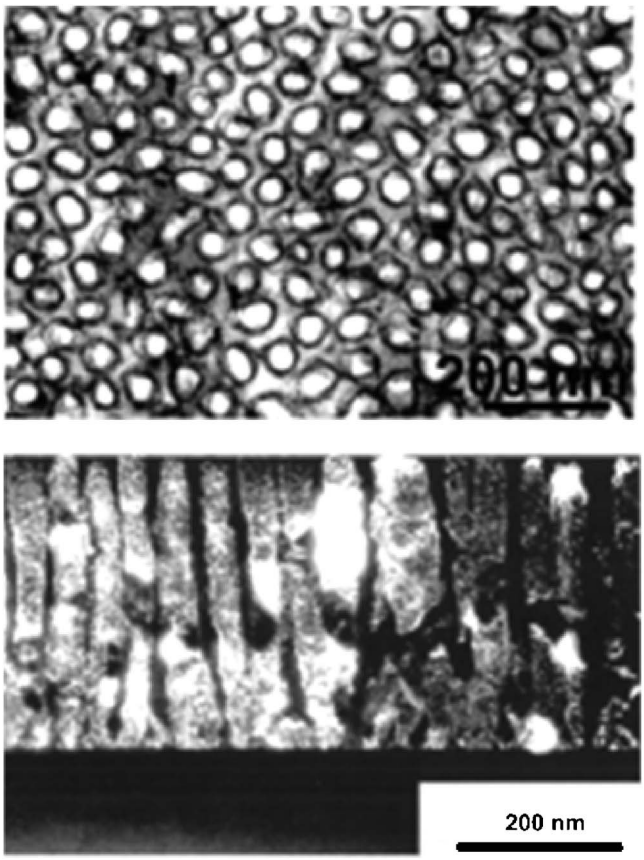

FIG. 39. Plan view TEM image and cross-sectional dark field TEM image of $CoFe_2O_4$ nanopillars embedded in the $BaTiO_3$ matrix [Zheng *et al.* (Ref. 80)].

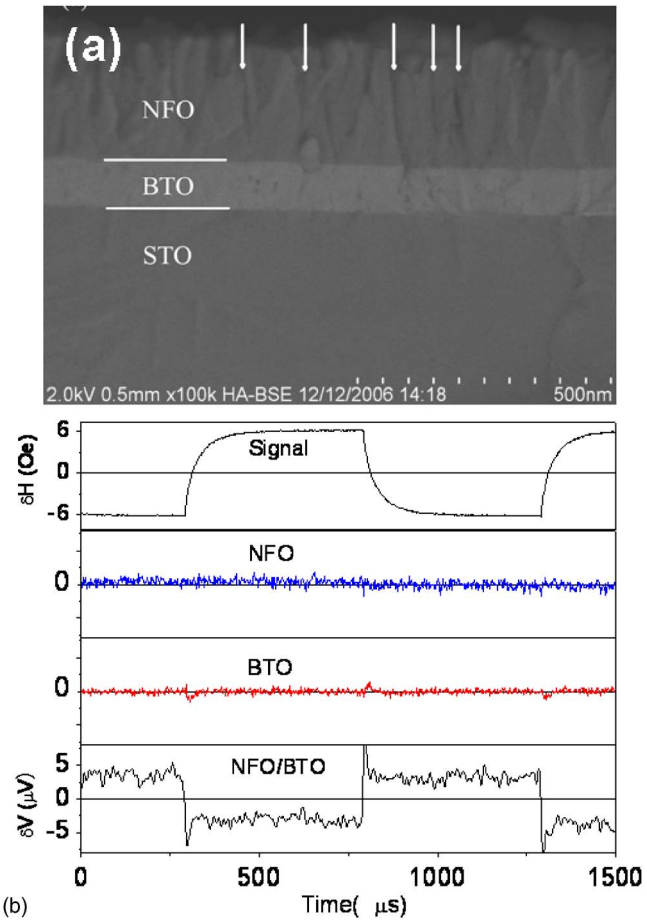

FIG. 40. (Color online) (a) A cross-sectional SEM image of the heterostructured NFO/BTO composite film grown in STO substrate; and (b) the ME response (induced ME voltage δV) of this film when the in-plane magnetic field is applied (ac magnetic field δH at 1 kHz with a bias magnetic field of 100 Oe). For comparison, the results for pure NFO and BTO films are also shown [Deng *et al.* (Ref. 177)].

can only be achieved if an additional weak magnetic field is superimposed to lift the time-reversal symmetry.

Although the ME coupling has been observed via microscopy in such vertical nanostructures,[81,176] through switching of the magnetization on reversal of the ferroelectric polarization, the ME coefficients could not be directly measured in the 1-3–type vertical heterostructures because of leakage problem resulting from low resistance of the magnetic pillars penetrating through the films or the magnetic matrix. The leakage problem would erase the promising direct ME effect in the vertical nanostructures.

B. 2-2–type horizontal heterostructures

In comparison with the vertical nanostructures, the 2-2–type horizontal heterostructures exhibit weak ME effects due to large in-plane constraint from substrates.[117] But the horizontal nanostructures are more easier to be fabricated, and rule out the leakage problem due to the ferroelectric layers shutting off circuit, which could lead to visible ME effect.

Murugavel *et al.*[83] and Singh *et al.*[84] reported $BaTiO_3$–$Pr_{0.7}Ca_{0.3}MnO_3$ perovskite superlattices grown on $SrTiO_3$ via PLD. Their studies found that the impedance and capacitance of the films varied with the applied magnetic field due to the ME coupling in the nanostructures. A negative magnetocapacitance value of 3 % / T at 1 kHz and 100 K was demonstrated.

Different 2-2–type combinations of ferroelectric perovskites (e.g., BTO, PZT) and magnetic oxides (e.g., $CoFe_2O_4$, $NiFe_2O_4$, and $La_{1.2}Sr_{1.8}Mn_2O_7$) have also been grown via PLD and sol-gel spin-coating method.[85,86,92,93] These layered films showed good coexistence of ferroelectric and ferromagnetic behaviors. For example, Fig. 40 shows a simple bilayer BTO-NFO nanocomposite film, and the measurements illustrate obvious ME response of the heterostructured film.[177] As seen from Fig. 40, when an in-plane alternating magnetic field signal δH is applied, the single-phase BTO and NFO films do not produce any ME output δV, by comparison, the heterostructured NFO/BTO film clearly yields the ME output following the switch of the magnetic excitation signal δH. The observation of the ME coupling in the heterostructures can only be achieved as a weak ac magnetic field δH is superimposed to lift the time-reversal symmetry.

In particular, a special horizontal heterostructure has been recently constructed by growing an epitaxial ferroelectric PZT film on a magnetostrictive layered manganite single crystal of composition LSMO,[89] and inversely, an epitaxial magnetic $LaCa(Sr)MnO_3$ film on a ferroelectric single crystals (e.g., $BaTiO_3$ and PMN-PT).[91,178] The efficient mechanical coupling at the interface results in a remarkable ME effect in such special horizontal heterostructures.

For example, in this PZT-film-on-LSMO structure,[89] the manganite crystal serves as the substrate for the PZT film growth, as the magnetostrictive element and as the bottom electrode in the device. Without the constraint from conventional substrates, such a geometry maximizes the efficiency of in-plane transfer of the magnetostrictive strain from LSMO to the PZT film. A large ME effect is observed at T_C (about 105 K) of LSMO where it exhibits the highest magnetostrictive sensitivity (0.13%) to an applied magnetic field, i.e., magnetically induced an abrupt 7.3% increase in switchable polarization of the PZT film.[89] This modulation of polarization originates from the contraction of the in-plane lattice parameters of LSMO at T_C. Most recently, Eerenstein *et al.*[91] have reported an epitaxial magnetic LSMO film on BTO single crystal and achieved sharp and persistent converse ME effect. In the LSMO-film-on-BTO structure, an applied electric field modifies the ferroelectric domain structure of the BTO substrate, and then the switching of BTO domains alters in LSMO the local strain, magnetic anisotropy, and thus the magnetization.

C. Theoretical modeling

In theoretical analyses, some characteristics of films, e.g., giant residual stress/strain resulting from the lattice misfit between the film and substrate and spontaneous polarization in epitaxial films, have been considered to understand the ME response in nanostructured films.[117] As a result, the constitutive equations for the coupling magnetic-mechanical-electric interactions in the nanostructured films can be expressed as

$$\boldsymbol{\sigma} = \boldsymbol{c}\boldsymbol{\varepsilon} - \boldsymbol{e}^T\boldsymbol{E} - \boldsymbol{c}\boldsymbol{\varepsilon}^{\mathrm{ms}} - \boldsymbol{\sigma}_s,$$

$$\boldsymbol{D} = \boldsymbol{e}\boldsymbol{\varepsilon} + \boldsymbol{\kappa}\boldsymbol{E} + \boldsymbol{\alpha}\boldsymbol{H} + \boldsymbol{P}_s,$$

$$\boldsymbol{B} = \boldsymbol{\mu}(\boldsymbol{\varepsilon},\boldsymbol{E},\boldsymbol{H})\boldsymbol{H} + \boldsymbol{M}_s. \quad (24)$$

In comparison to the constitutive equations for bulk composites, the residual stress $\boldsymbol{\sigma}_s$ (or residual strain $\boldsymbol{\varepsilon}_s$), spontaneous polarization $\boldsymbol{P}_s$ and magnetization $\boldsymbol{M}_s$ are incorporated for the multiferroic composite films. Based on the modified constitutive equations, the ME coupling interaction and magnetically induced polarization for nanostructured composite films were firstly calculated using Green's function technique.[117] It was revealed that the 1-3–type vertical heterostructures could exhibit large ME response which is even larger than that in their bulk counterparts if there is no leakage problem, while the 2-2–type horizontal heterostructures show much weaker ME coupling due to large in-plane constraint effect. Most recently, the calculations for the ME effects in nanobilayers, nanopillars, and nanowires of nickel ferrite and PZT on MgO substrates or templates have also shown that the ME coupling decreases with increasing substrate clamping.[179]

Because the magnetostriction of the magnetic phase can dynamically change the strain constraint in the nanostructured composite films, the magnetically induced polarization could also be calculated from the Landau–Ginsburg–Devonshire phenomenological thermodynamic theory,[118,121]

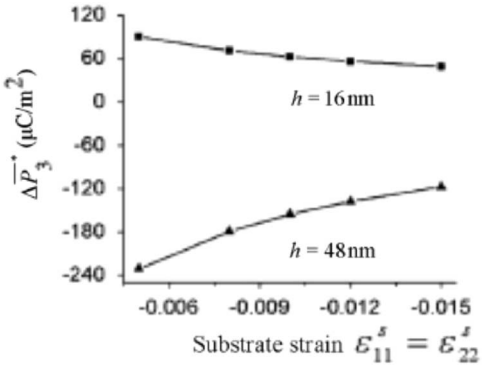

FIG. 41. Dependence of magnetic-field-induced electric polarization ΔP_3 on the substrate strains (h is the thickness of the film, the distance between neighboring magnetic pillars is d=64 nm, and the volume fraction of the magnetic pillars is 0.35) [Zhang *et al.* (Ref. 120)].

where the boundary conditions are related to the magnetic field. This method was found to yield some similar results to those using Green's function technique,[118] i.e., the calculation results showed that the 1-3–type nanostructured composite films exhibit a large ME coefficient, but the 2-2–type films exhibit much weaker ME coefficient due to large in-plane constraint.

A powerful approach, phase-field model, in which the elastic energy in the constrained thin film was incorporated including the effect of free film surface and the constraint from the substrate, has been recently developed for studying the ME coupling effect in the 1-3 nanocomposite thin films.[120] The phase-field calculations of the magnetic-field-induced electric polarization in 1-3–type $BaTiO_3$–$CoFe_2O_4$ nanocomposite film give similar results to Green's function technique. The phase-field simulation illustrates that the magnetic-field-induced electric polarization is highly dependent on the film thickness, morphology of the nanocomposite, and substrate constraint, which provide a number of degrees of freedom in controlling coupling in nanocomposite films, as shown in Fig. 41.

Recently, by first-principles density functional calculations of a model Fe/$BaTiO_3$ horizontal superlattice, Duan *et al.*[119] have demonstrated a ME effect in such a multiferroic heterostructure that arises from a purely electronic hybridization between Ti and Fe atoms, not mediated by strain. Thus this ME effect is driven by the coupling between ferroelectricity and magnetism through interface bonding. The displacement of atoms at the interface caused by ferroelectric instability alters the overlap between atomic orbitals at the interface, which in turn affects the interface magnetization, resulting in a ME effect. In this case, the ME effect is confined to the interface and represents a change of the interface magnetic moment at the coercive field of the ferroelectric. Such a ME effect, they argue, should be possible in both vertical and horizontal heterostructures. However, this remains in need of experimental verification.

VII. APPLICATIONS

So far only the bulk ME composites discussed above exhibit large ME effects above room temperature, which can exceed the intrinsic ME effect in single-phase compounds by

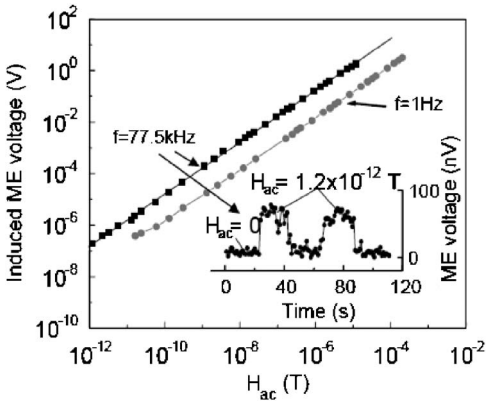

FIG. 42. Limit magnetic field sensitivity of Terfenol-D/PMN-PT ME laminate [Dong *et al.* (Ref. 166)].

many orders of magnitude. Thus the ME composites are ready for technological applications. Promising applications include magnetic field sensors (thus complementing Hall sensors and current measurement probes), transducer, filters, oscillators, phase shifters, memory devices, and so on. Since the magnetic field input is required to have two components, a dc bias and an ac probe, either of the two can be detected by providing the other component. The ME composite can thus be used as a magnetic probe for detecting ac or dc fields. At the resonance frequency the ME composite can be used as a transducer which converts the microwave magnetic field into a microwave electric field. Because of the shift in the resonance frequency in a static magnetic or electric bias field the composite materials hold promise in electrically tunable microwave applications such as filters, oscillators, and phase shifters. Due to the hysteretic nature of the ME effect, the composites may find applications in memory devices.[3] The linear ME effect has a positive or a negative sign, depending on the annealing conditions (parallel or antiparallel magnetic and electric fields). Thus the coupling could, in principle, permit data to be written electrically and read magnetically in memory technologies.

A. Magnetic sensors

The working principle of magnetic sensing in the ME composites is simple and direct.[180] When probing a magnetic field, the magnetic phase in the ME composites strains, producing a proportional charge in the piezoelectric phase. Highly sensitive magnetic field sensors can be obtained using the ME composites with high ME coefficients. The ME composites can be used as a magnetic probe for detecting ac or dc fields.

1. ac magnetic field sensors

Figure 42 shows the voltages induced across the two ends of a PMN-PT layer in a push-pull ME Terfenol-D/PMN-PT/Terfenol-D three-layer laminate [see Fig. 24(f)] as a function of ac magnetic field (H_{ac}) at drive frequencies of (i) $f=1$ kHz and (ii) $f=77.5$ kHz under a given H_{dc}. In this figure, the induced ME voltage can be seen to have a linear response to H_{ac} over a wide range of fields from $10^{-11} < H_{ac} < 10^{-3}$ T.[49,164,166] When the laminates were operated under resonance drive, an enhancement in sensitivity to small magnetic field variations was observed. The sensitivity limit of the ME laminates at ambient conditions was 1.2×10^{-12} T.[166] These results unambiguously demonstrate that ME laminates have an ultrahigh sensitivity to small ac magnetic field variations.

Apart from a bimorph,[164] a multilayer configuration[57] of ME laminates has been reported that enables ultralow frequency detection of magnetic field variations. This multilayer ME laminate is illustrated earlier in Fig. 24(h). This configuration can greatly improve the low-frequency capability because of its high ME charge coupling and large capacitance. Figure 43 shows the magnetic field induced voltages for multilayer Terfenol-D/PMN-PT ME laminates at frequencies of 100, 1, and 0.01 Hz. At an extremely low frequency of $f=10$ mHz, the multilayer ME laminates can still detect a small magnetic field variation as low as 10^{-7} T.

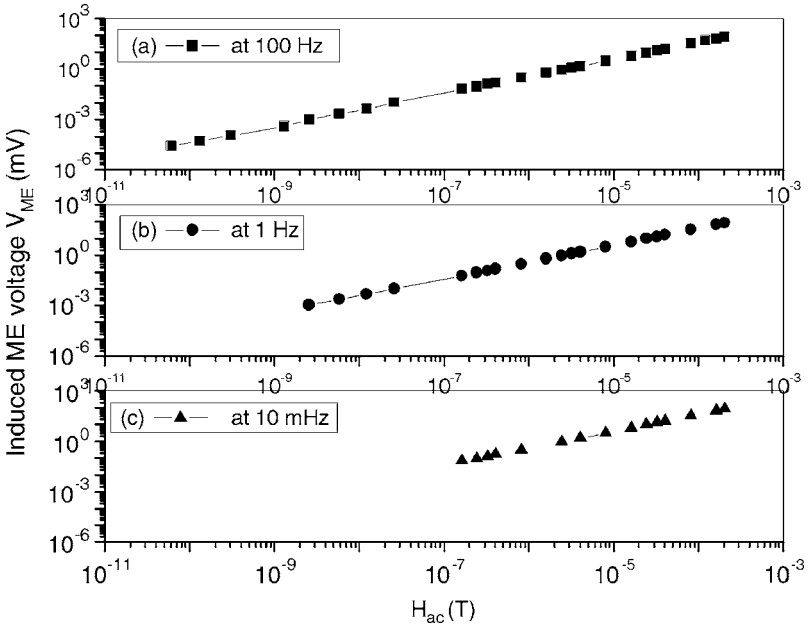

FIG. 43. Low-frequency response of a multi-*L-T* Terfenol-D/PMN-PT laminate [Dong *et al.* (Ref. 57)].

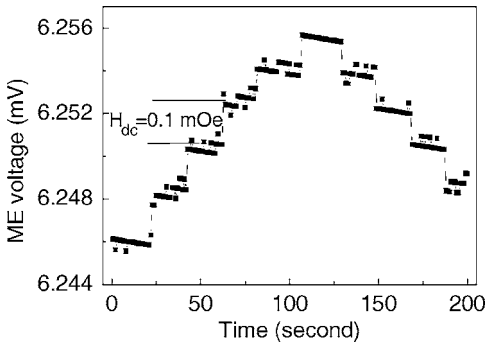

FIG. 44. Sensitivity limit of an *L-T* ME laminate to small dc magnetic field variations under resonant drive [Dong *et al.* (Ref. 61)].

2. dc magnetic field sensors

It has also been reported that small dc magnetic field variations can be detected using ME laminates based on magnetic bias effect[61] or inverse ME effect.[181,182] In fact, small long-type ME laminates of Terfenol-D and PZT are quite sensitive to small H_{dc} variations, when driven under a constant H_{ac}. The sensitivity limit is about 10^{-7} T using a constant amplitude low frequencies drive, which can be enhanced to 10^{-8} T under resonant drive.[61] Figure 44 shows the sensitivity limit of an *L-T* ME laminate to small dc magnetic field variations, while under resonant drive. It can be seen that dc magnetic field changes as small as 10^{-8} T were readily detected.

3. ME current sensors

The ME composites have also been shown to be good candidates for electric current sensors. A straight wire containing ac or dc current I will excite an ac or dc vortex magnetic field H_{vor} around this wire: $H_{vor}=I/\pi r$, where r is radius of the vortex magnetic field. Accordingly, ring-type ME laminates[53,54,58] are ideal configurations for vortex magnetic field detection, or current I detection. Previously, a ME ring-type laminate (see Fig. 27) has been made of a circumferentially magnetized Terfenol-D and a circumferentially poled piezoelectric PZT (or PMN-PT), which was shown to have a high ME sensitivity of up to 5.5 V/cm Oe at f =1 kHz to a vortex magnetic field. Figure 45(a) illustrates this ring-type ME laminate used as an electric current sensor, and Fig. 45(b) shows the ME voltage response to a square-wave current passing through the wire. Detection using a toroidal type variable reluctance coil (100 turns) exhibited a much smaller induced voltage (by a factor of 0.01 times) than that of this ME ring sensor.

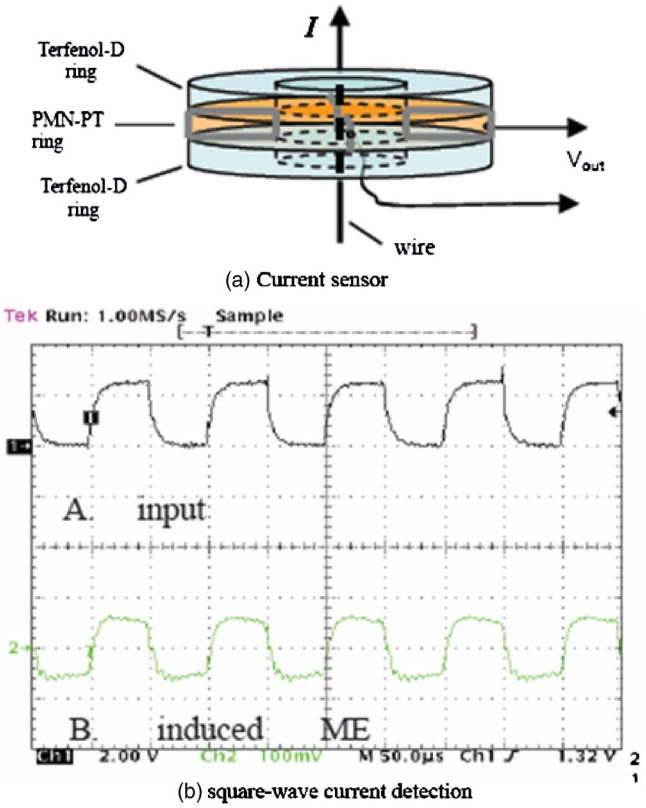

FIG. 45. (Color online) ME current sensor [Dong *et al.* (Ref. 58)].

B. Transformers and gyrators

ME transformers or gyrators have important applications as voltage gain devices, current sensors, and other power conversion devices. An extremely high voltage gain effect under resonance drive has been reported in long-type ME laminates consisting of Terfenol-D and PZT layers.[55,56] A solenoid with n turns around the laminate that carries a current of I_{in} was used to excite a H_{ac}. The input ac voltage applied to the coils was V_{in}. When the frequency of H_{ac} was equal to the resonance frequency of the laminate, the magnetoelectric voltage coefficient was strongly increased, and correspondingly the output ME voltage (V_{out}) induced in the piezoelectric layer was much higher than V_{in}. Thus, under resonant drive, ME laminates exhibit a strong voltage gain, offering potential for high-voltage miniature transformer applications.

Figure 46 shows the measured voltage gain V_{out}/V_{in} as a function of the drive frequency for a ME transformer consisting of Terfenol-D layers of 40 mm in length and a piezoelectric layer of 80 mm in length. A maximum voltage gain of ~260 was found at a resonance frequency of 21.3 kHz. In addition, at the resonance state, the maximum voltage gain of the ME transformer was strongly dependent on an applied H_{dc}, which was due to the fact that Terfenol-D has a large effective piezomagnetic coefficient only under a suitable H_{dc}.

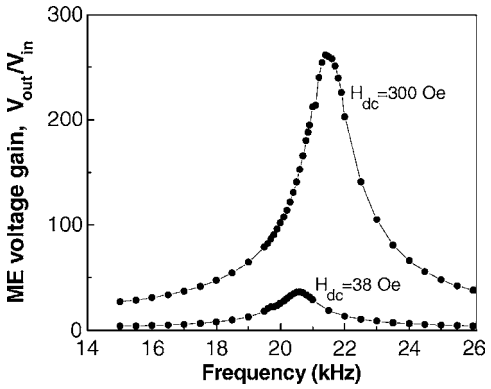

FIG. 46. Voltage gain of ME transformer as a function of the drive frequency [Dong *et al.* (Ref. 55)].

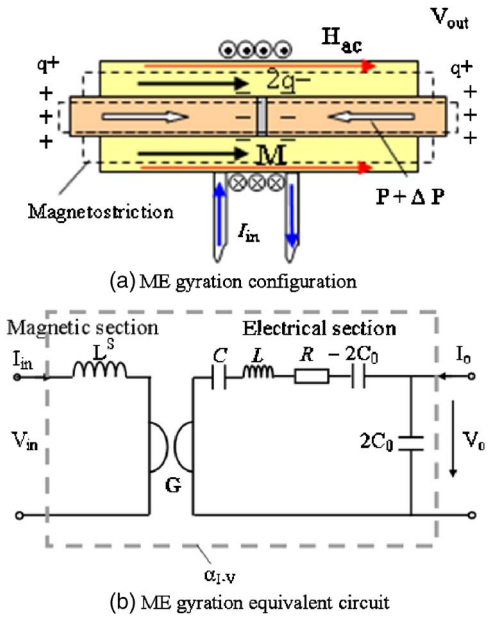

FIG. 47. (Color online) ME gyrator: (a) ME gyration configuration, and (b) ME gyration equivalent circuit [Dong *et al.* (Ref. 65)].

Other reports have shown that a ME laminate with a coil carrying current I_{in} has a unique current-to-voltage (I-V) conversion capability. ME laminates actually act as a I-V gyrator, with a high I-V gyration coefficient G.[65,66] Figure 49(a) illustrates the ME gyrator's configuration and Fig. 47(b) shows its ME gyration equivalent circuit. At electromechanical resonance, the ME gyrator shows a strong I-V conversion of ~2500 V/A, as shown in Fig. 48. We also observed (i) reverse gyration: an input current to the piezoelectric section induced a voltage output across coils, and (ii) impedance inversion: a resistor R_i connected in parallel to the primary terminals of the gyrator resulted in an impedance G^2/R_i in series with the secondary terminals.

C. Microwave devices

Since the composite ME effect is a "dynamic" effect, i.e., a pronounced linear ME response is only observed for an ac field oscillating in the presence of a stronger dc bias field, the composite ME effect is thus predetermined for microwave applications. Different frequency ranges are accessed

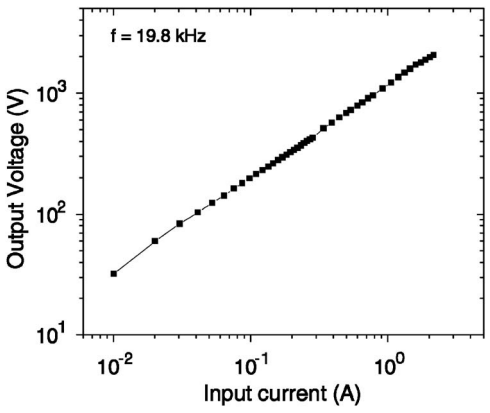

FIG. 48. I-V gyration of the ME gyrator [Dong *et al.* (Ref. 65)].

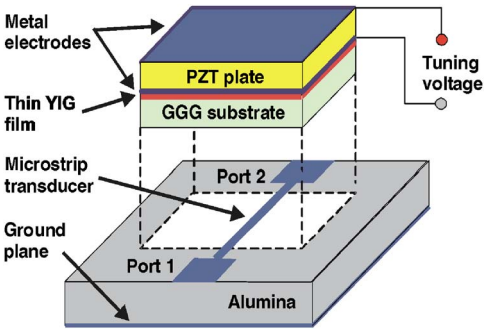

FIG. 49. (Color online) Example of a magnetic YIG film grown on gadolinium gallium garnet substrate and PZT electric field tunable microwave magnetic strip line device [Fetisov *et al.* (Ref. 189)].

by using the enhancement from the electromechanical resonance (~100 kHz), the ferromagnetic resonance (~10 GHz), or the antiferromagnetic resonance (~100 GHz). Among the ME ceramic composites (e.g., ferrite-piezoelectric ceramic composites) represent a promising new approach to build a new class of fast electric field tunable low power microwave devices. An electric field E applied to the piezoelectric transducer produces a mechanical deformation that couples to the ferrite and produces a shift in the resonance field.[127,183–185] Unlike the situation when magnetic fields are used for such tuning, the process is fast because there are no inductors, and the power budget is small because the biasing voltages involve minimal currents. This process has been demonstrated with ferromagnetic resonance and spin wave delay lines.[153,186–195] The critical goal for the future is in the development of a wide class of efficient wide band and low loss electrically tunable magnetic film devices for battlefield radar, signal processing, and secure and experimental evaluation of characteristics. The anticipated advantages of ME devices are yet to be exploited.

1. Tunable devices

In the microwave region of the electromagnetic spectrum, the ME effect can be observed in the form of a shift in FMR profile in an external electric field E.[127,183,184] The response can be realized with a device similar to the one shown in Fig. 49, i.e., a device concept based ferrite-piezoelectric microwave resonator that is dual electric and magnetic field tunable. Mechanical stress in the PZT layer due to the electric field is coupled to the ferrite, and this leads to a shift δH_E in the FMR resonance field.[189]

Figure 50 shows the data on the resonance field shift as a function of E for a bilayer of epitaxial YIG film and PMN-PT single crystal. The field shift δH_E converts to an equivalent frequency shift of about 3 MHz/Oe. This ME shift is determined by piezoelectric coupling, taken as d, and the magnetostriction λ. A large d and a large λ lead to a strong electric field induced shift. The data in Fig. 50 also provide the basis for a wide variety of *electric field tunable* FMR-based and spin wave based YIG signal processing devices.

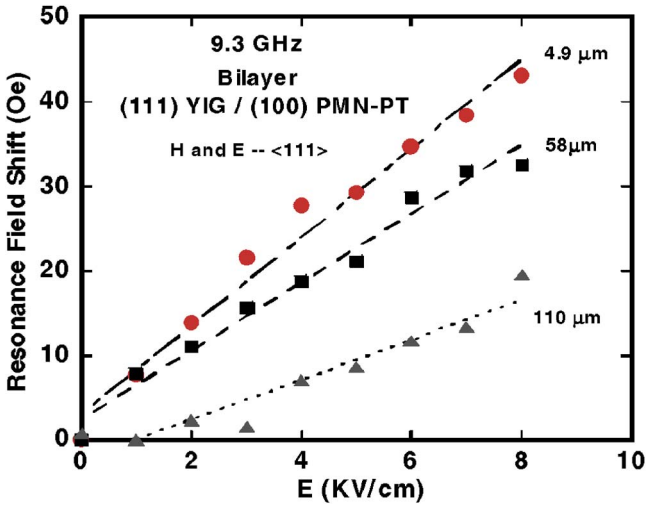

FIG. 50. (Color online) Data on FMR field shift vs electric field E for a YIG/PMN-PT bilayer [Tatarenko *et al.* (Ref. 186)].

2. Resonators

The device in Fig. 49 is a basic YIG/piezoelectric resonator. Such devices are useful in frequency selective microwave devices such as bandpass or band-stop filters.[186,190] The addition of the piezoelectric gives this important class of devices electric field tunability as shown above. Much work is needed if structures such as the one in Fig. 49 are to become viable components in real systems. This device can also serve as an ideal "test bed" for the selection of materials and device configurations for the full range of electric field tunable FMR and spin wave devices enumerated above. There are, for example, several issues.

(1) Options for different magnetic film components. Substituted YIG films can be used with higher magnetizations to cover different frequency ranges. Different substitutions also can give more or less of a ME interaction and better or worse tuning. Zinc substituted spinel ferrite can be used to achieve very high magnetizations for the low millimeter wave frequency range, and hexagonal ferrite[153] films can be used for frequencies up to 100 GHz or so.
(2) Options for different piezoelectric and ferroelectric layer components. There are many other options for the electric layers, including single crystal PMT-PT, PZT, and barium strontium titanate.
(3) Interplay of magnetic/electric/interface property loss and high power capabilities. Electric field tunability of FMR and spin wave devices may come at a price. It is clear that there will be interface modes. In the case of layered devices of the sort in Fig. 49, these effects can be controlled to some extent through the use of different bonding methods and materials.
(4) Tuning: It is well known that for basic magnetic film FMR and spin wave based microwave devices, one can also tune the frequency of operation by changing the direction of the field relative to the film plane or the direction of spin wave propagation. The field for the data shown above was applied perpendicular to the YIG film in Fig. 49. It is known that the magnetic loss can depend on the field orientation. The effect of field orientation on the ME coupling and the tunability remain to be determined.
(5) Speed of tuning: The obvious advantage of electric field tunability is speed. What are the limits? How can they be achieved in a useful device? What if the electric field tunability could be as fast as the microwave signal itself? This could lead to an entire class of completely new devices.

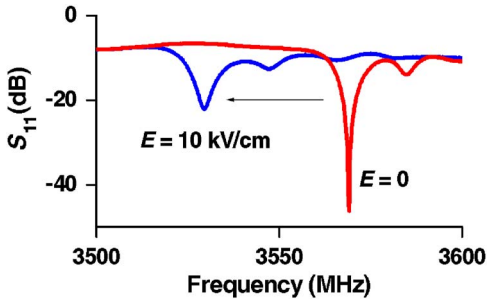

FIG. 51. (Color online) Electric field tunable 13 μm YIG/PMN-PT resonator with perpendicular magnetization (H=3010 Oe). The frequency shift is −50 MHz for E=10 kV/cm [Tatarenko *et al.* (Ref. 190)].

Figure 51 shows representative FMR data for YIG/PMN-PT with an electric field across PMN-PT. These data were with the static magnetic field perpendicular to the YIG film. The field shift in this case is negative as the electric field is applied. If the static field is in plane, it turns out that the shift is positive. The tuning shown in Fig. 51, with a δH_E of about 50 MHz, is obtained for an electric field of 10 kV/cm. This tuning is more than five times the width of FMR linewidth in the YIG film and is more than adequate for a variety of device applications. With optimized choices for the electric layer and the electric field, one should be able to obtain a tuning range of 0.5–1 GHz and an insertion loss of a few decibels at most.

3. Filters

The single-cavity ME filter,[190] shown in Fig. 52, consists of a 1 mm thick dielectric ground plane (permittivity of 10), input and output microstrips of nonresonance lengths, and a ME element. Power is coupled from input to output under FMR in the ME element. The ME element consisted of epitaxial YIG film bonded to PZT. A 110 μm thick YIG film grown by liquid-phase epitaxy on a (111) gadolinium gallium garnet was used. A PZT plate with the dimensions $4\times1\times0.5$ mm^3 was initially poled by heating up to 150 °C and cooling back to room temperature in an electric field of 10 kV/cm perpendicular to the sample plane. The layered structure was made by bonding the YIG film surface to PZT with 0.08 mm thick layer of ethyl cyanoacrylate, a fast-dry epoxy. The layered structure was placed between of the transducers as in Fig. 52 and was subjected to a field H parallel to the sample plane and perpendicular to the microstrips.

An input continuous-wave signal $P_{\text{in}}(f)=1$ mW was applied to the filter. The frequency dependence of the insertion loss L, i.e., the transmitted power through the ME element,

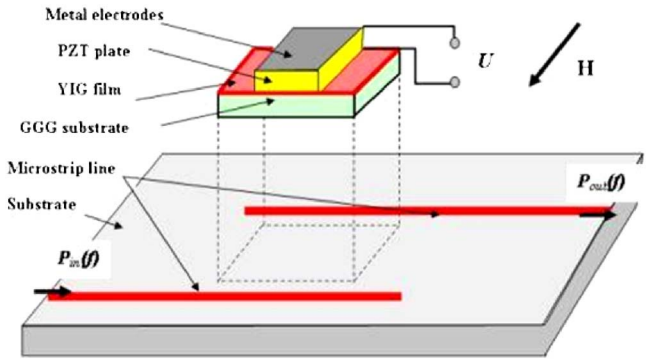

FIG. 52. (Color online) Diagram showing a microwave ME filter [Tatarenko *et al.* (Ref. 190)].

was measured at 4–10 GHz as a function of H and E applied across the PZT layer. Representative results are shown in Fig. 53. Consider first the profile for $E=0$. The maximum input-output coupling is observed at $f_r=6.77$ GHz that corresponds to FMR in YIG for an in-plane $H=1.7$ kOe, $4\pi M=1.75$ kG, and gyromagnetic ratio $\gamma=2.8$ GHz/kOe. The loss increases sharply below f_r and the off-resonance isolation is 20–25 dB. Above f_r, secondary maxima due to magnetostatic modes are seen in Fig. 53. A significant modification of frequency dependent L profile is observed (Fig. 53) when $E=1$ kV/cm is applied across PZT. f_r is downshifted by 28 MHz. The shift arises due to strain at YIG-PZT interface caused by the piezoelectric deformation in PZT. Further increase in E results in increase in the magnitude of the downshift, as shown in Fig. 53. An upshift in f_r can be observed when the direction of E was reversed by reversing the polarity of applied voltage, and is attributed to a switch from compressive to tensile strain in YIG. Thus, a microwave ME filter based on YIG/PZT layered structure has been designed and characterized. This filter can be tuned by 2% of the central frequency with a nominal electric field of 3 kV/cm.

4. Phase shifters and delay lines

A useful microstrip line structure for phase shift and delay time measurements is shown in Fig. 54.[187] We used YIG/piezoelectric elements and measured their phase shift, delay time, and E-field tunability. The bias field H is applied parallel to the transducer to excite magnetostatic surface wave

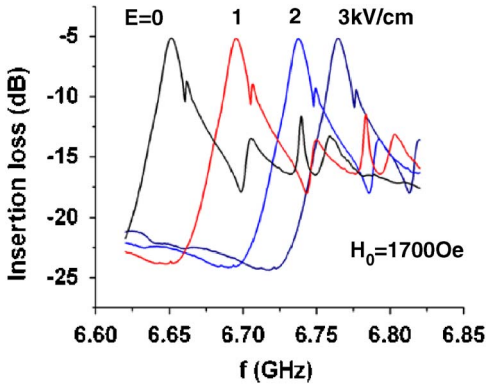

FIG. 53. (Color online) The transmission characteristics for ME microwave filter [Tatarenko *et al.* (Ref. 190)].

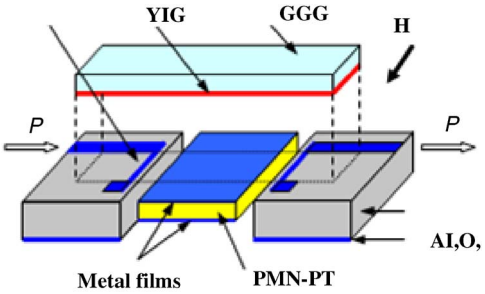

FIG. 54. (Color online) Stripline structure for phase shift and delay time measurements in YIG/PMN-PT [Fetisov *et al.* (Ref. 187)].

(MSSW). Typical results shown in Fig. 55 demonstrate the feasibility for realizing passive, electric field tunable phase shifter, and delay lines.

VIII. FUTURE DIRECTIONS

A. Bulk ceramic composites

Although bulk ME ceramic composites were considered to exhibit promising larger linear ME effects, the ME effect so far observed in cofired ceramic composites is ten times or more lower than that predicted, due mainly to their inherent preparation problems, such as atomic interfacial diffusion and/or reaction problems between two ceramic phases during high-temperature preparation. A large number of combinations of piezoelectric oxides and magnetic oxides (mainly ferrites) would be attained. However, several important issues remain to be solved, including, the following.

(1) For the particulate ceramic composites, the challenge remains in achieving good dispersion of high concentration of ferrite phase in the piezoelectric ceramic matrix, favorable coherent interfaces, and sufficient bulk density while avoiding possible reaction and interfacial diffusion between the two ceramic phases to occur. Recently, chemical solution processing and novel sintering techniques such as SPS and hot pressing have been employed to fabricate the particulate ceramic composites and some improvement has been achieved. But obviously, more work still remains.
(2) For the laminate ceramics, the control of well cofiring the ferrite and piezoelectric layers with good interfacial contact but without interfacial diffusion/reaction is a key issue, which is like the cofiring of multilayer ceramic devices.[196] For the ME applications, strong ME coupling

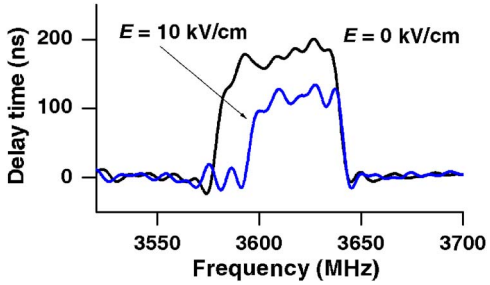

FIG. 55. (Color online) Delay time characteristics for MSSW excitations in YIG/PMN-PT for $H=701$ Oe [Fetisov *et al.* (Ref. 187)].

between these layers are desired. On the other hand, the laminate ceramics with high values of permittivity and permeability but minimum ME interaction are also highly desired for the integrated capacitor-inductor applications. The cofiring especially at low temperature of laminate ferroelectric and ferrite ceramics has been of technological importance.

(3) There have been a lot of theoretical works devoted to the constitutive problem of the ME ceramic composites, especially, many simulations from the micromechanics field. However, no work is done on the fatigue of the ME ceramic composites under bias fields, which is particularly of technological importance.

(4) The ME ceramic composites are ready for practical ME device applications due to their large ME effect above room temperature. Although some prototypes of microwave devices (see Sec. VII) based on the ME ceramic laminates have been proposed, much work still remains for their applications in real systems.

B. Magnetic alloy based composites

Among the ME composites, the magnetostrictive alloy (such as Terfenol-D) based composites have shown strongest ME coupling over wide frequency range. For example, the highest subresonant ME voltage coefficient of 5.5 V/cm Oe was observed for a *C-C* mode Terfenol-D/PZN-PT/Terfenol-D three-layer ring-type laminate. For such magnetic alloy based composites, the future directions include the following.

(1) Further optimizations for such ME laminate composites still remain, such as multilayer long or ring-type configurations for structure optimization, incorporation of even higher-μ third phases, and engineering controlled connectivity of the magnetic-piezoelectric phases. Actually, there are many possibilities that have not been tested.

Recently, Metglas ribbons have been used as the magnetostrictive layers.[62] Metglas has an extremely high magnetic permeability ($\mu_r \sim 30\,000$), but low magnetostriction. However, because of its ultrahigh μ_r, the effective piezomagnetic coefficient is high under small dc magnetic bias, making it an ideal candidate for incorporation into ME composites. Accordingly, a two-dimension Metglas layer connected with a one-dimension piezoelectric PZT fiber layer (i.e., a 2–1 type connectivity of Metglas/PZT fiber laminate, as shown in Fig. 56) has recently been shown to have a largely enhanced ME coupling. Figure 57 shows the ME voltage coefficient as a function of dc magnetic bias for longitudinal (L), width ($T1$), and thickness ($T2$) magnetizations. From this figure, it can be seen that the maximum dE/dH for the *L-L* mode is 22 V/cm Oe under a low H_{dc} of only 5 Oe. This is almost an order higher than that of corresponding *L-L* mode of Terfenol-D based ME laminates. Furthermore, under resonance drive, this value can be enhanced to ~500 V/cm Oe. Clearly, Metglas/PZT fibers in such 2-1 connectivity are an important direction for new ME laminate developments.

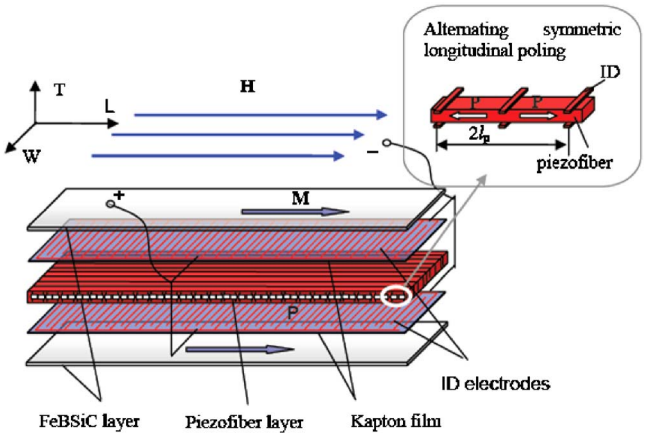

FIG. 56. (Color online) 2-1–type connectivity Metglas/PZT fiber laminate [Dong *et al.* (Ref. 62)].

Most recently, a small three-phase ME composite rod with a single PZT ceramic rod (see the inset in Fig. 58) embedded in Terfenol-D/epoxy (TDE) matrix has been reported.[197] The experimental results demonstrated that the coupling interaction between the PZT rod and TDE matrix can generate much larger ME response than other three-phase polymer-based composites. At high frequency where the electromechanical resonance appears, this ME rod showed a giant ME effect. This simple ME rod presented a size-dependent ME response, which implies that much smaller-sized ME rods (e.g., micro-ME rods) with large ME response can be obtained by using a single PZT fiber and promises future micro-ME devices.

(2) In the magnetic alloy based (two-phase or three-phase) composites, piezoelectric ceramics and magnetic alloys are bonded together by using polymer binders. The lifetimes of such ME composites are determined by the polymer binders. How do the polymer binders affect the ME response and the fatigue of such ME composites?

(3) Like the ME ceramic composites, these two-phase or three-phase magnetic alloy based ME composites are ready for practical ME device applications due to their

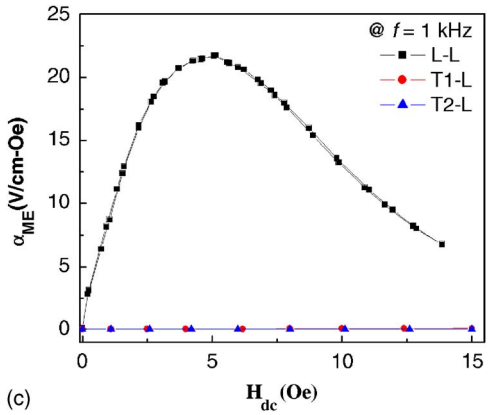

FIG. 57. (Color online) ME field coefficient as a function of dc magnetic bias for longitudinal (L), width ($T1$), and thickness ($T2$) magnetization [Dong *et al.* (Ref. 62)].

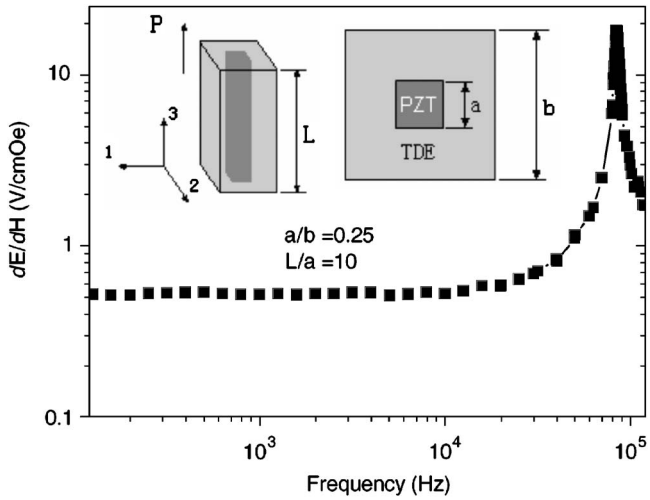

FIG. 58. Frequency dependence of the ME coefficients for the small ME composite rod (see the inset) with $a/b=0.25$ and $L/a=10$ ($a=1$ mm) [Ma *et al.* (Ref. 197)].

giant ME effect above room temperature. Although some prototypes of devices based on these composites have been proposed, much work also remains for their real applications.

C. Nanostructures

ME nanostructures have become an important topic of ever-increasing interest in last few years, since they, especially ME thin films, are easy to on-chip integration, which is a prerequisite for incorporation into microelectronic devices. But ME nanostructures are just in infant stage. The potential of ME nanostructures and their devices is almost limitless, but we must first overcome two fundamental challenges at least.

(1) The first is physical: how do we control the identity, placement, and function of every important atom in a ME nanostructure, in ways that are practical to apply to real-world ME materials and devices? In terms of nanostructure assembly, controlling the growth of desired ME nanostructures with precisely controlled composition, atomic arrangements, and interfaces is the most interesting but difficult problem. Indeed, this has been an ongoing quest in the field of nanomaterials and nanodevices, with recent progress also driven by directed assembly processes. For example, the formation of self-assembled, vertical nanostructures with long-range ordering will undoubtedly have great impact, not only in the field of multiferroics, but in a broad range of photonic applications.[198] High-quality horizontal heterostructures such as ME superlattices[199] hold particular promise for the rational design of new multiferroics and their devices.

(2) The second is conceptual: how do we understand systems that are too large to be handled by bruteforce calculation, but too small to be tackled by statistical methods? Many open questions regarding the ME coupling in nanostructures remain:[94] what is the timescale of the coupling process? How does the time dependence of the magnetism relate to the ferroelectric switching? What is the smallest value of magnetic field that can lead to full switching of the magnetization? How does the behavior depend on the chemistry of the nanostructures? Is there a critical dimension below which the coupling will disappear or change in nature?

(3) Like bulk ME composites, sensors, transducers, and heterogeneous read/write devices are among the suggested technical implementations of the composite ME effect in ME nanostructures.

ACKNOWLEDGMENTS

C.W.N. was supported by Ministry of Science and Technology of China (Grant Nos. 2002CB613303 and 2006AA03Z101) and the NSF of China (Grant Nos. 50621201 and 10574078). B.M.I. was supported by the Russian Foundation for Basic Research (Project Nos. 06-08-00896-a, No. 06-02-08071-ofi, and No. 05-02-39002-GFEN-a) and Program of Russian Ministry of Education and Science. S.D. and D.V. were supported by Office of Naval Research, U.S. Department of Energy, and DARPA.

[1] H. Schmid, Ferroelectrics **162**, 317 (1994).
[2] M. Fiebig, J. Phys. D **38**, R123 (2005).
[3] W. Eerenstein, N. D. Mathur, and J. F. Scott, Nature (London) **442**, 759 (2006).
[4] *Magnetoelectric Interaction Phenomena in Crystals, Proceedings of the MEIPIC-2*, edited by H. Schmid, Ascona, Switzerland, 13–18 September 1993, [Ferroelectrics **161–162** (1994)].
[5] *Proceedings of the MEIPIC-3*, edited by M. Bichurin, Novgorod, Russia, 16–20 September 1996 [Ferroelectrics **204** (1997)].
[6] *Proceedings of the MEIPIC-4*, edited by M. Bichurin, Novgorod, Russia, 16–19 October 2001 [Ferroelectrics **279–280** (2002)].
[7] *Magnetoelectric Interaction Phenomena in Crystals*, edited by M. Fiebig, V. V. Eremenko, and I. E. Chupis (Kluwer, Dordrecht, 2004); Proceedings of the MEIPIC-5, Sudak, Ukraine, 21–24 September 2003.
[8] N. A. Hill, J. Phys. Chem. B **104**, 6694 (2000).
[9] T. Kimura, T. Goto, H. Shintani, K. Ishizaka, T. Arima, and Y. Tokura, Nature (London) **426**, 55 (2003).
[10] J. Wang, J. B. Neaton, H. Zheng, V. Nagarajan, S. B. Ogale, B. Liu, D. Viehland, V. Vaithyanathan, D. G. Schlom, U. V. Waghmare, N. A. Spaldin, K. M. Rabe, M. Wuttig, and R. Ramesh, Science **299**, 1719 (2003).
[11] T. Goto, T. Kimura, G. Lawes, A. P. Ramirez, and Y. Tokura, Phys. Rev. Lett. **92**, 257201 (2004).
[12] T. Lottermoser, T. Lonkai, U. Amann, D. Hohlwein, J. Ihringer, and M. Fiebig, Nature (London) **430**, 541 (2004).
[13] N. Hur, S. Park, P. A. Sharma, J. S. Ahn, S. Guha, and S. W. Cheong, Nature (London) **429**, 392 (2004).
[14] W. Prellier, M. P. Singh, and P. Murugavel, J. Phys.: Condens. Matter **17**, R803 (2005).
[15] S. W. Cheong and M. Mostovoy, Nat. Mater. **6**, 13 (2007).
[16] J. van Suchtelen, Philips Res. Rep. **27**, 28 (1972).
[17] C. W. Nan, Phys. Rev. B **50**, 6082 (1994).
[18] R. E. Newnham, D. P. Skinner, and L. E. Cross, Mater. Res. Bull. **13**, 525 (1978).
[19] J. Boomgard, D. R. Terrell, R. A. J. Born, and H. F. J. I. Giller, J. Mater. Sci. **9**, 1705 (1974).
[20] A. M. J. G. Run, D. R. Terrell, and J. H. Scholing, J. Mater. Sci. **9**, 1710 (1974).
[21] J. Boomgard, A. M. J. G. Run, and J. Suchtelen, Ferroelectrics **10**, 295 (1976).
[22] J. Boomgard and R. A. J. Born, J. Mater. Sci. **13**, 1538 (1978).
[23] G. Harshe, J. P. Dougherty, and R. E. Newnham, Int. J. Appl. Electromagn. Mater. **4**, 145 (1993).
[24] S. Lopatin, I. Lopatin, and I. Lisnevskaya, Ferroelectrics **162**, 63 (1994).
[25] T. G. Lupeiko, I. V. Lisnevskaya, M. D. Chkheidze, and B. I. Zvyagintsev,

Inorg. Mater. **31**, 1245 (1995).
[26]M. I. Bichurin, I. A. Kornev, V. M. Petrov, and I. Lisnevskaya, Ferroelectrics **204**, 289 (1997).
[27]K. K. Patankar, S. A. Patil, K. V. Sivakumar, R. P. Mahajan, Y. D. Kolekar, and M. B. Kothale, Mater. Chem. Phys. **65**, 97 (2000).
[28]J. Ryu, A. V. Carazo, K. Uchino, and H. E. Kim, J. Electroceram. **7**, 17 (2001).
[29]K. K. Patankar, R. P. Nipankar, V. L. Mathe, R. P. Mahajan, and S. A. Patil, Ceram. Int. **27**, 853 (2001).
[30]V. L. Mathe, K. K. Patankar, U. V. Jadhav, A. N. Patil, S. D. Lotake, and S. A. Patil, Ceram. Int. **27**, 531 (2000).
[31]G. Srinivasan, E. T. Rasmussen, J. Gallegos, R. Srinivasan, Y. I. Bokhan, and V. M. Laletin, Phys. Rev. B **64**, 214408 (2001).
[32]G. Srinivasan, E. T. Rasmussen, B. J. Levin, and R. Hayes, Phys. Rev. B **65**, 134402 (2002).
[33]M. I. Bichurin, V. M. Petrov, R. V. Petrov, Y. V. Kiliba, F. I. Bukashev, A. Y. Smirnov, and D. N. Eliseev, Ferroelectrics **280**, 365 (2002).
[34]M. B. Kothale, K. K. Patankar, S. L. Kadam, V. L. Mathe, A. V. Rao, and B. K. Chougule, Mater. Chem. Phys. **77**, 691 (2003).
[35]G. Srinivasan, R. Hayes, and M. I. Bichurin, Solid State Commun. **128**, 261 (2003).
[36]G. E. Srinivasan, T. Rasmussen, and R. Hayes, Phys. Rev. B **67**, 014418 (2003).
[37]S. L. Kadam, K. K. Patankar, V. L. Mathe, M. B. Kothale, R. B. Kale, and B. K. Chougule, Mater. Chem. Phys. **78**, 684 (2003).
[38]S. Mazumder and G. S. Bhattacharyya, Ceram. Int. **30**, 389 (2004).
[39]J. Y. Zhai, N. Cai, Z. Shi, Y. H. Lin, and C. W. Nan, J. Phys. D **37**, 823 (2004).
[40]J. Y. Zhai, N. Cai, Z. Shi, Y. H. Lin, and C. W. Nan, J. Appl. Phys. **95**, 5685 (2004).
[41]M. Zeng, J. G. Wan, Y. Wang, H. Yu, J.-M. Liu, X. P. Jiang, and C. W. Nan, J. Appl. Phys. **95**, 8069 (2004).
[42]R. S. Devan, S. A. Lokare, D. R. Patil, S. S. Chougule, Y. D. Kolekar, and B. K. Chougule, J. Phys. Chem. Solids **67**, 1524 (2006).
[43]Y. J. Li, X. M. Chen, Y. Q. Lin, and Y. H. Tang, J. Eur. Ceram. Soc. **26**, 2839 (2006).
[44]J. P. Zhou, H. C. He, Z. Shi, G. Liu, and C. W. Nan, J. Appl. Phys. **100**, 094106 (2006).
[45]R. S. Devan, S. B. Deshpande, and B. K. Chougule, J. Phys. D **40**, 1864 (2007).
[46]S. S. Chougule and B. K. Chougule, Smart Mater. Struct. **16**, 493 (2007).
[47]J. Ryu, S. Priya, A. V. Carazo, K. Uchino, and H. E. Kim, J. Am. Chem. Soc. **84**, 2905 (2001).
[48]J. Ryu, A. V. Carazo, K. Uchino, and H. E. Kim, Jpn. J. Appl. Phys., Part 1 **40**, 4948 (2001).
[49]S. X. Dong, J. F. Li, and D. Viehland, Appl. Phys. Lett. **83**, 2265 (2003).
[50]S. X. Dong, J. F. Li, and D. Viehland, IEEE Trans. Ultrason. Ferroelectr. Freq. Control **50**, 1236 (2003).
[51]S. X. Dong, J. F. Li, and D. Viehland, J. Appl. Phys. **95**, 2625 (2004).
[52]S. X. Dong, J. F. Li, and D. Viehland, Appl. Phys. Lett. **85**, 2307 (2004).
[53]S. X. Dong, J. F. Li, and D. Viehland, J. Appl. Phys. **96**, 3382 (2004).
[54]S. X. Dong, J. F. Li, and D. Viehland, Appl. Phys. Lett. **85**, 2307 (2004).
[55]S. X. Dong, J. F. Li, and D. Viehland, Appl. Phys. Lett. **85**, 3534 (2004).
[56]S. X. Dong, J. F. Li, and D. Viehland, Appl. Phys. Lett. **84**, 4188 (2004).
[57]S. X. Dong, J. Y. Zhai, Z. P. Xing, J. F. Li, and D. Viehland, Appl. Phys. Lett. **86**, 102901 (2005).
[58]S. X. Dong, J. G. Bai, J. Y. Zhai, J. F. Li, G. Q. Lu, D. Viehland, S. J. Zhang, and T. R. Shrout, Appl. Phys. Lett. **86**, 182506 (2005).
[59]S. X. Dong, J. Y. Zhai, F. M. Bai, J. F. Li, D. Viehland, and T. A. Lograsso, J. Appl. Phys. **97**, 103902 (2005).
[60]S. X. Dong, J. Y. Zhai, N. G. Wang, F. M. Bai, J. F. Li, D. Viehland, and T. A. Lograsso, Appl. Phys. Lett. **87**, 222504 (2005).
[61]S. X. Dong, J. Zhai, J.-F. Li, and D. Viehland, Appl. Phys. Lett. **88**, 082907 (2006).
[62]S. X. Dong, J. Y. Zhai, J. F. Li, and D. Viehland, Appl. Phys. Lett. **89**, 252904 (2006).
[63]S. X. Dong, J. Y. Zhai, J. F. Li, and D. Viehland, Appl. Phys. Lett. **89**, 122903 (2006).
[64]S. X. Dong, J. F. Li, and D. Viehland, J. Appl. Phys. **100**, 124108 (2006).
[65]S. X. Dong, J. Y. Zhai, J. F. Li, D. Viehland, and M. I. Bichurin, Appl. Phys. Lett. **89**, 243512 (2006).
[66]J. Y. Zhai, J. F. Li, S. X. Dong, D. Viehland, and M. I. Bichurin, J. Appl. Phys. **100**, 124509 (2006).
[67]P. Li, Y. M. Wen, and L. X. Bian, Appl. Phys. Lett. **90**, 022503 (2007).
[68]X. M. Yin, N. Zhang, J. C. Bao, Phys. Lett. A **361**, 434 (2007).
[69]C. W. Nan, L. Liu, N. Cai, J. Zhai, Y. Ye, Y. H. Lin, L. J. Dong, and C. X. Xiong, Appl. Phys. Lett. **81**, 3831 (2002).
[70]J. G. Wan, J.-M. Liu, H. L. W. Chand, C. L. Choy, G. H. Wang, and C. W. Nan, J. Appl. Phys. **93**, 9916 (2003).
[71]C. W. Nan, N. Cai, L. Liu, J. Zhai, Y. Ye, and Y. H. Lin, J. Appl. Phys. **94**, 5930 (2003).
[72]N. Cai, J. Zhai, C. W. Nan, Y. H. Lin, and Z. Shi, Phys. Rev. B **68**, 224103 (2003).
[73]N. Cai, C. W. Nan, J. Y. Zhai, and Y. H. Lin, Appl. Phys. Lett. **84**, 3516 (2004).
[74]Y. H. Lin, N. Cai, J. Y. Zhai, G. Liu, and C. W. Nan, Phys. Rev. B **72**, 012405 (2005).
[75]C. W. Nan, N. Cai, Z. Shi, J. Zhai, G. Liu, and Y. H. Lin, Phys. Rev. B **71**, 014102 (2005).
[76]Z. Shi, C. W. Nan, J. Zhang, N. Cai, and J. F. Li, Appl. Phys. Lett. **87**, 012503 (2005).
[77]Z. Shi, C. W. Nan, J. Zhang, J. Ma, and J. F. Li, J. Appl. Phys. **99**, 124108 (2006).
[78]Z. Shi, J. Ma, Y. H. Lin, and C. W. Nan, J. Appl. Phys. **101**, 043902 (2007).
[79]H. Zheng, J. Wang, S. E. Lofland, Z. Ma, L. Mohaddes-Ardabili, T. Zhao, L. Salamanca-Riba, S. R. Shinde, S. B. Ogale, F. Bai, D. Viehland, Y. Jia, D. G. Schlom, M. Wuttig, A. Roytburd, and R. Ramesh, Science **303**, 661 (2004).
[80]H. Zheng, J. Wang, L. Mohaddes-Ardabili, M. Wuttig, L. Salamanca-Riba, D. G. Schlom, and R. Ramesh, Appl. Phys. Lett. **85**, 2035 (2004).
[81]F. Zavaliche, H. Zheng, L. Mohaddes-Ardabili, S. Y. Yang, Q. Zhan, P. Shafer, E. Reilly, R. Chopdekar, Y. Jia, P. Wright, D. G. Schlom, Y. Suzuki, and R. Ramesh, Nano Lett. **5**, 1793 (2005).
[82]J. G. Wan, X. W. Wang, Y. J. Wu, M. Zeng, Y. Wang, H. Jiang, W. Q. Zhou, G. H. Wang, and J. M. Liu, Appl. Phys. Lett. **86**, 122501 (2005).
[83]P. Murugavel, P. Padhan, and W. Prellier, Appl. Phys. Lett. **85**, 4992 (2004); P. Murugavel, D. Saurel, W. Prellier, C. Simon, and B. Raveau, *ibid.* **85**, 4424 (2004).
[84]M. P. Singh, W. Prellier, L. Mechin, C. Simon, and B. Raveau, J. Appl. Phys. **99**, 024105 (2006).
[85]J. P. Zhou, H. C. He, Z. Shi, and C. W. Nan, Appl. Phys. Lett. **88**, 013111 (2006).
[86]H. C. He, J. P. Zhou, J. Wang, and C. W. Nan, Appl. Phys. Lett. **89**, 052904 (2006).
[87]I. Levin, J. Li, J. Slutsker, and A. L. Roytburd, Adv. Mater. (Weinheim, Ger.) **18**, 2044 (2006).
[88]H. Zheng, F. Straub, Q. Zhan, P. L. Yang, W. K. Hsieh, F. Zavaliche, Y. H. Chu, U. Dahmen, and R. Ramesh, Adv. Mater. (Weinheim, Ger.) **18**, 2747 (2006).
[89]T. Wu, M. A. Zurbuchen, S. Saha, J. Mitchellm and S. K. Streiffer, Phys. Rev. B **73**, 134416 (2006).
[90]N. Ortega, P. Bhattacharya, and R. S. Katiyar, J. Appl. Phys. **100**, 126105 (2006).
[91]W. Eerenstein, M. Wiora, J. L. Prieto, J. F. Scott, and N. D. Mathur, Nat. Mater. **6**, 348 (2007).
[92]Y. G. Ma, W. N. Cheng, M. Ning, and C. K. Ong, Appl. Phys. Lett. **90**, 152911 (2007).
[93]H. C. He, J. P. Zhou, J. Wang, and C. W. Nan, Adv. Funct. Mater. **17**, 1333 (2007).
[94]R. Ramesh and N. A. Spaldin, Nat. Mater. **6**, 21 (2007).
[95]C. W. Nan, Prog. Mater. Sci. **37**, 1 (1993).
[96]C. W. Nan and D. R. Clarke, J. Am. Ceram. Soc. **80**, 1333 (1997).
[97]Y. Benveniste, Phys. Rev. B **51**, 16424 (1995).
[98]I. Getman, Ferroelectrics **162**, 45 (1994).
[99]T. Y. Chen, J. Mech. Phys. Solids **45**, 385 (1997); T. Y. Chen and S. C. Chiang, Acta Mech. **121**, 79 (1997).
[100]J. S. Lee, J. G. Boyd, and D. C. Lagoudas, Int. J. Eng. Sci. **43**, 790 (2005).
[101]J. Y. Li and M. L. Dunn, Philos. Mag. A **77**, 1341 (1998).
[102]J. Y. Li, Int. J. Eng. Sci. **38**, 1993 (2000); Q. J. Mech. Appl. Math. **56**, 35 (2003).
[103]S. Srinivas and J. Y. Li, Acta Mater. **53**, 4135 (2005).
[104]S. Srinivas, J. Y. Li, and Y. C. Zhou, J. Appl. Phys. **99**, 043905 (2006).
[105]L. J. Li and J. Y. Li, Phys. Rev. B **73**, 184416 (2006).
[106]J. H. Huang and W. S. Kuo, J. Appl. Phys. **81**, 1378 (1997).
[107]J. H. Huang, Phys. Rev. B **58**, 12 (1998).
[108]T. L. Wu and J. H. Huang, Int. J. Solids Struct. **37**, 2981 (2000).

[109] E. Pan, Z. Angew. Math. Phys. **53**, 815 (2002).
[110] D. A. Filippov, Tech. Phys. Lett. **30**, 351 (2004).
[111] H. T. Huang and L. M. Zhou, J. Phys. D **37**, 3361 (2004).
[112] M. I. Bichurin, V. M. Petrov, O. V. Ryabkov, S. V. Averkin, and G. Srinivasan, Phys. Rev. B **72**, 060408 (2005).
[113] Y. Zhou and F. G. Shin, J. Appl. Phys. **100**, 043910 (2006).
[114] C. W. Nan, M. Li, and J. H. Huang, Phys. Rev. B **63**, 144415 (2001).
[115] C. W. Nan, M. Li, X. Feng, and S. Yu, Appl. Phys. Lett. **78**, 2527 (2001).
[116] K. Mori and M. Wuttig, Appl. Phys. Lett. **81**, 100 (2002).
[117] C. W. Nan, G. Liu, Y. H. Lin, and H. Chen, Phys. Rev. Lett. **94**, 197203 (2005).
[118] G. Liu, C. W. Nan, and J. Sun, Acta Mater. **54**, 917 (2006); G. Liu, C. W. Nan, Z. K. Xu, and H. Chen, J. Phys. D **38**, 2321 (2005).
[119] C. G. Duan, S. S. Jaswal, and E. Y. Tsymbal, Phys. Rev. Lett. **97**, 047201 (2006).
[120] J. X. Zhang, Y. L. Li, D. G. Schlom, L. Q. Chen, F. Zavaliche, R. Ramesh, and Q. X. Jia, Appl. Phys. Lett. **90**, 052909 (2007).
[121] X. Lu, B. Wang, Y. Zheng, and E. Ryba, Appl. Phys. Lett. **90**, 133124 (2007); J. Phys. D **40**, 1614 (2007).
[122] C. W. Nan, J. Appl. Phys. **82**, 5268 (2002).
[123] R. Hill, J. Mech. Phys. Solids **12**, 199 (1964).
[124] M. Avellaneda and G. Harshe, J. Intell. Mater. Syst. Struct. **5** 501 (1994).
[125] M. I. Bichurin, V. M. Petrov, and G. Srinivasan, J. Appl. Phys. **92**, 7681 (2002); Phys. Rev. B **68**, 054402 (2003).
[126] M. I. Bichurin and V. M. Petrov, Sov. Phys. Tech. Phys. **33**, 1389 (1989).
[127] M. I. Bichurin, V. M. Petrov, and Y. V. Kiliba, Phys. Rev. B **66**, 134404 (2002).
[128] M. I. Bichurin, V. M. Petrov, and I. A. Kornev, Ferroelectrics **280**, 353 (2002).
[129] M. I. Bichurin, D. A. Filippov, and V. M. Petrov, Phys. Rev. B **68**, 132408 (2003).
[130] D. A. Filippov, M. I. Bichurin, and V. M. Petrov, Tech. Phys. Lett. **30**, 6 (2004).
[131] M. I. Bichurin and V. M. Petrov, Ferroelectrics **162**, 33 (1994).
[132] X. M. Chen, Y. H. Tang, and I. W. Chen, J. Appl. Phys. **96**, 6520 (2004).
[133] Y. H. Tang, X. M. Chen, and Y. J. Li, Mater. Sci. Eng., B **116**, 150 (2005).
[134] K. K. Patankar, V. L. Mathe, and A. N. Patil, J. Electroceram. **6**, 115 (2001); V. L. Mathe, K. K. Patankar, and U. V. Jadhav, Ceram. Int. **27**, 531 (2001).
[135] K. K. Patankar, V. L. Mathe, and R. P. Mahajan, Mater. Chem. Phys. **72**, 23 (2001); K. K. Patankar, P. D. Dombale, and V. L. Mathe, Mater. Sci. Eng., B **87**, 53 (2001).
[136] S. L. Kadam, K. K. Patankar, and V. L. Mathe, J. Electroceram. **9**, 193 (2002); Mater. Chem. Phys. **78**, 684 (2003).
[137] S. R. Kulkarni, C. M. Kanamadi, and K. K. Patankar, J. Mater. Sci. **40**, 5691 (2005); C. M. Kanamadi and K. K. Chougule, J. Electroceram. **15**, 123 (2005).
[138] Y. R. Dai, P. Bao, and J. S. Zhu, J. Appl. Phys. **39**, 1209 (2003).
[139] M. E. Botello-Zubiate, D. Bueno-Baques, and J. D. Vaquerizo, Integr. Ferroelectr. **83**, 33 (2006).
[140] C. M. Kanamadi, L. B. Pujari, and B. K. Chougule, J. Magn. Magn. Mater. **295**, 139 (2005).
[141] M. Zeng, J. G. Wan, Y. Wang, and J. M. Liu, J. Appl. Phys. **95**, 8069 (2004).
[142] R. A. Islam and S. Priya, Jpn. J. Appl. Phys., Part 2 **45**, L128 (2006).
[143] V. M. Petrov, G. Srinivasan, V. Laletsin, and M. I. Bichurin, Phys. Rev. B **75**, 174442 (2007).
[144] S. Q. Ren, L. Q. Weng, and S. H. Song, J. Mater. Sci. **40**, 4375 (2005).
[145] G. Srinivasan, C. P. DeVreugd, and C. S. Flattery, Appl. Phys. Lett. **85**, 2550 (2004).
[146] Q. H. Jiang, Z. J. Shen, J. P. Zhou, Z. Shi, and C. W. Nan, J. Eur. Ceram. Soc. **27**, 279 (2007).
[147] Z. J. Shen and M. Nygren, Chem. Rec. **5**, 173 (2005).
[148] L. Q. Weng, Y. D. Fu, and S. H. Song, Scr. Mater. **56**, 465 (2007).
[149] J. G. Wan, H. Zhang, and X. W. Wang, Appl. Phys. Lett. **89**, 122914 (2006).
[150] V. Corral-Flores, D. Bueno-Baques, and D. Carrillo-Flores, J. Appl. Phys. **99**, 08J503 (2006).
[151] R. A. Islam and S. Priya, Appl. Phys. Lett. **89**, 152911 (2006); N. Zhang, W. Ke, and T. Schneider, J. Phys.: Condens. Matter **18**, 11013 (2006).
[152] I. V. Lisnevskaya, I. A. Bobrova, and E. A. Bikyashev, Inorg. Mater. **42**, 1147 (2006).
[153] G. Srinivasan, I. V. Zavislyak, and A. S. Tatarenko, Appl. Phys. Lett. **89**, 152508 (2006).
[154] C. W. Nan, Y. H. Lin, and J. H. Huang, Ferroelectrics **280**, 319 (2002).
[155] C. W. Nan, G. Liu, and Y. H. Lin, Appl. Phys. Lett. **83**, 4366 (2003).
[156] S. X. Dong, J. F. Li, and D. Viehland, IEEE Trans. Ultrason. Ferroelectr. Freq. Control **50**, 1253 (2003).
[157] S. X. Dong, J. F. Li, and D. Viehland, J. Mater. Sci. **41**, 97 (2006).
[158] S. X. Dong, J. R. Cheng, J. F. Li, and D. Viehland, Appl. Phys. Lett. **83**, 4812 (2003).
[159] Y. X. Liu, J. G. Wan, J. M. Liu, and C. W. Nan, J. Appl. Phys. **94**, 5111 (2003); **94**, 5118 (2003).
[160] G. Liu, C. W. Nan, N. Cai, and Y. H. Lin, J. Appl. Phys. **95**, 2660 (2004); Int. J. Solids Struct. **41**, 4423 (2004).
[161] Y. M. Jia, S. W. Or, and H. L. Chan, Appl. Phys. Lett. **88**, 242902 (2006).
[162] H. Yu, M. Zeng, and Y. Wang, Appl. Phys. Lett. **86**, 032508 (2005); N. Zhang, X. M. Yin, and W. Ke, J. Phys.: Condens. Matter **18**, 10965 (2006); S. S. Guo, S. G. Lu, Z. Xu, X. Z. Zhao, and S. Or, Appl. Phys. Lett. **88**, 182906 (2006).
[163] J. G. Wan, Z. Y. Li, Y. Wang, M. Zeng, G. H. Wang, and J.-M. Liu, Appl. Phys. Lett. **86**, 202504 (2005).
[164] J. Y. Zhai, Z. Xing, S. X. Dong, J. F. Li, and D. Viehland, Appl. Phys. Lett. **88**, 062510 (2006).
[165] S. X. Dong, J. F. Li, and D. Viehland, IEEE Trans. Ultrason. Ferroelectr. Freq. Control **51**, 794 (2004).
[166] S. X. Dong, J. Y. Zhai, F. Bai, J. F. Li, and D. Viehland, Appl. Phys. Lett. **87**, 062502 (2005).
[167] J. Y. Zhai, S. X. Dong, Z. P. Xing, J. F. Li, and D. Viehland, Appl. Phys. Lett. **89**, 083507 (2006).
[168] K. Zhao, K. Chen, Y. R. Dai, J. G. Wan, and J. S. Zhu, Appl. Phys. Lett. **87**, 162901 (2005).
[169] V. M. Laletin, N. Paddubnaya, and G. Srinivasan, Appl. Phys. Lett. **87**, 222507 (2005).
[170] S. N. Babu, T. Bhimasankaram, and S. V. Suryanarayana, Bull. Mater. Sci. **28**, 419 (2005).
[171] Y. M. Jia, S. W. Or, and K. H. Lam, Appl. Phys. A: Mater. Sci. Process. **86**, 525 (2007).
[172] Z. Shi, C. W. Nan, J. M. Liu, and M. I. Bichurin, Phys. Rev. B **70**, 134417 (2004).
[173] D. A. Filippov, M. I. Bichurin, C. W. Nan, and J. M. Liu, J. Appl. Phys. **97**, 113910 (2005).
[174] S. X. Dong, J. Y. Zhai, J. F. Li, and D. Viehland, J. Appl. Phys. **100**, 124108 (2006).
[175] J. Slutsker, I. Levin, J. H. Li, A. Artemev, and A. L. Royburd, Phys. Rev. B **73**, 184127 (2006).
[176] F. Zavaliche, T. Zhao, H. Zheng, F. Straub, M. P. Cruz, P.-L. Yang, D. Hao, and R. Ramesh, Nano Lett. **7**, 1586 (2007).
[177] C. Y. Deng, Y. Zhang, J. Ma, Y. H. Lin, and C. W. Nan, J. Appl. Phys. **102**, 074114 (2007).
[178] C. Thiele, K. Dorr K, O. Bilani O, J. Roedel, and L. Schultz, Phys. Rev. B **75**, 054408 (2007).
[179] G. Srinivasan, C. P. De Vreugd, and M. I. Bichurin, Appl. Phys. Lett. **86**, 222506 (2005); R. V. Chopdekar and Y. Suzuki, *ibid.* **89**, 182506 (2006).
[180] V. M. Petrov, G. Srinivasan, M. I. Bichurin, and A. Gupta, Phys. Rev. B **75**, 224407 (2007).
[181] L. P. M. Bracke and R. G. van Vlite, Int. J. Electron. **51**, 255 (1981); J. L. Prieto, C. Aroca, E. Lopez, M. C. Sanchez, and P. Sanchez, J. Magn. Magn. Mater. **215**, 756 (2000); E. Quandt, S. Stein, and M. Wuttig, IEEE Trans. Magn. **41**, 3667 (2005); R. Bergs, R. A. Islam, and M. Vickers, J. Appl. Phys. **101**, 024108 (2007).
[182] J. G. Wan, J. M. Liu, G. H. Wang, and C. W. Nan, Appl. Phys. Lett. **88**, 182505 (2006).
[183] Z. Huang, J. Appl. Phys. **100**, 114104 (2006).
[184] M. I. Bichurin, I. A. Kornev, V. M. Petrov, A. S. Tatarenko, Yu. V. Kiliba, and G. Srinivasan, Phys. Rev. B **64**, 094409 (2001).
[185] S. Shastry, G. Srinivasan, M. I. Bichurin, V. M. Petrov, and A. S. Tatarenko, Phys. Rev. B **70**, 064416 (2004).
[186] M. I. Bichurin, R. V. Petrov, and Y. V. Kiliba, Ferroelectrics **204**, 311 (1997).
[187] A. S. Tatarenko, M. I. Bichurin, and G. Srinivasan, Electron. Lett. **41**, 596 (2005).
[188] Y. K. Fetisov and G. Srinivasan, Appl. Phys. Lett. **87**, 103502 (2005); Electron. Lett. **41**, 1066 (2005).
[189] A. A. Semenov, S. F. Karmanenkov, V. E. Demidov, B. A. Kalinikos, G. Srinivasan, A. N. Slavin, and J. V. Mantese, Appl. Phys. Lett. **88**, 033503 (2006).
[190] Y. K. Fetisov and G. Srinivasan, Appl. Phys. Lett. **88**, 143503 (2006).

[191] A. S. Tatarenko, G. Srinivasan, and M. I. Bichurin, Appl. Phys. Lett. **88**, 183507 (2006); A. S. Tatarenko, V. Gheevarughese, and G. Srinivasan, Electron. Lett. **42**, 540 (2006).
[192] A. A. Semenov, S. F. Karmanenko, B. A. Kalinikos, G. Srinivasan, A. N. Slavin, and J. V. Mantese, Electron. Lett. **42**, 641 (2006).
[193] G. Srinivasan and Y. K. Fetisov, Integr. Ferroelectr. **83**, 89 (2006).
[194] A. B. Ustinov, V. S. Tiberkevich, G. Srinivasan, A. N. Slavin, A. A. Semenov, S. F. Kamanenko, B. A. Kalinikos, J. V. Mantese, and R. Ramer, J. Appl. Phys. **100**, 093905 (2006).
[195] G. Srinivasan and Y. K. Fetisov, Ferroelectrics **342**, 65 (2006).
[196] N. Setter and R. Waser, Acta Mater. **48**, 151 (2000).
[197] J. Ma, Z. Shi, and C. W. Nan, Adv. Mater. (Weinheim, Ger.) **19**, 2571 (2007).
[198] A. Figotin and I. Vitebskiy, Phys. Rev. E **63**, 066609 (2001); **68**, 036609 (2003).
[199] M. P. Singh and W. Prellier, Philos. Mag. Lett. **87**, 211 (2007).